A daily reconstruction of historical weather to study past climate variability and impacts

Inaugural dissertation
of the Faculty of Science,
University of Bern

presented by

Noemi Imfeld

from Lungern OW

Supervisor of the doctoral thesis:

Prof. Dr. Stefan Brönnimann

Institute of Geography, University of Bern.

A daily reconstruction of historical weather to study past climate variability and impacts

Inaugural dissertation
of the Faculty of Science,
University of Bern

presented by

Noemi Imfeld

from Lungern, OW

Supervisor of the doctoral thesis:

Prof. Dr. Stefan Brönnimann

Institute of Geography, University of Bern.

Accepted by the Faculty of Science.

Bern, 18th December 2023

The Dean:
Prof. Dr. Marco Herwegh

Supervisor:

Prof. Dr. Stefan Brönnimann

Institute of Geography

University of Bern

External examiner:

Prof. Dr. Ed Hawkins

Department of Meteorology

University of Reading

Summary

Studying daily weather of the past can provide relevant insights into the decadal variability of weather events and climate impacts that are not resolved in current climate reconstructions. While monthly to seasonal reconstructions have been evaluated for the past several hundred years, the daily time scale has received little attention, mainly because the necessary data sets are scarce.

In this thesis, a daily reconstruction of high-resolution (1x1 km^2) temperature and precipitation fields from 1763 to 1960 is presented, that forms together with present-day fields a 258-year-long gridded data set for Switzerland (Chapter 2). Further, reconstructions for sea level pressure and temperature for several short periods in the late 18th and early 19th century for Europe are presented (Sect. 1.3 and Appendix A). These data sets allow for new analyses of daily weather and daily-based climate indices that were hitherto not possible. The meteorological fields were reconstructed using the Analogue Resampling Method (ARM) to generate a first guess of the meteorological fields, and subsequently improved by assimilating temperature and pressure observations and bias-correcting precipitation fields. For Switzerland, cross-validation results of the temperature reconstruction show good skill even for the very early periods before 1864, when observations were sparse. The reconstruction skill for precipitation is lower than for temperature, but wet days frequencies compare well to independent observations.

Based on this gridded data set, we calculated climate indices and two phenological phases to evaluate spring weather over the 258-year-long period (Chapter 3). Although it receives less attention than winter and summer, the spring season is important because adverse weather conditions in spring delay plant growth, and late frosts can damage vegetation. Climate and phenological indices impressively depict the warming of the recent decades compared to the pre-industrial reference period 1871 to 1900. Cherry flowering, for example, advanced by up to 20 days in the Swiss Plateau since the pre-industrial reference period. In the 258-year-long series, the spring of 1785 stands out of the reconstruction with a mean temperature of only 4.10 °C and up to 30 days of frost registered in the Swiss Plateau. Further data sets and historical sources confirm that this was a record-breaking cold spring, with prolonged inversion conditions in the Swiss Plateau.

Among the ten warmest summer half years in Switzerland, only one summer from the 20th century remains, the summer of 1947 (Chapter 4). It still ranks as the fifth warmest summer on record based on a time series for the Swiss Plateau since 1756. In some parts of

Switzerland, precipitation deficits are still the lowest since 1864. The repeated occurrence of blocking anticyclones led to a total of five heat waves in some parts of Switzerland between May and September, contributing to the anomalously warm temperatures. The warm and dry conditions had severe consequences such as extensive glacier ice loss, drying out of lakes, and forest damage. If we compare the warm summers to their mean climatic state, the summer of 1947 was indeed as extreme as 2003. However, the summer of 2022, the second warmest summer on record, was a fairly normal summer compared to its mean climate. Compared to the summer temperatures expected by the end of the century (2070 - 2099), the record summers of 1947, 2003, and 2022 would only be fairly normal summers under an emissions reduction scenario (RCP2.6), and such summers would be exceptionally cold if no emissions reductions are achieved (RCP8.5).

Contents

List of Figures

List of Tables

List of Abbreviations

Data sets

20CRv3	20th Century Reanalysis Version 3
CH2018	Swiss climate scenarios
ECA&D	European Climate Assessment and Dataset
EKF400v2	Ensemble Kalman Fitting Paleo-Reanalysis Version 2.0
EOBS	E-OBS daily gridded meteorological data for Europe from 1950 to present derived from in-situ observations
ERA5	5th generation ECMWF reanalysis
ModE-RA	Modern Era Reanalysis
NBCN	Swiss National Basic Climate Network
RhiresD	Daily gridded precipitation sum data set (1961 - present) from MeteoSwiss
RrecabsM1864	Monthly gridded precipitation data set with long-term consistency from MeteoSwiss
SPN	Swiss Phenology Network
TabsD	Daily gridded mean temperature data set (1961 - present) from MeteoSwiss
TrecabsM1864	Monthly gridded temperature data set with long-term consistency from MeteoSwiss

Projects and scientific programs

CHIMES	Swiss Early Instrumental Measurements for Studying Decadal Climate Variability
DigiHom	Digitalisieren und Homogenisieren von historischenKlimadaten des Swiss NBCN
ETCCDI	Expert Team on Climate Change Detection and Indices
PALAEO-RA	A Palaeoreanalysis To Understand Decadal Climate Variability

Variables and parameters

$\tilde{K}$	Reduced Kalman gain matrix
H	Forward operator to extract observations from model space
K	Kalman gain matrix
P^b	Model error covariance matrix
R	Observation error covariance matrix
x^a	Analysis, best estimate of true atmospheric state
x^b	Background state, first guess
y	Observations
CSDI	Cold Spell Duration Index
d	days
E	East, indifferent weather type
F_{crit}	Threshold when phenological phase is reached
FD	Frost Days
GDD	Growing Degree Days
GSS	Growing Season Start
HP	High pressure over Europe weather type
L_i	Daylength at a location dependent on latitude i
LFD	Last Frost Days
N	North, cyclonic weather type
NE	Northeast, indifferent weather type
R_g	Growing degree days temperature response
S_{frc}	State of forcing
SD	Snowfall Days
t_0	Start day for temperature accumulation
T_{base}	Base temperature for temperature accumulation
W	Westerly flow over Northern Europe weather type
WC	Westerly flow over Southern Europe, cyclonic weather type
WD	Wet Days
WSDI	Warm Spell Duration Index
WSW	West-southwest, cyclonic, flat pressure weather type

Other abbreviations

ARM	Analogue Resampling Method
EnKF	Ensemble Kalman Fitting
ERA-20C	ECMWF Reanalysis of the 20th Century
MCH	National Weather Service of Switzerland, MeteoSwiss
MSESS	Mean Squared Error Skill Score
PTT	Photo Thermal Time phenology model

RCP2.6	Representative Concentration Pathway 2.6
RCP4.5	Representative Concentration Pathway 4.5
RCP8.5	Representative Concentration Pathway 8.5
RMSE	Root Mean Squared Error
TT	Thermal Time phenology model
WRF	Weather Research and Forecasting model

Chapter 1

Introduction

1.1 The relevance of historical weather

Monthly to annual climate reconstructions have provided important insights into climate variability and climate change over the past several hundred years. For example, they have helped to understand the processes of the climate system and the mechanisms of climate change, and have contributed to the study of past extreme events (Ljungqvist et al., 2019; Luterbacher et al., 2004; Valler et al., 2022; Casty et al., 2005; Pauling et al., 2006). However, in terms of impacts, often the extreme weather events that occur on synoptic timescales have caused severe damage and are therefore relevant to society and ecosystems (e.g. Stucki et al., 2015; Brönnimann et al., 2019). Recent events have been studied extensively to understand the underlying mechanisms and to prevent future damage, but studying historical events could further contribute to our understanding of past and present weather. This is, however, often hampered because data sets do not extend further back in time, they are too coarse, they do not cover a sufficient spatial scale, or they do not represent an event adequately. For studying daily weather of the past at least 200 years, there are mainly two types of data available, the 20th century reanalysis, 20CRv3, that covers a period from 1806 to 2015, but at a rather coarse resolution ($0.75°$), and early instrumental records dating back to the 18th, but only available at specific locations. More insights can, however, be gained when spatio-temporally complete data is available.

Studying historical weather in a spatio-temporal comprehensive way is important for several reasons. (1) Since extreme events are rare by nature, we can extend the sample of events when considering also the 18th and 19th centuries. Improved data assimilation in 20th century reanalysis 20CRv3 resulted in a better representation and, thus, a better understanding of the dynamics of the storm Ulysses (Hawkins et al., 2023). (2) Comparing historical events with current events allows us to assess how extreme an event was,

for example, when placing the hot summer of 1947 into its climatological context (Imfeld et al., 2022b), or by comparing the occurrence of heat waves in the past with more recent heat waves (e.g. Yule et al., 2023). (3) We can gain knowledge by assessing the climate-related risk of past extreme events by running impact models, as it has been shown for floods and crop losses in the cold summers of 1816 and 1817 (Brönnimann et al., 2019; Flückiger et al., 2017; Rössler and Brönnimann, 2018). (4) Finally, daily data at a high spatio-temporal resolution is needed to extend various applications further back in time, such as hydrological modelling, snow pack modelling, and phenological modelling.

More than 75 years ago, the heat waves of the summer of 1947 and the prolonged drought conditions between 1945 and 1952 caused significant ecosystem and societal impacts in Switzerland (Imfeld et al., 2022a). But, the 18th and 19th centuries also saw their share of extreme weather and climate. In Switzerland, a prominent example is the infamous "year without a summer" in 1816 causing a famine, which has been studied in-depth concerning its causes and impacts (e.g. Flückiger et al., 2017). Less is known about other events, such as the warm summer of 1807, the cold spring in 1785 (Pappert et al., 2021), or the multi-year cold and wet anomaly around 1770 (Collet, 2018).

In this thesis, we present continuous daily reconstructions of temperature and precipitation fields for Switzerland covering a period from 1763 to 2020 (Chapt. 2), and some examples of temperature and pressure reconstructions for Europe (Sect. 1.3). These reconstructions make it possible to study such historical events and contribute to gaining a first understanding of their extent and impact (Chapt. 3).

1.2 Historical weather data

Historical observations are the key to studying past weather, and therefore the key to reconstructing weather and assessing the impact of past weather events. With the establishment of the national weather service in Switzerland in the 1860s, systematic measurements of meteorological data with standard procedures were introduced (Hupfer, 2019). Since 1864, a dense network of homogenized high-quality station data of temperature, precipitation, and pressure has been available (Begert et al., 2005). Long time series are, however, also available for the 18th and 19th centuries (e.g. for Basel, Bider et al., 1958), and any other series exist in Switzerland, measured by dedicated societies and individuals interested in meteorology. In the project CHIMES (Swiss Early Instrumental Measurements for Studying Decadal Climate Variability), these so-called early instrumental data have been imaged, digitized, and quality controlled (Pfister et al., 2019; Brugnara et al., 2020), and a dense network of observations for the 18th and 19th century is now digitally available for Switzerland.

When using early observations in climatological studies certain challenges have to be addressed and not all are easy to overcome. Here, we attempt to list some examples. The historical instruments often had different scales and their measurements have to be converted to today's standard units. This is not always straightforward, for example, when it is unclear what units have been used. Temperature measurements can suffer from exposure to direct or scattered solar radiation and to precipitation creating biases in the data that are difficult to correct (Wallis et al., 2023; Böhm et al., 2010). For air pressure, uncertainties arise depending on the barometer construction, from unknown temperature corrections of the pressure observations, and from missing temperature measurements representative of the barometer temperature (Brugnara et al., 2020). Common to many observations are also missing, vague, or inaccurate observation times, which complicate the calculation of daily mean values, especially for temperature. Despite these challenges, overall, there is a large amount of data that can be used to reconstruct and study historical weather on a daily time scale over the past few hundred years.

1.3 Reconstructing historical daily weather

Different approaches have been used to reconstruct daily weather fields of the past 250 years (see e.g. Brönnimann, 2022). Some widely used daily data sets cover periods back to the 19th century. The reanalysis 20CRv3, for example, covers a period from 1806 to 2015 at a resolution of about 0.75 ° latitude by longitude and is solely based on assimilating pressure observations (Slivinski et al., 2019). 20CRv3 is valuable for studying past historical weather events since it is possible to study the entire atmospheric column, i.e. the upper-level dynamics in the atmosphere as well as 2 m temperature and sea level pressure fields (e.g. Yule et al., 2023; Meyer et al., 2022; Slivinski et al., 2021). A daily global gridded temperature product is EUSTACE which covers a period since 1850, is based on observational data only, and relies for its generation on geostatistical approaches (Rayner et al., 2020). Other data sets cover smaller areas but have a higher spatial resolution. For example, Devers et al. (2021) produced a high-resolution reanalysis of temperature and precipitation based on the SCOPE climate reconstruction (Caillouet et al., 2019) starting in 1890 for France. For the UK, Keller et al. (2015) interpolated daily and monthly precipitation fields back to 1890 using a geostatistical approach.

A comparatively simple and computationally cheap approach for weather reconstruction is the analogue resampling method (ARM). This method relies on the assumption that the spatial patterns that can be observed in a reference period are stationary over time. Analogue fields based on reference fields from present-day gridded products or climate models have been widely used for annual, seasonal, and monthly time scales (Gómez-Navarro et al., 2017; Franke et al., 2011; Zorita and von Storch, 1999). On a daily basis, Flückiger et al.
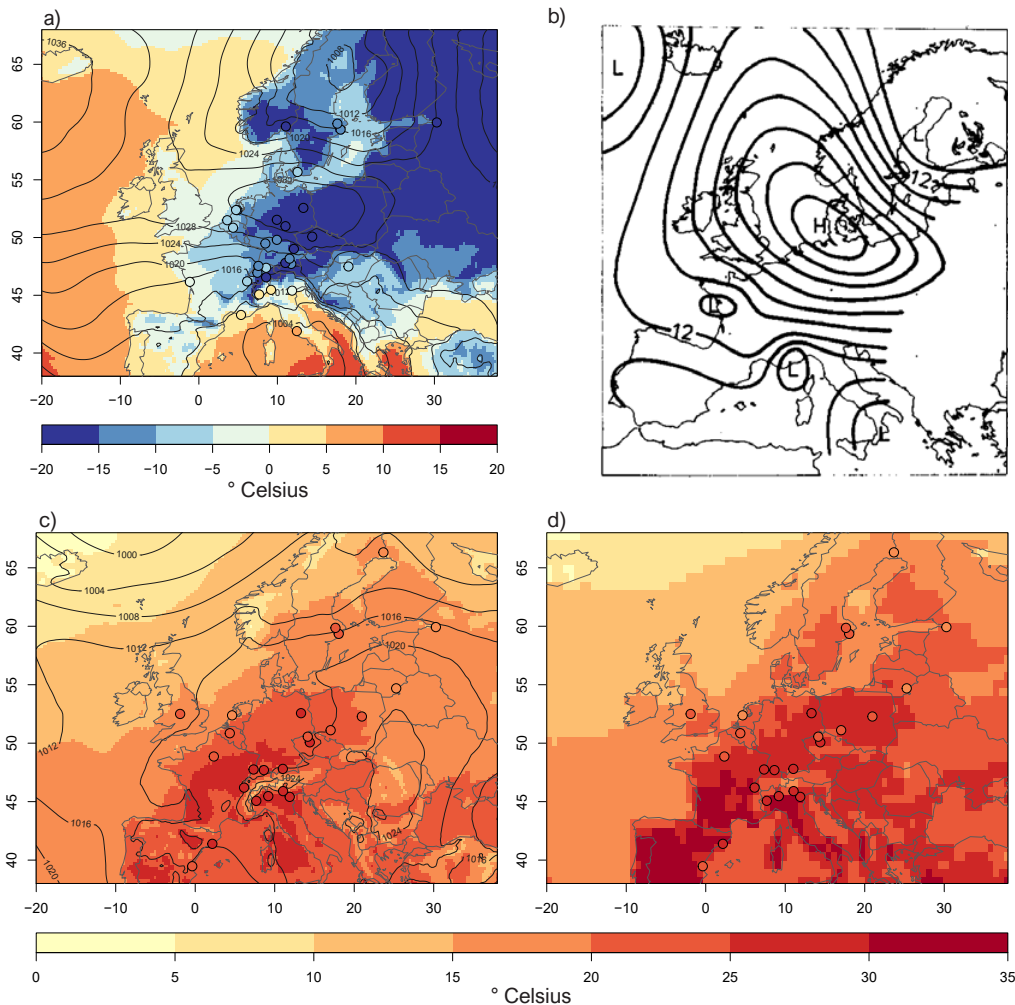
Figure 1.1: Comparison of reconstruction methods for two days in the years 1785 and 1807. a) Reconstructed temperature and sea level pressure for 28th February 1785 with ARM and data assimilation. b) hand-drawn sea level pressure maps by Kington (1988) for 28th February 1785. c) as in (a) but for the 13th July 1807 and d) temperature field from 20CRv3 with additional assimilation of temperature observations for the 13th July 1807. Temperature observations entering the reconstructions in a,c, and d are shown as filled circles.

(2017) used the ARM for studying the impacts of the cold and wet conditions in the "year without a summer" in 1816. For Switzerland, Pfister et al. (2020) reconstructed daily fields of precipitation and temperature back to 1864 using the ARM. Pappert et al. (2022) showed that this method is also feasible for a larger region by reconstructing daily sea level pressure and temperature fields for the very cold winter of 1788/89 in Europe. For such early periods, gridded weather data are rarely available. Attempts to study the daily synoptic conditions of Europe for the years from 1781 to 1785 were made by Kington (1988)

by hand drawing surface pressure maps based on observations and secondary information. These maps have been used for many years, for example, as a basis for understanding the Laki volcanic gaze over Europe (e.g. Thordarson and Self, 2003). While such maps help gain a general understanding, objective methods that provide numerical fields are often more valuable for further analysis. The ARM offers a simple way to reconstruct such fields. Figure 1.1a and b compare the ARM-based 2 m temperature and sea level pressure reconstruction with subsequent data assimilation to the hand-drawn map by Kington (1988). Both fields depict a pronounced anticyclone on the 28th February of 1785 that led to very cold conditions over Europe, but the extent of the anticyclone differs. Figure 1.1 c and d compare the ARM-based 2 m temperature and sea level pressure reconstruction to a 2 m temperature field from 20CRv3 with additional offline data assimilation for the 13th July 1807, a very hot day in the year 1807 (as in Brönnimann, 2022). The summer of 1807 has been described in many sources as very warm, as evidenced by the high temperatures in Central Europe in both reconstructions. Both reconstructions for 1785 and 1807 were produced as part of this thesis and based on the ERA5 reanalysis between 1950 and 2020 (Hersbach et al., 2020) and historical observations. The method follows mainly the description in Chapter 2 and Pappert et al. (2022) with analogue resampling and subsequent data assimilation.

Also, artificial intelligence has been used for the reconstruction of past climate states across several centuries for monthly-to-annual scales (Wegmann and Jaume-Santero, 2023; Jaume-Santero et al., 2022). On the daily time scale, generative adversarial networks proved useful for downscaling wind fields (Miralles et al., 2022) from 1961 to 2020 for Switzerland, but similar methods have not yet been extended back to e.g. the early instrumental period.

In addition to the statistical methods, there are also numerical methods for the periods for which fields from reanalyses are available as boundary conditions. Historical extreme events, such as the snow-rich winter of 1916/17 and the severe foehn storm of 1925, have been dynamically downscaled using the Weather Research and Forecasting (WRF) model (Brugnara et al., 2017; Stucki et al., 2015). For both cases, reanalyses provided the initial and lateral boundary conditions driving the regional, high-resolution model. Dynamical downscaling can be improved when combining it with data assimilation (Stucki et al., in preparation), but this requires careful work ahead. Early instrumental data, for example, sometimes lack precise observation times, which complicates at what time step to assimilate an observation. Both downscaling approaches produce high-resolution fields of the entire atmosphere, but since they are computationally intensive only a few studies have covered longer periods (e.g. Koenigseder et al., 2023).

Overall, different data set exists, or have been created within this thesis to study daily weather since around the mid-18th century (Fig. 1.2). The Swiss reconstruction pro-

vides high-resolution daily temperature and precipitation fields for Switzerland since 1763 (Chapt. 2). For Europe, several short reconstructions have been performed around the 1780s and in 1807 using the ARM (e.g. Pappert et al., 2022). Different events have been downscaled with WRF relying on reanalyses as boundary conditions. The 20CRv3 reanalysis itself is a valuable source for studying the daily weather between 1806 and 2015. Further, there are long observational series at various locations in Europe. As an example, the Swiss Plateau series based on early instrumental data from Bern and Zurich covers together with the data from the Swiss weather service a period from 1756 to present. Lastly, daily weather types have been reconstructed by Schwander et al. (2017) since 1763 and allow the study of synoptic conditions over Europe.

In this thesis, these data sets are used to study different historical extreme events, such as the cold and wet summer of 1770, the cold spring of 1785, and the warm summer of 1947 (marked as grey bars in Fig. 1.2). The data sets also allow other applications, such as phenological modeling, which will be introduced in the next section.
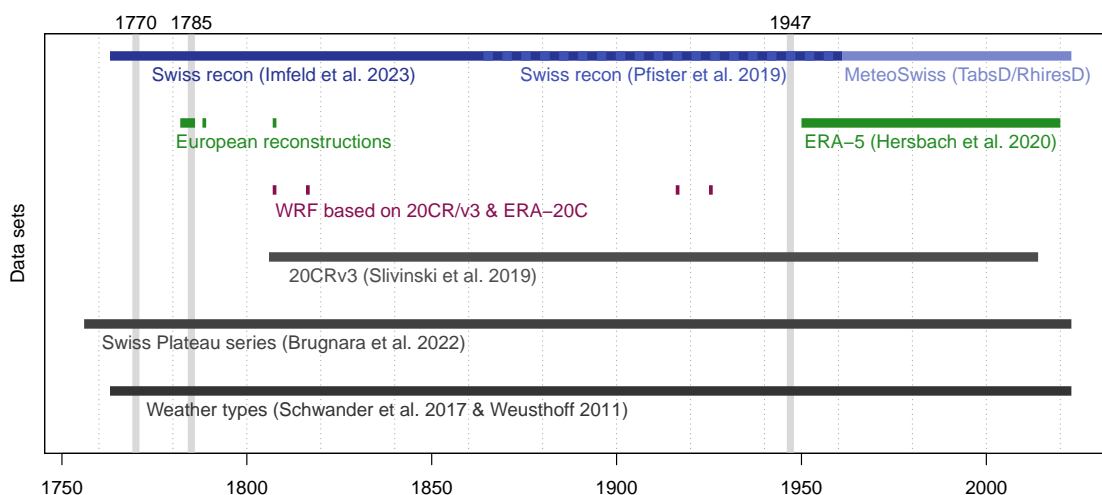
Figure 1.2: Overview of available historical daily data sets between the mid-18th century and present. Each data set consists of different variables. For WRF, examples of downscale events are shown, but the examples are not exclusive. Grey bars denote events that have been studied in this thesis.

1.4 Phenological applications to study weather impacts

Meteorological variables are one of the main drivers of vegetation growth. Cold weather delays crop growth, frost can destroy plant tissues, and droughts wither species. To study the impacts of weather on vegetation, we can study the phenological stages of different plants, i.e., when their bud bursts, when they flower, or when leaves unfold. Already in

the 18th century, Réaumur (1735) proposed the simple growing degree days model to model phenology. This model is still applied today though in modified versions. The growing degree day model assumes that the occurrence of phenological phases is proportional to the summation of daily temperatures (Fu et al., 2020). A variety of process-oriented models have been used to study the onset of phenological phases (e.g. Basler, 2016; Hufkens et al., 2018; Meier and Bigler, 2023), differing in the functions describing the temperature accumulation or by considering the daylength through a photoperiod term. Phenological models need to be parameterized using observations. However, finding the optimal parameters is not straightforward because the parameters are often intercorrelated and local minima of the model functions make it more difficult to find the optimal parameters. Generalized simulated annealing has been used for many years for optimization of the models since it is straightforward to implement (Meier et al., 2018; Hufkens et al., 2018; Basler, 2016). However, Bayesian optimization algorithms have grown in popularity due to their ability to estimate parameter uncertainty and assess model convergence, for example when a model oscillates between local minima (Meier and Bigler, 2023; Fu et al., 2012).

Studying phenological phases based on historical weather data is, therefore, a simple way to study the impacts of weather on e.g. vegetation since it does not involve running complex models. Furthermore, reports on phenological phases are often found in historical sources (e.g. Pfister et al., 2017) providing a suitable basis for comparison. In this thesis, we apply phenological models to gain an idea of how the weather conditions in late winter and spring affected the onset of phenological phases.

1.5 Outline and objectives of the thesis

The main objective of this thesis is to create a daily gridded data set of temperature and precipitation for Switzerland that covers the period 1763 to 2020 and to evaluate decadal variability in Swiss weather and historical extreme events based on this data set. The thesis is structured into three main Chapters (2 to 4), Conclusions and Outlook in Chapter 5, and an Appendix A.

In Chapter 2 the development of a 258-year-long data set of temperature and precipitation for Switzerland since 1763 is described. This includes the input data used for the reconstruction, the different development steps, the skill analyses, and a case study of a wet and cold summer in Switzerland in 1770. With the development of the data set, several questions can be tackled:

- Can we consistently reconstruct temperature and precipitation fields back to 1763 based on the available observational data?

- What are the skills of the reconstruction method for the early period when very few

observations are available?

- Can we improve the precipitation reconstruction by using information on precipitation occurrence?

Further, we used the data set to calculate climate indices and phenological phases to study spring weather and climate across 258 years, which is described in Chapter 3. Spring weather is relevant because, e.g. cold spells in spring can have a significant impact on vegetation growth and delay vegetation onset. In this Chapter, we addressed the following questions:

- How did climate and phenological indices change over the 258-year-long period?

- What extreme cases of spring weather have happened in the past, and how are they represented in climate indices and phenological phases of our reconstruction

- Can we confirm these extreme cases of spring with historical sources?

During the writing of this thesis in 2022, a historical extreme event, the hot and dry summer of 1947, had its 75th anniversary. This summer had been the warmest summer for many years and remains the driest summer in certain regions of Switzerland, acting as a harbinger of the more recent hot and dry summers. For this occasion, we created a booklet and a movie about the causes and impacts of hot and dry summers in Switzerland, with a specific focus on the summers of 1947, 2003, and 2018. As an addendum, we also wrote a summary about the summer of 2022 placing it into context with past and future summers (Imfeld et al., 2022a,b). A part of this booklet is presented in Chapter 4, Sections 4.3 and 4.4, including a contextualization of the summer of 1947 in the 258-year-long Swiss reconstructions and the Swiss series of Bern and Zurich (Sect. 4.2). The booklet aims at a general audience from different fields of research, and, thus, does not answer specific research questions.

We highlight the Conclusions of the thesis and present further research questions based on the results of this thesis in Chapter 5. In the Appendix A, we present an article on the reconstruction of sea level pressure and temperature fields for the cold winter of 1788/89 based on the analog method, for which I contributed as a co-author (Pappert et al., 2022).

Bibliography

Basler, D.: Evaluating phenological models for the prediction of leaf-out dates in six temperate tree species across central Europe, Agricultural and Forest Meteorology, 217, 10–21, doi:10.1016/j.agrformet.2015.11.007, 2016.

Begert, M., Schlegel, T., and Kirchhofer, W.: Homogeneous temperature and precipitation series of Switzerland from 1864 to 2000, International Journal of Climatology, 25, 65–80, doi:10.1002/joc.1118, 2005.

Bider, M., Schüepp, M., and von Rudloff, H.: Die Reduktion der 200jährigen Basler Temperaturreihe, Archiv für Meteorologie, Geophysik und Bioklimatologie, Serie B, 9, 360–412, doi:10.1007/BF02243047, 1958.

Böhm, R., Jones, P. D., Hiebl, J., Frank, D., Brunetti, M., and Maugeri, M.: The early instrumental warm-bias: a solution for long central European temperature series 1760–2007, Climatic Change, 101, 41–67, doi:10.1007/s10584-009-9649-4, 2010.

Brönnimann, S.: From climate to weather reconstructions, PLOS Climate, 1, e0000 034, doi:10.1371/journal.pclm.0000034, 2022.

Brugnara, Y., Brönnimann, S., Zamuriano Carbajal, J. M., Schild, J., Rohr, C., and Segesser, D.: Reanalysis sheds lights on 1916 avalanche disaster, ECMWF Newsletter, pp. 28–34, doi:10.21957/h9b197, 2017.

Brugnara, Y., Pfister, L., Villiger, L., Rohr, C., Isotta, F. A., and Brönnimann, S.: Early instrumental meteorological observations in Switzerland: 1708–1873, Earth System Science Data, 12, 1179–1190, doi:10.5194/essd-12-1179-2020, 2020.

Brönnimann, S.: Historical Observations for Improving Reanalyses, Frontiers in Climate, 4, doi:10.3389/fclim.2022.880473, 2022.

Brönnimann, S., Martius, O., Rohr, C., Bresch, D. N., and Lin, K.-H. E.: Historical weather data for climate risk assessmenty, Annals of the New York Academy of Sciences, 1436, 121–137, doi:10.1111/nyas.13966, 2019.

Caillouet, L., Vidal, J.-P., Sauquet, E., Graff, B., and Soubeyroux, J.-M.: SCOPE Climate: a 142-year daily high-resolution ensemble meteorological reconstruction dataset over France, Earth System Science Data, 11, 241–260, doi:10.5194/essd-11-241-2019, 2019.

Casty, C., Wanner, H., Luterbacher, J., Esper, J., and Böhm, R.: Temperature and precipitation variability in the European Alps since 1500, International Journal of Climatology, 25, 1855–1880, doi:10.1002/joc.1216, 2005.

Collet, D.: Die doppelte Katastrophe: Klima und Kultur in der europäischen Hungerkrise 1770–1772., vol. 18 of *Umwelt und Gesellschaft*, Vandenhoeck & Ruprecht, doi:10.13109/9783666355929, 2018.

Devers, A., Vidal, J.-P., Lauvernet, C., and Vannier, O.: FYRE Climate: a high-resolution reanalysis of daily precipitation and temperature in France from 1871 to 2012, Climate of the Past, 17, 1857–1879, doi:10.5194/cp-17-1857-2021, 2021.

Flückiger, S., Brönnimann, S., Holzkämper, A., Fuhrer, J., Krämer, D., Pfister, C., and Rohr, C.: Simulating crop yield losses in Switzerland for historical and present Tambora climate scenarios, Environmental Research Letters, 12, 074 026, doi:10.1088/1748-9326/aa7246, 2017.

Franke, J., González-Rouco, J. F., Frank, D., and Graham, N. E.: 200 years of European temperature variability: insights from and tests of the proxy surrogate reconstruction analog method, Climate Dynamics, 37, 133–150, doi:10.1007/s00382-010-0802-6, 2011.

Fu, Y., Li, X., Zhou, X., Geng, X., Guo, Y., and Zhang, Y.: Progress in plant phenology modeling under global climate change, Science China Earth Sciences, 63, 1237–1247, doi:10.1007/s11430-019-9622-2, 2020.

Fu, Y. H., Campioli, M., Demarée, G., Deckmyn, A., Hamdi, R., Janssens, I. A., and Deckmyn, G.: Bayesian calibration of the Unified budburst model in six temperate tree species, International journal of biometeorology, 56, 153–164, doi:10.1007/s00484-011-0408-7, 2012.

Gómez-Navarro, J. J., Zorita, E., Raible, C. C., and Neukom, R.: Pseudo-proxy tests of the analogue method to reconstruct spatially resolved global temperature during the Common Era, Climate of the Past, 13, 629–648, doi:10.5194/cp-13-629-2017, 2017.

Hawkins, E., Brohan, P., Burgess, S. N., Burt, S., Compo, G. P., Gray, S. L., Haigh, I. D., Hersbach, H., Kuijjer, K., Martínez-Alvarado, O., McColl, C., Schurer, A. P., Slivinski, L., and Williams, J.: Rescuing historical weather observations improves quantification of severe windstorm risks, Natural Hazards and Earth System Sciences, 23, 1465–1482, doi:10.5194/nhess-23-1465-2023, 2023.

Hersbach, H., Bell, B., Berrisford, P., Hirahara, S., Horányi, A., Muñoz-Sabater, J., Nicolas, J., Peubey, C., Radu, R., Schepers, D., et al.: The ERA5 global reanalysis, Quarterly Journal of the Royal Meteorological Society, 146, 1999–2049, doi:10.1002/qj.3803, 2020.

Hufkens, K., Basler, D., Milliman, T., Melaas, E. K., and Richardson, A. D.: An integrated phenology modelling framework in r, Methods in Ecology and Evolution, 9, 1276–1285, doi:10.1111/2041-210X.12970, 2018.

Hupfer, F.: Das Wetter der Nation: Meteorologie, Klimatologie und der schweizerische Bundesstaat, 1860–1914, Chronos Verlag, 2019.

Imfeld, N., Stucki, P., Brönnimann, S., Bader, S., Bürgi, M., Calanca, P., Gubler, S., Holzkämper, A., Hövel, L. B., Isotta, F. A., et al.: Hot and dry summers in Switzerland. Causes and impacts of the record summers 1947, 2003, and 2018, doi:10.4480/GB2022.G98.03, 2022a.

Imfeld, N., Stucki, P., Brönnimann, S., Bürgi, M., Calanca, P., Holzkämper, A., Isotta, F. A., Nussbaumer, S., Scherrer, S. C., Staub, K., et al.: 2022: Ein ziemlich normaler zukünftiger Sommer, doi:10.4480/GB2022.G100, 2022b.

Jaume-Santero, F., Barriopedro, D., García-Herrera, R., and Luterbacher, J.: Monthly North Atlantic Sea level pressure reconstruction back to 1750 CE using artificial intelligence optimization, Journal of Climate, 35, 3395–3410, doi:10.1175/JCLI-D-21-0155.1, 2022.

Keller, V., Tanguy, M., Prosdocimi, I., Terry, J., Hitt, O., Cole, S., Fry, M., Morris, D., and Dixon, H.: CEH-GEAR: 1 km resolution daily and monthly areal rainfall estimates for the UK for hydrological and other applications, Earth System Science Data, 7, 143–155, doi:10.5194/essd-7-143-2015, 2015.

Kington, J.: The Weather of the 1780s Over Europe, Cambridge University Press, doi:10.1017/CBO9780511735721, 1988.

Koenigseder, S., Barrows, T., Fisher, J., Evans, J., and MacColl, C.: Performance evaluation of 20CRv3 downscaling using WRF over southern Alaska with focus on temperature and precipitation in glaciated areas, Tech. rep., doi:10.5194/egusphere-egu23-10585, 2023.

Ljungqvist, F. C., Seim, A., Krusic, P. J., González-Rouco, J. F., Werner, J. P., Cook, E. R., Zorita, E., Luterbacher, J., Xoplaki, E., Destouni, G., García-Bustamante, E., Aguilar, C. A. M., Seftigen, K., Wang, J., Gagen, M. H., Esper, J., Solomina, O., Fleitmann, D., and Büntgen, U.: European warm-season temperature and hydroclimate since 850 CE, Environmental Research Letters, 14, 084 015, doi:10.1088/1748-9326/ab2c7e, 2019.

Luterbacher, J., Dietrich, D., Xoplaki, E., Grosjean, M., and Wanner, H.: European Seasonal and Annual Temperature Variability, Trends, and Extremes Since 1500, Science, 303, 1499–1503, doi:10.1126/science.1093877, 2004.

Meier, M. and Bigler, C.: Process-oriented models of autumn leaf phenology: ways to sound calibration and implications of uncertain projections, EGUsphere, 2023, 1–43, doi:10.5194/egusphere-2022-1423, 2023.

Meier, M., Fuhrer, J., and Holzkämper, A.: Changing risk of spring frost damage in grapevines due to climate change? A case study in the Swiss Rhone Valley, International journal of biometeorology, 62, 991–1002, doi:10.1007/s00484-018-1501-y, 2018.

Meyer, E. M. I., Weisse, R., Grabemann, I., Tinz, B., and Scholz, R.: Reconstruction of wind and surge of the 1906 storm tide at the German North Sea coast, Natural Hazards and Earth System Sciences, 22, 2419–2432, doi:10.5194/nhess-22-2419-2022, 2022.

Miralles, O., Steinfeld, D., Martius, O., and Davison, A. C.: Downscaling of Historical Wind Fields over Switzerland Using Generative Adversarial Networks, Artificial Intelligence for the Earth Systems, 1, e220 018, doi:10.1175/AIES-D-22-0018.1, 2022.

Pappert, D., Brugnara, Y., Jourdain, S., Pospieszyńska, A., Przybylak, R., Rohr, C., and Brönnimann, S.: Unlocking weather observations from the Societas Meteorologica Palatina (1781–1792), Climate of the Past, 17, 2361–2379, doi:10.5194/cp-17-2361-2021, 2021.

Pappert, D., Barriendos, M., Brugnara, Y., Imfeld, N., Jourdain, S., Przybylak, R., Rohr, C., and Brönnimann, S.: Statistical reconstruction of daily temperature and sea-level pressure in Europe for the severe winter 1788/9, Climate of the Past Discussions, pp. 1–35, 2022.

Pauling, A., Luterbacher, J., Casty, C., and Wanner, H.: Five hundred years of gridded high-resolution precipitation reconstructions over Europe and the connection to large-scale circulation, Climate Dynamics, 26, 387–405, doi:10.1007/s00382-005-0090-8, 2006.

Pfister, C., Rohr, C., and Jover, A. C. C.: Euro-Climhist: eine Datenplattform der Universität Bern zur Witterungs-, Klima-und Katastrophengeschichte, Wasser Energie Luft, 109, doi:10.7892/boris.97013, 2017.

Pfister, L., Hupfer, F., Brugnara, Y., Munz, L., Villiger, L., Meyer, L., Schwander, M., Isotta, F. A., Rohr, C., and Brönnimann, S.: Early instrumental meteorological measurements in Switzerland, Climate of the Past, 15, 1345–1361, doi:10.5194/cp-15-1345-2019, 2019.

Pfister, L., Brönnimann, S., Schwander, M., Isotta, F. A., Horton, P., and Rohr, C.: Statistical reconstruction of daily precipitation and temperature fields in Switzerland back to 1864, Climate of the Past, 16, 663–678, doi:10.5194/cp-16-663-2020, 2020.

Rayner, N. A., Auchmann, R., Bessembinder, J., Brönnimann, S., Brugnara, Y., Capponi, F., Carrea, L., Dodd, E. M., Ghent, D., Good, E., et al.: The EUSTACE project: delivering global, daily information on surface air temperature, Bulletin of the American Meteorological Society, 101, E1924–E1947, doi:10.1175/BAMS-D-19-0095.1, 2020.

Réaumur, R.: Observations du thermomètre faites à Paris pendant l'année 1735, comparées avec celles qui ont été faites sous la ligne, à l'Isle de France, à Alger et quelques unes de nos iles de l'Amérique, Mémoires l'Académie R des Sci, pp. 545–576, 1735.

Rössler, O. and Brönnimann, S.: The effect of the Tambora eruption on Swiss flood generation in 1816/1817, Science of The Total Environment, 627, 1218–1227, doi:https://doi.org/10.1016/j.scitotenv.2018.01.254, 2018.

Schwander, M., Brönnimann, S., Delaygue, G., Rohrer, M., Auchmann, R., and Brugnara, Y.: Reconstruction of Central European daily weather types back to 1763, International Journal of Climatology, 37, 30–44, doi:10.1002/joc.4974, 2017.

Slivinski, L. C., Compo, G. P., Whitaker, J. S., Sardeshmukh, P. D., Giese, B. S., McColl, C., Allan, R., Yin, X., Vose, R., Titchner, H., et al.: Towards a more reliable historical reanalysis: Improvements for version 3 of the Twentieth Century Reanalysis system, Quarterly Journal of the Royal Meteorological Society, 145, 2876–2908, doi:10.1002/qj.3598, 2019.

Slivinski, L. C., Compo, G. P., Sardeshmukh, P. D., Whitaker, J., McColl, C., Allan, R., Brohan, P., Yin, X., Smith, C., Spencer, L., , Vose, R. S., Rohrer, M., Conroy, R. P., Schuster, D. C., Kennedy, J. J., Ashcroft, L., Brönnimann, S., Brunet, M., Camuffo, D., Cornes, R., Cram, T. A., Domínguez-Castro, F., Freeman, J. E., Gergis, J., Hawkins, E., Jones, P. D., Kubota, H., Lee, T. C., Lorrey, A. M., Luterbacher, J., Mock, C. J., Przybylak, R. K., Pudmenzky, C., Slonosky, V. C., Tinz, B., Trewin, B., Wang, X. L., Wilkinson, C., Wood, K., and Wyszyński, P.: An evaluation of the performance of the twentieth century reanalysis version 3, Journal of Climate, 34, 1417–1438, doi:10.1175/JCLI-D-20-0505.1, 2021.

Stucki, P., Brönnimann, S., Martius, O., Welker, C., Rickli, R., Dierer, S., Bresch, D. N., Compo, G. P., and Sardeshmukh, P. D.: Dynamical downscaling and loss modeling for the reconstruction of historical weather extremes and their impacts: a severe Foehn storm in 1925, Bulletin of the American Meteorological Society, 96, 1233–1241, doi:10.1175/BAMS-D-14-00041.1, 2015.

Stucki, P., Pfister, L., Brugnara, Y., Auchmann Varga, R., Martynov, A., Hari, C., and Bönnimann, S.: Dynamical downscaling and regional data assimilation for a cold-air

outbreak in the European Alps during the Year Without Summer 1816, Climate of the Past, in preparation.

Thordarson, T. and Self, S.: Atmospheric and environmental effects of the 1783–1784 Laki eruption: A review and reassessment, Journal of Geophysical Research: Atmospheres, 108, AAC 7–1–AAC 7–29, doi:10.1029/2001JD002042, 2003.

Valler, V., Franke, J., Brugnara, Y., and Brönnimann, S.: An updated global atmospheric paleo-reanalysis covering the last 400 years, Geoscience Data Journal, p. 89–107, doi:10.1002/gdj3.121, 2022.

Wallis, E., Osborn, T., and Taylor, M.: Estimating exposure biases in early instrumental land surface temperature data, Tech. rep., EGU23-8119, Copernicus Meetings, 2023.

Wegmann, M. and Jaume-Santero, F.: Artificial intelligence achieves easy-to-adapt nonlinear global temperature reconstructions using minimal local data, Communications earth & environment, 4, 217, doi:10.1038/s43247-023-00872-9, 2023.

Yule, E. L., Hegerl, G., Schurer, A., and Hawkins, E.: Using early extremes to place the 2022 UK heat waves into historical context, Atmospheric Science Letters, 24, e1159, doi:10.1002/asl.1159, 2023.

Zorita, E. and von Storch, H.: The Analog Method as a Simple Statistical Downscaling Technique: Comparison with More Complicated Methods, Journal of Climate, 12, 2474 – 2489, doi:10.1175/1520-0442(1999)012<2474:TAMAAS>2.0.CO;2, 1999.

Chapter 2

A 258-year-long data set of temperature and precipitation fields for Switzerland since 1763

Noemi Imfeld[1,2], Lucas Pfister[1,2], Yuri Brugnara[1,2], and Stefan Brönnimann[1,2]

1. Oeschger Center for Climate Change Research, University of Bern, Switzerland.
2. Institute of Geography, University of Bern, Switzerland.

Abstract

Climate reconstructions give insights in monthly and seasonal climate variability in the past few hundred years. However, for understanding past extreme weather events and for relating them to impacts, for example through crop yield simulations or hydrological modelling, reconstructions on a weather timescale are needed. Here, we present a data set of 258 years of daily temperature and precipitation fields for Switzerland from 1763 to 2020. The data set was reconstructed with the analogue resampling method, which resamples meteorological fields for a historical period based on the most similar day in a reference period. These fields are subsequently improved with data assimilation for temperature and bias correction for precipitation. Even for an early period prior to 1800 with scarce data availability, we found good validation results for the temperature reconstruction especially in the Swiss Plateau. For the precipitation reconstruction, skills are considerably lower, which can be related to the few precipitation measurements available and the heterogeneous nature of precipitation. By means of a case study of the wet and cold years from 1769 to 1772, which triggered widespread famine across Europe, we show that this data set allows more detailed analyses than hitherto possible.

2.1 Introduction

Reconstructions of atmospheric variables on monthly, seasonal, and annual timescales have allowed the study of climate variability in the past few hundred years and helped to gain relevant insights into long-term changes and variability (e.g. Luterbacher et al., 2004; Casty et al., 2005, 2007; Dobrovolnỳ et al., 2010; Murphy et al., 2020; Valler et al., 2022). However, for various applications, such as assessing climate impacts, rather than the monthly or seasonal variability, daily weather is more relevant (Brönnimann, 2022). Temperature and precipitation fields on a daily timescale for past extreme events allow us to conduct impact modelling, for example of crop yields (Flückiger et al., 2017), phenological stages of specific species (Rutishauser et al., 2020), runoff (Rössler and Brönnimann, 2018), and avalanche disposition (Brugnara et al., 2017; Pfister et al., 2020). Numerous historical sources report past extreme weather events with severe impacts on society (e.g. Pfister and Wanner, 2021) that could be better understood using daily weather fields. One example that will be followed up in this article are the wet and cold anomalies in the late 18th century in Europe that led to widespread famine (Collet, 2018).

In Europe, efforts have been undertaken to reconstruct meteorological fields dating back to the 19th century. For example, Devers et al. (2021) created a high-resolution reanalysis covering France for the period of 1870 to 2012. They assimilated daily temperature and precipitation observations into the SCOPE climate reconstruction (Caillouet et al., 2019) using an offline ensemble Kalman filter. When sufficient data are available, fields can be reconstructed based on interpolation methods such as for the UK for daily precipitation fields dating back to 1890 (Keller et al., 2015). Single weather events have been reconstructed by resampling present-day meteorological fields (Pappert et al., 2022; Flückiger et al., 2017) and by dynamically downscaling historical reanalysis data (e.g. Stucki et al., 2015; Brugnara et al., 2017). Both reconstruction methods yielded insights into the evolution and spatial extent of these past weather and climate events. Also, the use of documentary sources from weather diaries has been explored for reconstructing past weather with different approaches (Harvey-Fishenden and Macdonald, 2021; Wang et al., 2021). For Switzerland, Pfister et al. (2020) reconstructed daily temperature and precipitation fields for 1864 to 2017 based on the analogue resampling method (ARM). This method resamples meteorological fields for a historical period based on the most similar day in a reference period. Subsequently, temperature measurements were assimilated onto the temperature fields and quantile mapping was applied to correct for biases in the precipitation fields. Both variables showed a very good reconstruction performance as illustrated by a case study on the avalanche winter of 1887/88 (Pfister et al., 2020). The analogue method has been widely used in climate and weather reconstruction (e.g. Schenk and Zorita, 2012; Gómez-Navarro et al., 2017) with considerable skill.

Weather recording peaked for the first time as early as around the late 18th century (Brönnimann et al., 2019). However, only a few attempts have been made to reconstruct weather back to this time using quantitative data (e.g. Pappert et al., 2022). For this period, only a few data records have so far been available because it is a tremendous amount of work to find, image, digitize, quality check, and homogenize these data. For Switzerland, recent data rescue projects made available a unique set of historical instrumental data before 1864, the so-called early instrumental data (Brugnara et al., 2020b; Pfister et al., 2019). These data make it possible to reconstruct temperature and precipitation fields for Switzerland back to the mid-18th century.

Here, we present a new data set of daily temperature and precipitation fields for Switzerland with a higher resolution spanning 258 years. It consists of two subsets: (1) a new reconstruction from 1763 to 1863 described in this article and (2) an update of the reconstruction by Pfister et al. (2020) with a higher resolution of 1 km and spanning 1864 to 2020. Reconstructions were made with the analogue resampling method and subsequent data assimilation for temperature and bias correction for precipitation. This data set allows further applications to other fields, such as environmental impact studies and crop yield modelling.

During the years 1769 to 1772, Europe suffered from one of the most severe famines of the Little Ice Age (Collet, 2018; Pfister and Brázdil, 2006), which has been related to a cultural crisis and a climatic wet-cold anomaly. We use this event to exemplarily calculate climate indices that had an impact on crop growth in Switzerland and to compare these to documentary data describing the event (Collet, 2018; Pfister and Brázdil, 2006).

The paper is structured as follows. Section 2 describes the data needed for the reconstruction. Section 3 describes the reconstruction method and how we evaluate the reconstruction skill. Section 4 shows and discusses these evaluation results and in Sect. 5 we showcase the use of the reconstruction based on a case study. The conclusion is found in Sect. 6. The data set is available online in PANGAEA (https://doi.pangaea.de/10.1594/PANGAEA.950236) (Imfeld et al., 2022).

2.2 Data

2.2.1 Historical instrumental data

Systematic measurements of meteorological data in Switzerland only started in the 1860s with the establishment of the national weather service (Hupfer, 2019; Begert et al., 2005). To reconstruct weather in the late 18th and early 19th century we, therefore, relied on data that have been rescued by various initiatives (Brugnara et al., 2020b; Pfister et al.,

2019; Camuffo and Jones, 2002; Klein Tank et al., 2002; Füllemann et al., 2011; Brugnara et al., 2022). Such early instrumental data are challenging to work with because common measurement standards had not yet been developed when the observations were recorded. Difficulties with early instrumental data arise for example from the construction of the ancient measurement devices, unknown measurement devices and liquids, inappropriate location of the devices, exposure to radiation, and missing or ambiguous observation times (Brugnara et al., 2020b). For early temperature measurements, for example, unstable glasses contracting with age, differences in the expansion rate of the liquids in the glass, and exposure to radiation or precipitation can create errors in the measurements (Brugnara et al., 2020b; Winkler, 2006; Böhm et al., 2010). It was already recognized in the 18th century that a thermometer needs to be sheltered from solar radiation (Pfister, 1988). However, even thermometers placed on north-facing walls, as was common after 1760, were still influenced by radiation (Böhm et al., 2010) and often showed warm biases. Sources of errors for pressure measurements include device-related issues (Brugnara et al., 2020a) but also the required temperature corrections due to the thermal expansion of the liquid in the barometers. Temperature corrections can introduce errors in pressure measurements when no attached thermometer is available, when temperature measurements are not representative of the barometer, or when the corrections applied are unclear. The manual measurements in our network were taken between two and eight times per day. Calculating an arithmetic daily mean for temperature and pressure based on only a few measurements a day or on varying measurement times introduces biases in daily means. Also, observation times of early instrumental data can be ambiguous, for example when the time is denoted as "morning" or "evening", and it is therefore not straightforward to include these in a daily mean estimation. These above-described examples affect the quality of the measurements used for the reconstruction, and corrections are often difficult. The quality of early instrumental data thus has to be kept in mind when working with the reconstruction.

For the reconstruction from 1763 to 1863, we selected time series that showed sufficient data quality (Brönnimann, 2020) and that cover at least 7 continuous years to keep the reconstruction as spatially and temporally consistent as possible. However, the network changes considerably throughout time (Fig. 2.1), and coverage is much sparser compared to the network after 1864, which has been used for the reconstruction from 1864 to 2020 in Pfister et al. (2020) (Fig. 2.1d and e). At the start of the reconstruction period in 1763, around 11 to 12 series are available (Fig. 2.1a), which then increases to around 30 series (Fig. 2.1c). To increase the number of observations for this early period we also used time series from nearby locations in Italy and Germany. In total, the reconstruction is based on 17 pressure series, 18 temperature series, and 6 precipitation and precipitation occurrence series. Because only very few precipitation measurements were available, we also include

precipitation occurrence as a variable that has been derived from weather notes. Figure 2.1f shows the evolution of monthly data availability, and Table 2.1 lists all time series used for the reconstruction period 1763 to 1863.

Most of the instrumental data for the reconstruction were already available in modern units, and their quality was checked on a subdaily basis (for details, see Brugnara et al., 2020b). The data preparation necessary thus included the calculation of daily mean values, pressure reduction where not available, additional quality control on daily means and the homogenization of the time series.

To adjust the daily mean value based on only a few subdaily measurements, we subtracted a correction according to the historical measurement times. These corrections were calculated for every month of the year separately based on the anomalies of the 10 min monthly means from automatic weather stations for the period 1981 to 2010. If no weather stations were available in the surrounding area, the corrections were calculated from the hourly 2 m temperature of the closest grid point from ERA5-Land (Muñoz-Sabater et al., 2021) of 1981 to 2010. The anomalies were calculated by subtracting the daily mean of each month from the 10 min measurements. The final correction value was obtained by taking the mean of the anomalies according to the closest measurement times. For pressure, the daily mean correction was applied for all time series using the closest grid point from hourly ERA5-Land surface pressure data for 1981 to 2010. If no observation times were available, we tried to estimate the observation times by comparing the subdaily values to the daily cycle derived from present-day measurements, which, however, can introduce additional errors. For three time series, a temperature reduction in pressure was not conducted because no attached temperature measurements have been found. Therefore, we reduced the pressure to 0° C based on the climatology of daily mean temperature data for the period of 1850 to 1900 from the reanalysis 20CRv3 (Slivinski et al., 2019; Brugnara et al., 2020b). For subdaily weather notes, every day containing at least one precipitation event was transformed into a precipitation day. We did not convert descriptions such as dew and rime to precipitation, because they were not available for all stations.

Further, we performed a standard quality control on the daily means of each time series as implemented in Brugnara et al. (2019) and a spatial quality control using linear regression between the nearby five stations (Estévez et al., 2018). Together with the standard quality control, we flagged between 0 to 1.16 % of the values (with a mean of 0.12 %) depending on the time series. For precipitation occurrence, we calculated the monthly wet-day frequency for the series and excluded series that substantially deviated from other series or that showed substantial visual breaks.

We homogenized the quality-controlled series using surface temperature, and pressure from the closest grid point of the EKF400v2 reanalysis (Valler et al., 2022) as a reference series

(see Sect. 2.4). Break point detection was performed with the penalized maximal t test (Wang et al., 2007) and the penalized maximal F test (Wang, 2008), which are implemented in Wang and Feng (2013). Only break points that were significant without metadata were considered since only very few metadata are available. For Bern, Zurich, Basel, and Geneva homogenized series were used which are based on various short series (Brugnara et al., 2022; Brugnara, 2022).

As an independent evaluation of our reconstruction, we used seven temperature time series and one time series of precipitation occurrence during 1763 and 1863 (see asterisks in Fig. 2.1a and Table 2.2). The temperature time series were prepared following the same approach as for the series used in the reconstruction itself, but no homogenization was performed.
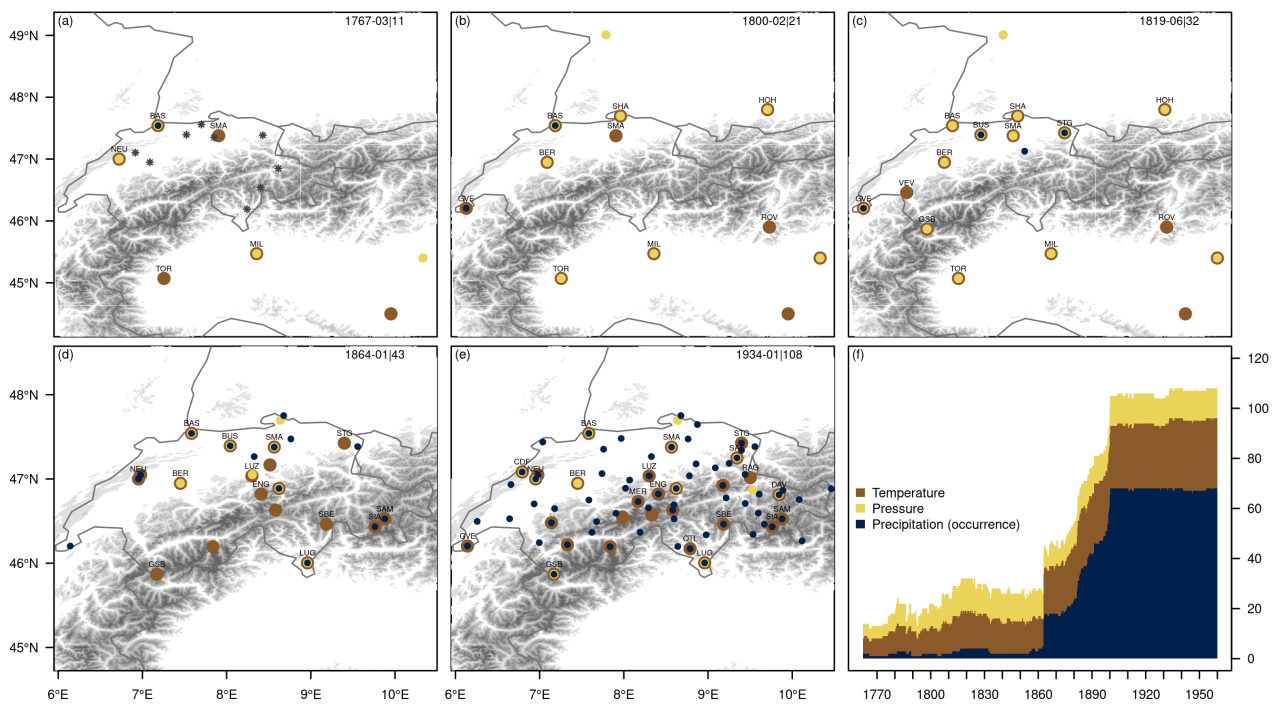
Figure 2.1: a-e) Station measurements as they are available for five different months from 1763 to 1960. The upper right numbers denote the example month and the total number of measurements for this time step. Labeled stations are used in the ensemble Kalman fitting. d and e) show the networks as used in Pfister et al. (2020). Asterisks in (a) denote locations of independent measurements, which are used for an evaluation of the reconstruction. f) Evolution of temperature, pressure, and precipitation measurements throughout the entire period. Precipitation includes precipitation occurrence and precipitation measurements.

Table 2.1: *Stations used for the reconstruction of the 1763 to 1863 period. The letters for the variables are as follows: p - pressure; ta - air temperature; rr - precipitation rate; rr0 - precipitation occurrence. A description of the CHIMES data set and where it is available is found in Brugnara et al. (2020b). If additional evaluations of the station exist, the respective reference is noted in the column "Hist. sources". For the reference data, MCH denotes station observations from the Swiss National Weather Service. For further abbreviations refer to Sect. 2.2.*

ID	Station	Country	Long	Lat	Altitude m a.s.l.	Variable	Hist. period	Hist. source	Ref. source
BAS	Basel	CH	7.588	47.558	253	p,ta,rr0	1763-1863	CHIMES Brönnimann and Brugnara (2020a; 2021)	MCH
BER	Bern	CH	7.452	46.948	554	p,ta,rr	1763-1863	CHIMES Brugnara et al. (2022)	MCH
BOL	Bologna	IT	11.353	44.497	-	ta	1763-1863	PALAEO-RA/ECA&D	EOBS
BUS	Aarau	CH	8.043	47.393	384	p,ta,rr0	1807-1863	CHIMES	TabsD, RhiresD MeteoSwiss (2021b,a)
ENS	Einsiedeln	CH	8.752	47.127	906	rr0	1817-1858	CHIMES Faden et al. (2020)	RhiresD MeteoSwiss (2021a)
FON	Fontaines	CH	6.900	47.044	767	ta	1843-1862	CHIMES	TabsD MeteoSwiss (2021b)
GOT	Gotthard	CH	8.568	46.555	2093	p,ta	1781-1792	CHIMES Brönnimann and Brugnara (2020a)	MCH
GSB	Gst Bernhard	CH	8.568	46.555	2093	p,ta	1817-1863	CHIMES Brönnimann and Brugnara (2020b)	MCH
GVE	Geneva	CH	6.143	46.204	411	p,ta,rr	1782-1863	CHIMES/Digihom Häderli et al. (2020) Brönnimann et al. (2020)	MCH
HOH	Hohen-peissenberg	D	11.020	47.800	995	p,ta	1781-1863	Deutscher Wetterdienst Winkler (2006)	Deutscher Wetterdienst Winkler (2006)
KAR	Karlsruhe	D	8.404	49.008	122	p	1778-1863	Palaeo-RA	ECA&D

LUZ	Lucerne	CH	8.404	49.008	122	p	1826-1832	CHIMES, Brönnimann and Brugnara (2022)	MCH
MIL	Milano	IT	9.180	45.470	132	p,ta	1763-1863	Improve	EOBS
NEU	Neuenburg	CH	6.930	46.991	434	p,ta	1763-1782	CHIMES Wyer et al. (2021)	MCH
PAD	Padua	IT	11.870	45.400	31	p,ta	1766-1863	PALAEO-RA	ECA&D
ROV	Rovereto	IT	11.050	45.900	200	ta	1800-1839	PALAEO-RA	EOBS
SHA	Schaffhausen	CH	8.639	47.696	400	p,ta	1794-1845	CHIMES	MCH
SMA	Zurich	CH	8.538	47.370	410	p,ta	1763-1863	CHIMES Brugnara et al. (2022)	MCH
STG	St.Gallen	CH	9.379	47.425	676	p,ta,rr0	1813-1853	CHIMES Hürzeler et al. (2020)	MCH
TOR	Torino	IT	7.680	45.070	281	p,ta	1763-1863	Improve	EOBS (p), ECA&D (ta)
VEV	Vevey	CH	6.844	46.460	378	ta	1805-1840	CHIMES, Brönnimann and Brugnara 2022	TabsD MeteoSwiss (2021b)
ZUG	Zug	CH	8.515	47.166	424	ta	1843-1863	CHIMES, Brönnimann and Brugnara 2022	TabsD MeteoSwiss (2021b)

Table 2.2: Stations used for independent evaluation of the 1763 to 1863 period from CHIMES. A description of the CHIMES data set and where it is available is found in Brugnara et al. (2020b). If additional evaluation of the station exists, the respective reference is noted under "Hist. sources".

CHIMES ID	Station	Country	Long	Lat	Altitude (m a.s.l.)	Variable	Hist. period	Hist. source
BE01_Bern_Studer	Bern	CH	7.452	46.948	534	rr0	1807-1818	CHIMES, Hari et al. (2022)
AG01_Aarau_Bronner	Aarau	CH	8.043	47.393	384	ta	1857-1865	CHIMES, Faden et al. (2020)
AG02_Tegerfelden	Aarau	CH	8.285	47.559	364	ta	1843-1853	CHIMES
AR01_Herisau_Merz	Herisau	CH	9.279	47.385	770	ta	1821-1831	CHIMES, Weber et al. (2020)
FR01_Fribourg	Fribourg	CH	7.158	46.807	627	ta	1829-1836	CHIMES, Brönnimann and Brugnara (2022)
GR11_Nufenen	Nufenen	CH	9.245	46.539	1580	ta	1834-1846	CHIMES
LU01_Luzern_Ineichen	Luzern	CH	8.304	47.052	435	ta	1826-1832	CHIMES, Brönnimann and Brugnara (2022)
TI02_Bellinzona	Bellinzona	CH	9.023	46.191	230	ta	1826-1832	CHIMES, Brönnimann and Brugnara (2022)

2.2.2 Present-day instrumental data

For every historical time series, the analogue selection requires an equivalent series in the reference period from 1961 to 2020. The long historical time series in Switzerland are mainly found in large cities. These locations also have a measurement station in the Swiss National Basic Climate Network (NBCN) (Füllemann et al., 2011; Begert et al., 2007). Precipitation and temperature time series from this network are quality controlled and homogenized by the Swiss Meteorological Service (Begert et al., 2005). For locations in Switzerland, where no data from the NBCN are available, we extracted the closest grid point from the daily temperature and precipitation fields (TabsD and RhiresD: for details about data sets, see the next section), and for sea level pressure we used the European EOBS data set v23.1 (Cornes et al., 2018). For time series in Germany and Italy, we used daily ECA&D station data (Klein Tank et al., 2002) if available or also the closest grid points from EOBS. To create time series of precipitation occurrences in the reference period, we used individual thresholds between 0.1 and 1 mm for each series for a rainy day. This is needed since the historical time series differ in how a wet day has been written down. To be able to use the full reference period as an analogue pool, all series in the reference period were gap filled by applying quantile mapping between the gridded data set (mainly EOBS) and the non-missing data of the time series. This bias correction is needed because a grid cell does not capture the local characteristics of a station and may thus have systematic biases. We choose empirical quantile mapping that estimates empirical cumulative distribution functions for the grid cell and station time series for 99 percentiles with a linear interpolation between the percentiles (Gudmundsson et al., 2012). The quantile mapping was calculated for every day of the year individually including +/- 15 d around the target day because the biases between the grid and stations showed an annual cycle. The same approach was used to extend the station data up to 2020 or back to 1961 if they did not cover the full period from 1961 to 2020. Further, if it had not been yet done, we homogenized the series with the closest homogenized NBCN stations as a reference using the penalized maximal t test (Wang et al., 2007) and the penalized maximal F test (Wang, 2008) as implemented in Wang and Feng (2013) for break point detection. Table 1 summarizes the information on the reference stations.

2.2.3 Gridded data sets

The analogue fields are resampled from the two daily spatial data sets from MeteoSwiss for temperature (TabsD) and precipitation (RhiresD) (MeteoSwiss, 2021b,a). These data sets are available for the period from 1 January 1961 to 31 December 2020 at a resolution of 1x1 km^2. The temperature fields represent the free-air temperature at 2 m above ground and are interpolated from approximately 90 homogeneous long-term station series with

a deterministic analysis method using nonlinear vertical temperature profiles and non-Euclidean distance (Frei, 2014). The precipitation fields cover all hydrological catchments that drain to locations within the Swiss border (MeteoSwiss, 2021a), i.e. also areas outside Switzerland. For the reconstruction, we only use the area that is covered during the entire 60 years excluding catchments to the south of Valais. The precipitation fields are generated using around 650 rain-gauge measurements within Switzerland and from neighbouring countries. They are based on the spatially interpolated monthly mean precipitation of a given day and spatial interpolations of relative anomalies (MeteoSwiss, 2021a).

2.2.4   Additional data sets

We want to restrict the selection of analogue days to days of similar weather. Therefore, we used a reconstruction of daily weather types covering the period of 1763 to 2009 from Schwander et al. (2017). This reconstruction is based on instrumental station records across Europe and the weather type classification by Weusthoff (2011). The weather type reconstruction also contains probabilities of the weather types for each day to account for the uncertainty in the reconstruction. For the period after 2009, we used the weather types provided by MeteoSwiss (Weusthoff, 2011).

The pre-processing steps of the gridded fields and observational data require additional reanalysis data. We use the palaeo-reanalysis EKF400v2 (Valler et al., 2022) for the homogenization of station data and for calculating a climatic offset between the reference period and the historical period to account for the warming since the pre-industrial period. This palaeo-reanalysis is based on atmosphere-only general circulation model simulations and assimilates a variety of data, such as early instrumental temperature and pressure data, documentary data, and tree-ring records. The reanalysis ERA5 (Hersbach et al., 2020) was used to remove temperature trends in the reference period (see Sect. 3.1).

In addition, we use the two monthly reconstructed gridded data sets for Switzerland TrecabsM1864 and RrecabsM1864, which cover the period of 1864 to 2020 and which have been constructed with a focus on high temporal consistency (MeteoSwiss, 2021c).

2.3   Method

For the analogue reconstruction, we mainly followed the approach implemented in Pfister et al. (2020). Some adaptations were necessary to reconstruct the early period from 1763 to 1863 because of the different network densities, and different data types and because the data set extended further back in time. This adapted approach is described in the following sections. The period of 1864 to 1960 was reconstructed as in Pfister et al. (2020) with the exception that we removed the trend in the temperature data of the reference period

(see Sect. 3.1), we changed the error covariance calculation of the observations for the assimilation procedure (see Sect. 3.3), and we implemented a quantile mapping approach considering the annual cycle of the precipitation bias (see Sect. 3.4). Figure 2.2 shows all required steps for creating the final reconstruction, including the data preparation, the reconstruction, and the cross-validation.

2.3.1 Pre-processing

Before the analogue selection, the observations had to be pre-processed to make the historical observations comparable to the observations in the reference period from 1961 to 2020. Firstly, we removed the trend for the temperature data (observations and grids) in the reference period to make it equally likely to choose days from warmer years of the 21st century as analogues. To remove a trend representing average climatic changes and not local climatic changes, we calculated a linear trend for the 2 m temperatures from the zonal mean of the ERA5 reanalysis covering the period of 1961 to 2020 centred on 1991. For each grid cell and station, the trend of the closest latitude was subtracted. Secondly, for the analogue selection and for the resampling in the historical period before the year 1864, we removed a climatic offset from the reference temperature observations and the grid because the temperature data are warmer in the reference period than in the historical period of 1763 to 1863. A monthly transient offset was calculated based on the difference between the zonal mean temperature of a 31-year window centred on the reconstructed year (e.g. from 1748 to 1778 for the year 1763) and the zonal mean temperature in the reference period of 1961 to 2003 considering land areas only. In this case, the reference period is shorter, because the EKF400v2 reanalysis ends in 2003. This offset was then subtracted from the data in the reference period (grid and observation) for every reconstructed day. Further, the historical stations had to be homogeneous with respect to their reference station. We performed a simple homogenization by calculating monthly differences between the historical and the reference stations over the full available period with respect to the closest grid points of the respective variable from the reanalysis EKF400v2 (Valler et al., 2022). The resulting difference between these two series is subtracted from the historical series to adjust them to EKF400v2. Lastly, we removed the seasonal cycle of temperature by fitting the first two harmonics of the temperature time series for observations and grid cells using least squares (see Pfister et al. (2020), for the equation).

2.3.2 Analogue reconstruction

The ARM samples meteorological fields for a historical period from the most similar days in a reference period. The most similar days, called the analogue days, are the days with the smallest differences calculated between the observational data in the historical period
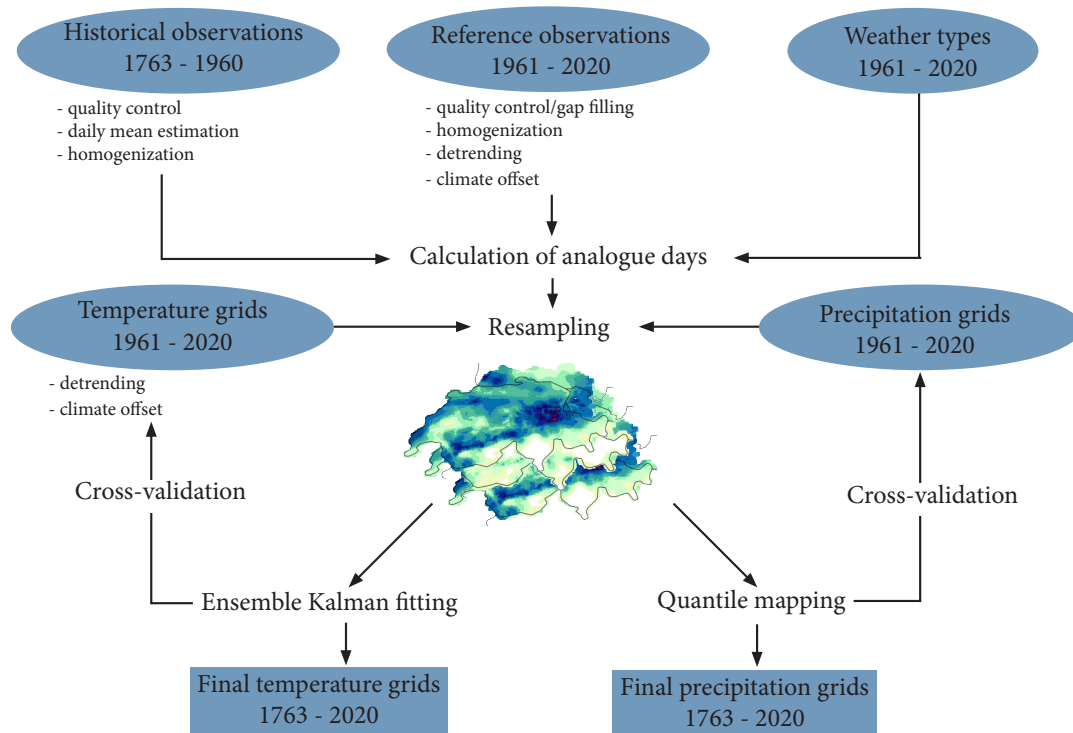
Figure 2.2: Schematic of temperature and precipitation reconstruction. Blue ellipses show input data. The necessary data preparation steps are listed below the input data. Blue rectangles show the final output data. Details on the individual steps are found in Chapter 3.

and observational data in the reference period. Our historical period starts in 1763 and is limited at the lower end by the availability of reconstructed weather types (Schwander et al., 2017). The reference period covers the period of the two gridded data sets TabsD and RhiresD from 1961 to 2020. These gridded data are resampled to generate a first reconstruction based on the best analogue day. To ensure that only physically plausible analogue days were chosen, the analogue selection was constrained to days with a similar weather type and days within the same season. All weather types with a cumulative probability of 95 % for the target days were admitted to the analogue pool to account for the uncertainty in the weather type reconstruction. This means we added up the probabilities of the most likely weather types until they reached 95 % together. Weather type probabilities were lower for the early days of the reconstruction in the 18th and beginning at the 19th century. For individual days, probabilities were so low (e.g. for 1803-03-01) that all weather types were included in the analogue pool. But the days of

the analogue pool were still constrained by the seasons. A season was defined based on a moving window of $+/-$ 60 d centred on the target day.

To reconstruct fields before 1864, we also used daily weather notes transformed into binary values of precipitation occurrence. The distance metrics used to find the closest analogue days in Pfister et al. (2020), i.e. the root mean squared error (RMSE), can however not be applied to categorical data (i.e. precipitation occurrence). Instead, we used the Gower distance, which allows for distances to be calculated for different variable types, such as continuous and count data (Gower, 1971; Kuhn and Johnson, 2019). It is defined as the average of partial distances across the variables (Eq. 2.1):

$$d(ij) = \frac{1}{k} \sum_{k=1}^{k} d(i, j, k) \tag{2.1}$$

The partial distances are calculated as a range-normalized Manhattan distance for the quantitative variables temperature, pressure, and precipitation sum. For the binary variable precipitation occurrence, the partial distances are calculated as follows. If $x_i k = x_j k$, then the partial distance is $d_i j k = 0$, and otherwise if $x_i k$ is not equal to $x_j k$, $d_i j k = 1$. We used an unweighted Gower distance. Thus, the distance metric for precipitation occurrence was either minimal (0) or maximal (1) which increased the weight of precipitation occurrence in the selection of the closest analogue. A first reconstruction was then obtained by resampling the fields based on the analogue day with the closest distance. To update the newer period from 1864 to 1960 we used the RMSE as a distance measure because a lot more precipitation measurements were available (compared to the earlier period) and the RMSE penalizes large errors. Changing the distance measure within the reconstruction period could lead to inhomogeneities. However, evaluations with both measures showed that the differences between the measures are small and the differences caused by the network changes are much larger.

2.3.3   Data assimilation for temperature fields

In a next step, the resampled temperature fields were improved by assimilating the available temperature measurements using ensemble Kalman fitting. This is an offline data assimilation approach, where the analysis is not passed to the next time step i.e. every time step is handled individually (Bhend et al., 2012; Valler et al., 2022). Data assimilation tries to find an optimal representation of the true atmospheric state between the best guess of an atmospheric field (our best analogue field) and the observations by minimizing a cost function (Franke et al., 2017). In the case of normally distributed errors, this cost function can be minimized with a Kalman filter. The best estimate of a true atmospheric

state, the analysis x^a, is given by Eq. (2.2):

$$x^a = x^b + P^b H^T (H P^b H^T + R)^{-1} (y - H x^b) \tag{2.2}$$

where x^b refers to the best estimate (the resampled analogue fields), P^b is the model error covariance matrix calculated from the 50 best analogues for each target day, H extracts the observations from the model space, and R is the observation error covariance matrix. The second part on the right-hand side of Eq. (2.2), $P^b H^T (H P^b H^T + R)$, is referred to as the Kalman gain K. To account for a bias in the covariance analysis, we used the ensemble square root filter as proposed by Whitaker and Hamill (2002) and updated the ensemble mean and the anomaly from the ensemble mean, individually yielding to separate equations Eq. (3) and (4).

$$\bar{x}^a = \bar{x}^b + K(\bar{y} - H\bar{x}^b) \tag{2.3}$$
$$x'^a = x'^b + \tilde{K}(y' - Hx'^b) \quad \text{with } y' = 0 \tag{2.4}$$

The Kalman gain for the mean K and anomaly $\tilde{K}$ were then calculated as follows.

$$K = P^b H^T (H P^b H^T + R)^{-1} \tag{2.5}$$
$$\tilde{K} = P^b H^T ((\sqrt{H P^b H^T + R}^{-1})^T \times (\sqrt{H P^b H^T + R} + \sqrt{R})^{-1} \tag{2.6}$$

Often localization of the background error covariance matrix P^b is used in data assimilation to avoid spurious error covariance. Testing different types of distance-, altitude-, and correlation-adjusted localization as proposed by Devers et al. (2021) did not improve results in our rather small area. Therefore, we did not apply localization.

We estimated the observation error covariance assuming that there is a linear relationship with distance between the variance of the differences in neighbouring observations as proposed by Wartenburger et al. (2013). The error covariance was estimated individually for the three periods 1763 to 1863, 1864 to 1960, and 1961 to 2020. As was expected, errors in the last period of 1961 to 2020 were smaller, and thus the skill of the cross-validation was overestimated. Due to the few available measurements within Switzerland in the period of 1763 to 1863, we also assimilated the temperature data from Hohenpeissenberg, Torino, Milano, and Rovereto. To do this, the observations from the best analogue days of the stations outside Switzerland (and therefore outside our grid) were added to the background x^b, and, subsequently, the H operator was adjusted and P^b was calculated including these

observations. The observation errors for these stations outside Switzerland were calculated as described above. For the years after 1864, only stations with correlation values above 0.975 are used for assimilation (see named stations in Fig. 1d and e). Before assimilating the observations we removed a monthly bias calculated between the observation and the closest grid points from the observations because the observations are biased with respect to the model grid.

2.3.4 Quantile mapping for precipitation fields

Despite using the same grids, precipitation biases occurred in the analogue-based reconstruction because precipitation measurements are very scarce and unevenly distributed across the area, leading to systematic biases in areas with no precipitation observations. To correct for these biases, we apply empirical quantile mapping calibrated between the reconstruction in the reference period and the original data set (RhiresD) for every grid cell (Gudmundsson et al., 2012; Feigenwinter et al., 2018; Rajczak et al., 2016). Correction factors were estimated for the 1st to 99th percentile using a linear interpolation between the percentiles. A wet-day threshold was set to 0.1 mm. Because quantile mapping showed seasonal biases of up to 1 mm per day in southern Switzerland, when the quantile mapping was estimated for the entire year, we calculated it in 15 d steps throughout the year based on a 91 d window centered around these 15 d. This yielded a total of 24 steps, which was a compromise between making a bias correction for every day of the year individually and doing the bias correction only for the four seasons. Because the biases in the precipitation reconstruction changed considerably based on the station network, quantile mapping was computed for the different networks (see Fig. 2.1) and then applied to the historical reconstruction depending on what network the historical period corresponded to best. Note that Fig. 2.1 only shows three examples of networks for the period before 1864. Quantile mapping was conducted for six different set-ups based on the station combinations occurring most often.

2.3.5 Evaluation

To evaluate the skill of the reconstructions, we (1) performed a cross-validation in the reference period of 1961 to 2020 and (2) compared the reconstructed fields with time series in the early period that have not been used for the reconstruction. For the cross-validation, we reconstructed the temperature and precipitation fields for the reference period of 1961 to 2020. For every day, the best analogue days were calculated by leaving out -/+ 5 d around the target day. The reconstructed fields were then compared to the original fields using five standard measures. We calculated the root mean squared error (RMSE), Pearson correlation, mean bias, and the mean squared error skill score (MSESS) on the de-

seasonalized temperature anomalies. For the MSESS, we used climatology as a reference, which is 0 in the case of anomalies. For precipitation, we used the Spearman correlation, RMSE, mean bias, and the Brier score (Wilks, 2011). We used the Brier score to evaluate how well the reconstruction assigns wet and dry days. Therefore, instead of probabilities, the Brier score was calculated for wet and dry days, using 0.1 mm as a threshold. The Brier score returns the percentage of days that are wrongly assigned to wet or dry days. To assess the temporal persistence of the reconstruction on the day-to-day timescales in more detail, we performed two additional analyses. For temperature, we calculated the autocorrelation at a 1-20 d lag for all networks and compared these values to the autocorrelation in the original grid TabsD. For precipitation, we used two persistence indices suggested by Moon et al. (2019) to assess the mean persistence characteristics of precipitation and compared these to the persistence calculated with the original RhiresD grid.

Because the station network changes heavily over time, we performed the cross-validation for the different network set-ups shown in Fig. 2.1. The evaluation is done individually for every grid cell, i.e. evaluating the reconstruction in time. For the network shown in Fig.2.1c, we also compared the original and reconstructed grids area-wise by calculating the above-mentioned measures in space and for two different altitude levels from 0 to 1000 m a.s.l. and from 1000 to 2000 m a.s.l. for an area in Central Switzerland between 7.4 and 9.1° E and 46.5 and 47.3° N. This gives insights, into how well the spatial structure is reproduced. The final reconstruction is, however, run on all available data.

For an independent evaluation, we compare the reconstruction with station data from seven entirely independent temperature series in the period of 1763 to 1863 (see Table 2.2) based on the same measures as described above. The mean bias was not calculated for series with seasonality removed but for the absolute temperature series. At the location of Bern, the precipitation reconstruction was compared to an independent series based on the Brier score and to monthly wet-day frequencies of the observation and the closest grid cell of the reconstruction. Furthermore, we explore the representation of the long-term variability by comparing our reconstructions to other data sets covering the same or similar periods.

2.4 Results and discussion

2.4.1 Cross-validation during reference period

Cross-validation results for de-seasonalized temperature anomalies using the network as in Fig. 1c (i.e. a dense network for the historical period) show correlation values between 0.67 and 0.99 and an average of 0.92 and 0.95 (Fig. 2.3a to e) for all seasons and the annual evaluation. All periods show a spatial pattern with the highest correlations in the Swiss Plateau, lower values in the Alpine region, and the lowest in the Canton of Ticino.

The winter months (December to February) show the lowest correlation values, especially in the Alpine region, followed by autumn (SON) and spring (MAM). These spatial and seasonal differences are also present in the RMSE and MSESS evaluation (Fig. 2.3f to o). RMSEs range between 0.45 and 3.82° C, with an average of 1.04 to 1.59° C for all time aggregations. In winter, the errors are largest in the very south and east of Switzerland and in the Jura. MSESS values range between 0.34 and 0.98. The lowest values are found in the valleys Ticino, especially around Lago Maggiore in winter and autumn. Mean biases range between -0.34 and +0.08° C (Fig. 2.3p to t). In winter, pronounced cold biases are present in the Alpine region, southern Switzerland, and the Jura. This is also the case for autumn, but biases are smaller. In spring, the largest cold biases are mainly found in the Alps but not in the Ticino, whereas in summer, biases range only between -0.06 and +0.08° C.

Spatial correlations do not show large differences in their performance with respect to the different deciles of the area mean for summer and winter and both altitude groups (Fig.2.4a and b). In winter, RMSEs are larger for the coldest and the warmest days, while days in the middle of the distribution show lower errors. At altitudes above 1000 m a.s.l. in particular, the warmest days show larger RMSEs. In summer, cold days have low RMSEs, and the RMSEs increase with increasing temperatures. This effect is more pronounced for the higher-altitude group. The mean bias in the low-altitude group (below 1000 m a.s.l.) does not show differences in the deciles. However, for the higher altitude group, the very cold days are too warm in the reconstruction and the very warm days are too cold. In summer, such an effect is not visible, but the spread of the mean bias distribution is generally larger for warm days than cold days.

Cross-validation results of the different networks, however, vary considerably. The network with only 11 measurements (Fig. 2.1a) has the lowest correlations, with values ranging between 0.58 and 0.99 for winter and 0.64 and 0.99 for summer (Fig. 2.5a and b). In the winter months in particular, this network performed worse with respect to correlation, RMSE, and MSESS. In summer, differences between networks are much smaller (Fig. 2.5b). The increase in observations in 1864 showed much better performance for all metrics, however, the change in the network from 41 observations to 108 did not lead to substantial improvements in the reconstructions. The spatial analyses of all five networks are shown in Figure A.1 in Appendix A for the annual evaluation.

Further, the persistence of day-to-day temperature variability is slightly underestimated in the reconstructions compared to the original grid (Appendix, Fig. A.3) with differences in the autocorrelations reaching up to 0.15 for the sparse networks. In the alpine areas in particular, autocorrelation at lags of up to 10 d is lower than in the original grid. This can be related to the network density and set-up. The sparser networks have lower

autocorrelation values in the areas with very few observations.

These spatial and seasonal differences may be related to the sparse and unevenly distributed station network and the seasonal meteorological situations typical of Switzerland. In the winter half year (October to March) during calm flow situations, radiation fog and lifted fog (i.e. low stratus clouds) are a frequent phenomenon in the Swiss Plateau (Scherrer and Appenzeller, 2014). Such situations block direct radiation, leading to significantly lower temperatures below the cloud layer. Because temperature data were mainly available in the Swiss Plateau below this inversion layer, a day that is too cool for the Alpine area may be selected as an analogue day and the temperature assimilation may be too cold because to the Alpine inversion layer is not well captured. An evaluation of fog days showed these large biases for the Alpine area (not shown). This is confirmed by the biases seen in Figure 2.3k-o and would also lead to lower correlations and MSESS and larger RMSE. The overall better performance in summer compared to winter for all networks (Fig. 2.5a and b) can also be related to such badly captured inversion layers, which are not present in summer months. For a reconstruction of monthly temperature, Isotta et al. (2019) found that the magnitude of the warm anomalies in the areas above the inversion is not reproduced if only a few stations are available in the Alpine regions. For the network with only 11 stations (Fig. 2.1a), the temperature bias in winter is actually smaller compared to the network with 21 and 32 measurements (Fig. 2.1b and c). Network 2 and 3 already contain the German station in Hohenpeissenberg at an altitude of 995 m a.s.l. and they also have more stations in the Swiss Plateau. An inversion layer captured wrongly because of the station distribution may also cause a larger bias.

The cross-validation of the precipitation reconstruction shows a lower performance compared to de-seasonalized temperature (Fig. 2.5 and 2.6). Spearman correlations range between 0.39 and almost 1 for all seasons and the annual evaluation considering the network with 32 measurements (Fig. 2.5c). The Alpine region does not stand out in as pronounced a way for the temperature validation. However, southern Switzerland, the Ticino, and the southern Grison valleys do have correlation values of only 0.35. In contrast with temperature, correlations are generally higher for winter than for summer months. RMSE ranges between 3.09 and 26.89 and is highest during the summer months in the Ticino. The Brier score is close to 0 around the locations, where precipitation occurrence is registered and decreases with distance. As for the other metrics, especially in the summer months, the southern Ticino and southern Grison have very low values. The mean bias in all seasons is close to 0, because we conducted quantile mapping taking into account the annual cycle of precipitation differences between the reconstruction and the original data set (Fig. 2.5p to t).

With respect to the intensity of events in winter, days with more precipitation on an
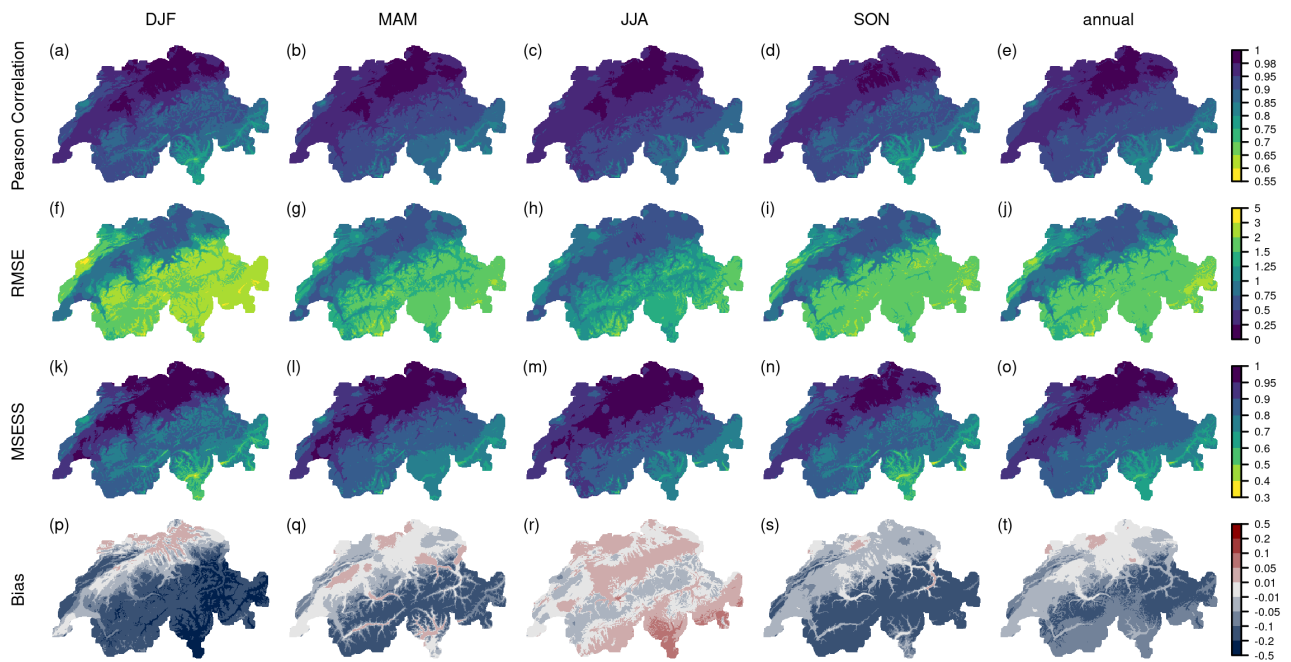
Figure 2.3: Cross-validation results of a network of 32 stations as in Fig. 1c for temperature anomalies during 1961-2020 for the four seasons (DJF, MAM, JJA, SON) and annually. a-e) Pearson correlation, f-j) RMSE, k-o) MSESS, and p-t) mean bias.

area-wide basis show higher correlations than days with less precipitation (Fig. 2.4c). In summer, spatial correlations do not vary in the median with respect to the area average intensity; however, the spread of the correlation increases for days with higher total precipitation. As is to be expected, the RMSE increases with increasing intensity of a rainy day. In summer in particular, the RMSE can reach very high values for the strongest events. For higher altitudes, the values are even larger. These high values come from an underestimation of the strong precipitation events in both winter and summer, which is shown in the lowest row. Despite the bias correction, extreme precipitation is underestimated in the reconstruction by a median up to 10 mm.

Differences between the networks are substantial for summer and winter (Fig. 2.5c and d), but the performance is generally better in winter than in summer. The sparsest network has a median correlation of 0.68, which increases considerably when stations are added. For the two networks after 1864 however, no more substantial changes occur. RMSEs are between 3.09 and 29.45 mm for the three networks of the early period and between 1.72 and 12.74 mm afterwards in winter. For the summer season, they are almost twice as large. For the annual evaluation of precipitation, the spatial analyses of all networks are shown in Figure A.2 in Appendix A.

Also, the persistence of dry and wet spells is underestimated in the reconstructions, al-
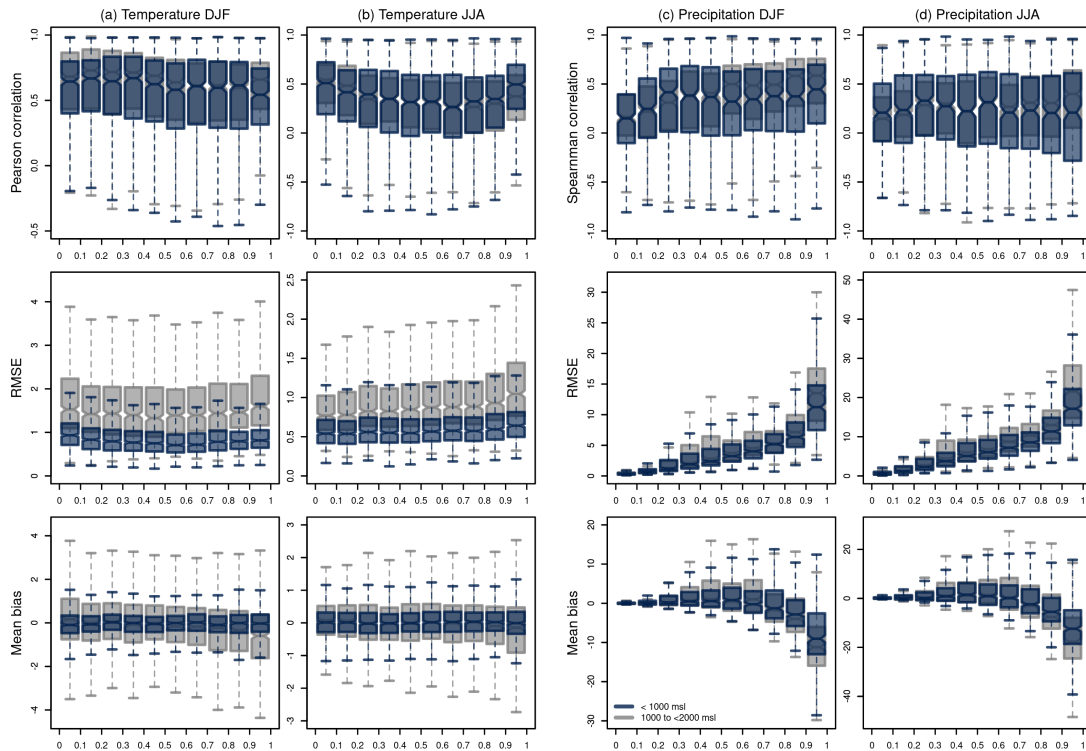
Figure 2.4: Spatial evaluation of the reconstruction ordered according to the deciles of the area mean between 7.4 and 9.1° E and 46.5 and 47.3° N for the original data set. a-b) DJF and JJA temperature evaluation with removed seasonality for Pearson correlation, RMSE, and mean bias. c-d) DJF and JJA precipitation evaluation for Spearman correlation, RMSE, and mean bias. Blue values show all grid cells below 1000 m a.s.l.; grey values show grid cells above 1000 m a.s.l.. The boxes range from the first to the third quartile and whiskers extend to 1.5 times the interquartile range outside the box.

though only slightly and with regional differences (Appendix Fig. A.4). The fraction of dry (wet) days followed by dry (wet) days is up to 0.14 smaller in the reconstruction compared to the original data. The underestimation of the wet-days persistence is largest in the Ticino and for the sparse networks, indicating that wet spells are less well captured. For the dry-day persistence, no spatial pattern is visible. A lower persistence for both wet and dry days in the reconstruction can be expected since the analogue resampling does not consider temporal information.

The lower performance of the precipitation reconstruction can be expected, since precipitation is a much more heterogeneous variable than temperature on a daily timescale impeding daily reconstruction, especially when only very few precipitation data are available. The performance differences in the reconstruction between winter and summer can be related to the type of precipitation occurring in these seasons. In summer, precipitation can be convective and very local, while in winter, precipitation is often stratiform, cov-
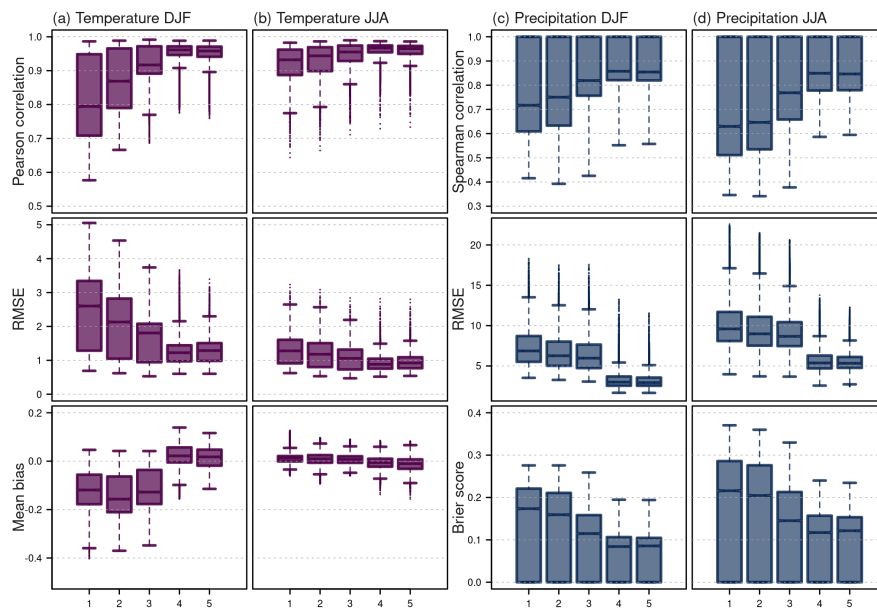
Figure 2.5: Cross-validation results for the five networks shown in Figure 1 for temperature anomalies during 1961-2020 a) in winter (DJF) and b) summer (JJA), showing Pearson correlation, RMSE, and mean bias, and for precipitation c) in winter (DJF) and d) summer (JJA), showing Spearman correlation, RMSE, and Brier score.

ering larger areas. This stratiform precipitation is easier to reconstruct. The Brier score decreases faster around the stations in summer than in winter. The poor performance with large RMSEs in the Ticino and the south-eastern Grison valley may come from convective or orographic precipitation not being captured at all in the precipitation data covering only northern Switzerland. But intense precipitation events are also difficult to capture in northern Switzerland (Fig. 2.4c and d). In contrast with Pfister et al. (2020), the mean bias of the uppermost percentile (Fig. 2.4c and d, lowest row) is on average negative; i.e. the reconstructed values are too low compared to the original. This may be because very few precipitation measurements enter the reconstruction, and thus days with high precipitation are not selected from the analogue pool.

The cross-validation results give us an impression of the performance of our reconstruction. However, they have some limitations. The cross-validation was performed based on station data in the reference period. These measurement data have a much higher quality than what we know from early instrumental data (see Sect 2.1). Further, our analogue pool covers the same period as our reconstruction period. Therefore, it covers the same longer-scale variabilities but not necessarily in the same way as they occur in the early period between 1763 and 1863. With respect to temperature, we calculated an offset in order to account for the climatic change between the 18th century and the late 20th and early 21th centuries. This offset is based on a state-of-the-art data set but may not be accurate for the
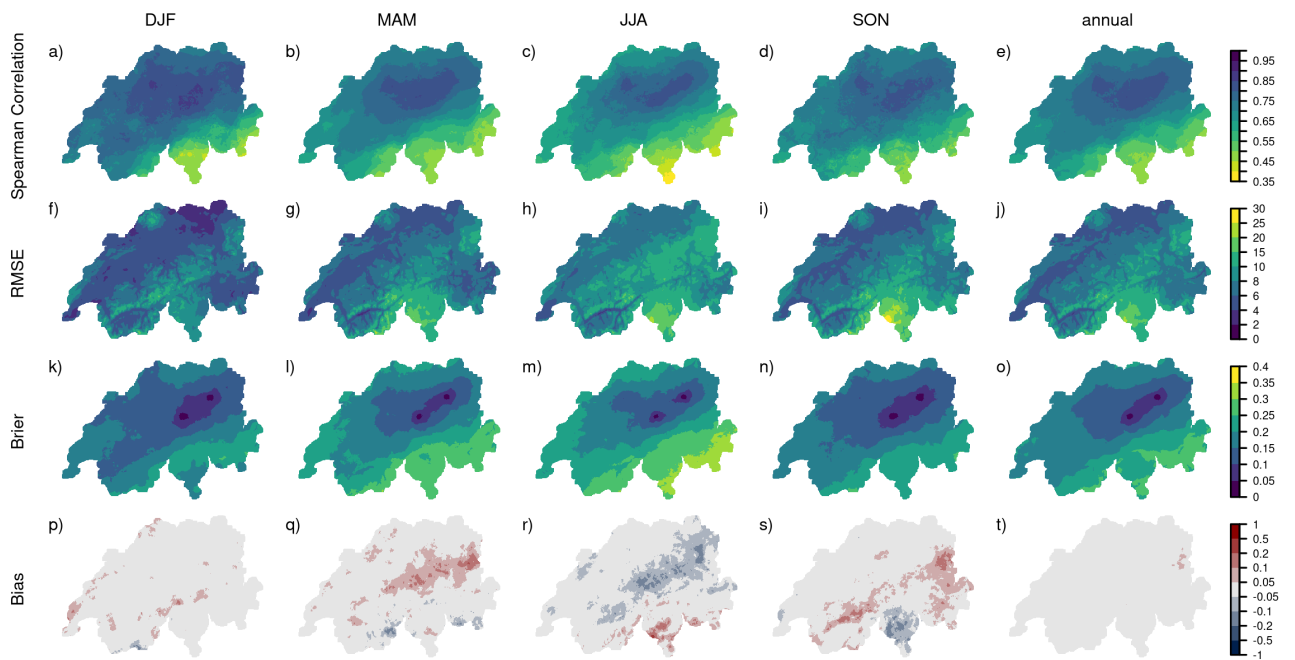
Figure 2.6: Cross-validation results of a network of 31 stations as in Figure 1c for precipitation during 1961-2020 for the four seasons (DJF, MAM, JJA, SON) and annually. a-e) Spearman correlation, f-j) RMSE, k-o) Brier score, p-t) mean bias. The RhiresD data set also contains the northern catchments in addition to Switzerland .

small and topographically heterogeneous area of Switzerland, thus adding an additional source of errors to the reconstruction.

2.4.2 Evaluation with independent data

A comparison with independent observations allowed us to assess the performance of the reconstruction in the reconstructed period itself, but the quality of the observations has to be considered. Temperature observations with removed seasonality in Aarau, Fribourg, Herisau, and Tegerfelden show Pearson correlations mostly above 0.85 (Fig. 2.7a-d). Nufenen, Bellinzona, and Luzern show considerably lower values. The same pattern is also seen for the MSESS. RMSEs range between 1 and 4° C. Again, Aarau, Fribourg, Herisau, and Tegerfelden have the smallest errors. The mean bias based on absolute values is mostly between -2 and 2° C for Fribourg, Herisau, and Tegerfelden. For Bellinzona, Luzern, and Nufenen, the reconstruction shows colder values than the observations in all seasons.

Fribourg, Herisau, Tegerfelden, and Aarau are all located in areas with a high station density (see Fig. 2.1). This contributes to the better performance of the reconstruction in these areas, but their good agreement confirms that for the Swiss Plateau our reconstruction provides useful results. Nufenen and Bellinzona show the lowest correlation values

and the largest biases. For Bellinzona, Brönnimann and Brugnara (2022) showed that the subdaily measurements in July are considerably warmer than what is expected from the daily cycle representative of this area, most likely because of radiative biases. This would explain the fact that the reconstruction is colder than the observations, which is especially pronounced in summer (Fig. 2.7e). Furthermore, Bellinzona lies in an area with no nearby observations used in the reconstruction. Due to this we would expect cold mean biases for winter as seen in the cross-validation but not for summer (Fig. 2.3). For Nufenen, the closest grid cell in the reconstruction corresponds to an altitude of 1866 m a.s.l., whereas the village Nufenen, where the measurements were taken, is at 1580 m a.s.l. Thus, 300 m of altitudinal difference can explain the large negative biases found between observation and reconstruction.

For precipitation, a comparison with independent observations is only possible for a series of precipitation occurrence in Bern between 1807 and 1818. Based on the cross-validation, we can expect a Brier score of between 0.15 and 0.2 (i.e. up to 20 % of the days are wrongly assigned to a wet or dry day) for this location and the respective network. The Brier-score between the closest grid cell in Bern and the precipitation occurrence series from weather notes yields 0.24, and is thus, higher than the cross-validation results. However, we compare a station measurement with a grid cell (of 1x1 km) covering a slightly different scale. Also, precipitation occurrence may have a problem with accounting for nighttime precipitation correctly for the exact day of the weather notes. The gridded data are a daily sum between 06:00 in the morning and 06:00 the next day, while this may not be entirely clear for the weather notes. Figure 2.7f shows precipitation occurrence for a dry (1811) and a very wet year (1816). Long-lasting dry spells such as in March and April 1811 are captured by the reconstruction, as well as the overall wet summer of 1816, but for individual days, reconstructions deviate from observations. This is also seen in the comparison of the monthly wet-day frequency from the reconstruction and observation (Fig. 2.7g), which agree well overall (Pearson correlation of 0.84).

2.4.3 Assessment of long-term variability

The 258-year-long reconstructions should reproduce daily weather and long-term variability in temperature and precipitation over Switzerland. We assess this long-term variability by comparing the field mean of our data set to other data sets covering the same or similar periods (Valler et al., 2022; Casty et al., 2005; Brugnara et al., 2022; MeteoSwiss, 2021c). These data sets consist either of only observations, statistical reconstructions based on proxy data and observations, or reanalyses. The data sets are not independent from the Swiss reconstruction since they rely on the same or similar input data and they are also not independent from each other. For details about the input data refer to the references.

The annual temperature anomalies with respect to the 1871 to 1900 climatology agree well in all data sets for the reconstruction period from 1864 to 2020 (Fig. 2.8a). This period has good coverage of temperature data with high quality, and, thus, a good agreement can be expected. Only the reconstruction by Casty et al. (2005) (hereafter referred to as Casty) is colder in the first half of the 20th century. Also, the data sets with a lower spatial resolution (EKF400v2, Casty) do not capture the steep warming at the end of the 20th century. Before 1864, deviations between the data sets are larger. The annual mean of the Swiss reconstruction is up to 0.5 ° C warmer than EKF400v2 and the Swiss Plateau series before 1800. The temperature differences are larger in winter than in summer (not shown). There are several reasons this might lead to the warmer temperatures in the Swiss reconstruction. EKF400v2 is used for homogenization and for calculating an offset between the reference period and the historical period. This offset might be too small especially in winter, since EKF400v2 is colder than the Swiss data in winter in the reference period.

The agreement between the precipitation reconstructions is much lower (Fig. 2.8b). After 1864, all data sets reproduce similar patterns, but with different magnitudes. Differences in the anomalies reach up to 3 % when comparing our reconstruction to RrecabsM1864 (MeteoSwiss, 2021c). Before 1864, differences among the data sets are considerable. Whereas the reconstruction of Casty partly agrees in terms of the direction of the signal with the Swiss reconstruction, EKF400v2 does not agree at all. Also, the Swiss reconstruction is on average drier before 1864 compared to the period after 1864. The smoothed time series only shows periods (around 1770 and 1850) with wetter conditions than the average from 1871 to 1900. Since very little information on absolute precipitation enters the reconstruction and the bias correction might not fully correct the dry bias, too dry a reconstruction can be expected. However, individual years, such as 1816, the "year without a summer" (e.g. Luterbacher and Pfister, 2015), and the wet summer of 1770 (see next section), do show large positive precipitation anomalies (Fig. 2.8b and Fig. A.5d). The precipitation reconstruction, therefore, needs to be used with care. Also, note that the main aim of the reconstruction was to create daily fields rather than creating a reconstruction with good long-term consistency. This needs to be considered when using the data set.
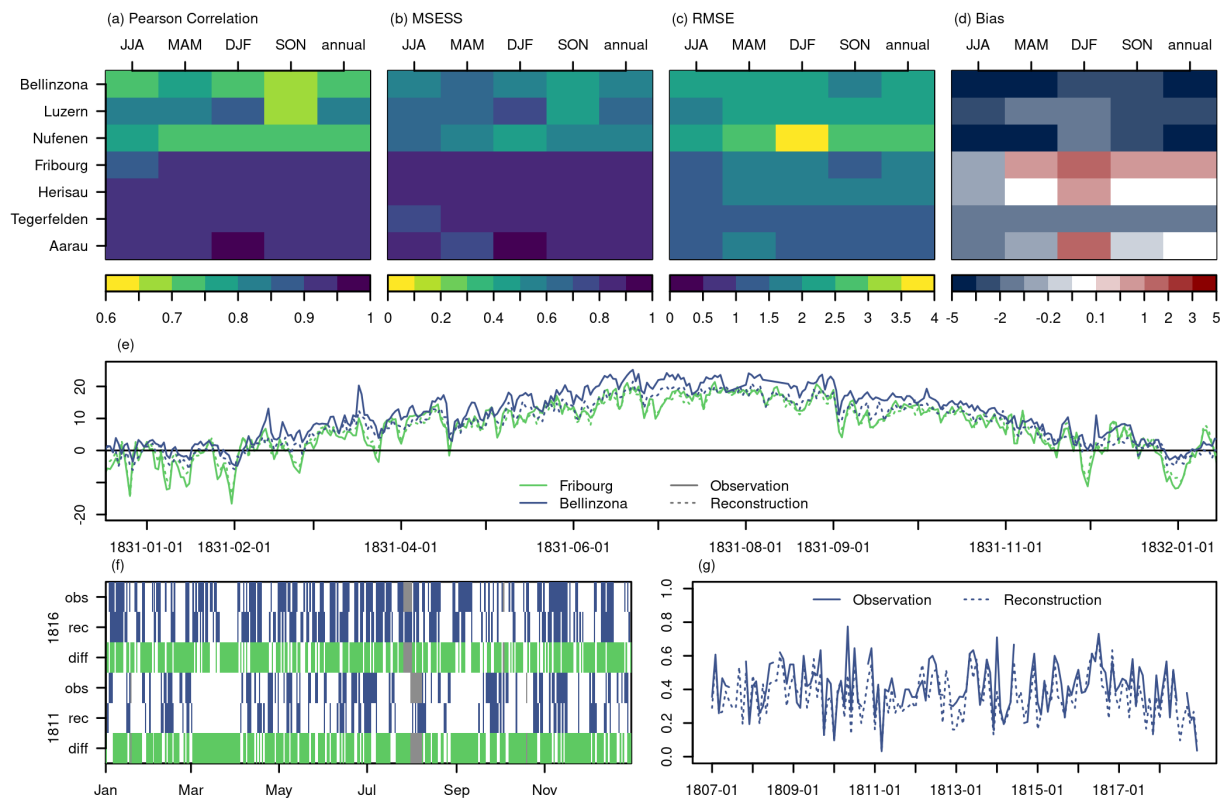
Figure 2.7: Evaluation of the closest grid point from the reconstruction and the observations for values with removed seasonality. a) Pearson correlation, b) RMSE, c) MSESS, and d) mean bias. Each box shows the four seasons and annual values on the top x axis and the different locations on the y axis. Locations are marked with an asterisk in Fig. 1a. e) Time series of two observations in Fribourg and Bellinzona and the closest grid points of the reconstruction for the year 1831. f) Wet days for the observations from weather notes in Bern and reconstruction for 2 years 1811 and 1816. A wet day is marked with a blue bar and a missing observation is marked with a grey bar. Green bars show the days that are correctly assigned to wet and dry. g) Comparison of the monthly wet-day frequency for the period of 1807 to 1818 for the data from f).
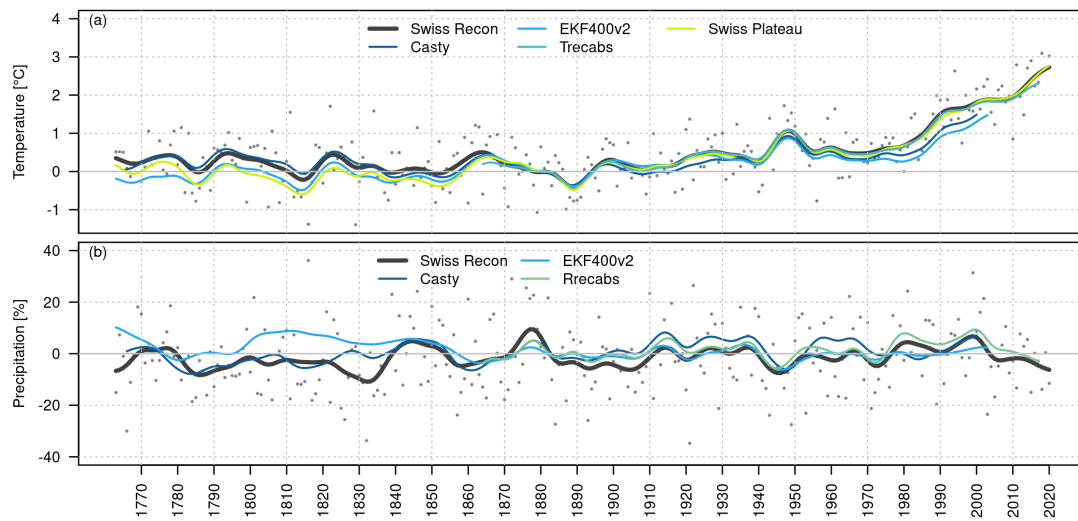
Figure 2.8: a) Long-term evolution of annual temperature anomalies in different data sets. b) Long-term evolution of annual precipitation anomalies as a percentage deviation from the mean. The time series are smoothed with a Gaussian filter (sigma = 3 years). Grey dots show reconstructed annual anomalies. All anomalies are calculated with respect to the 1871-1900 climatology for each data set. The time series either represent the field means (Trecabs/Rrecabs, Swiss reconstruction) or the closest grid point of the data set. The Swiss Plateau time series is based on the Bern and Zurich series as described in (Brugnara et al., 2022).

2.5   Case study: the European famine years 1770 to 1772

During the years 1770 to 1772 central Europe was hit by a severe famine which was considered one of the most devastating socio-ecological extreme events of the Little Ice Age. According to Collet (2018), the famine may have been of a similar magnitude to the famines of the 1315s and 1570s, causing hundreds of thousands of deaths. The crisis was related to long-lasting wet and cold conditions between 1769 and 1772 from France to Ukraine and Switzerland to Scandinavia. It hit a society with low coping capacities, and a very high cereal dependence beyond mere consumption; cereals were the key staple food but also served as a means of payment and taxation. This "cereal society" in Europe was highly vulnerable to adverse weather conditions, especially during the summer months. In the Czech Republic, around 10 % of the population died due to consecutive crop failures in the third year of the famine from 1771 to 1772 (Pfister and Brázdil, 2006). In contrast, for Switzerland, Pfister and Brázdil (2006) demonstrated that despite a loss of harvest, the famine was less severe due to a low social vulnerability by contemporary standards, effective interventions by the state, and the climate anomaly affecting only two harvests.

Collet (2018) summarized data from societal and natural archives describing the climate anomaly across Europe. According to him, the devastating impacts of the adverse weather were related to its length rather than its intensity. In fact, it has not been shown to be an outstanding climate anomaly with respect to magnitudes of temperature and precipitation anomalies in climate reconstructions (Luterbacher et al., 2004; PAGES2kConsortium, 2013; Pauling et al., 2006). A composite of 1769 to 1771 from the old world drought atlas shows however very wet conditions mainly for a limited area of south-eastern Germany, northern Austria, and the western Czech Republic (Cook et al., 2015).

For Switzerland, we summarized documentary sources that reported the wet and cold weather conditions and related impacts for the summer half year of 1770 (Table 2.3). These reports include, for example, late snowfall, continuous snow cover, rain and flood impacts, and poor harvests. With our reconstructed daily fields, we tried to confirm the long-lasting wet and cold conditions described. However, the lack of precipitation observations in the reconstruction in particular has to be kept in mind.

Table 2.3: *Selection of registered weather impacts from the wet and cold weather in Switzerland in the summer half year of 1770 based on our own sources (Brugnara et al., 2020b) and Euro-Climhist (Pfister et al., 2017).*

Time	Location	Impacts	Source
Spring	Geneva	snow impact on agriculture	Piuz (1974)
April	Adelboden (BE)	abundant snow	Baertschi (1916)
April	Gurzelen (BE)	snow impacts on agriculture	Oekonomische Gesellschaft Bern, metadata in Pfister et al. (2019)
April	Bern (BE)	snow impacts on agriculture	Oekonomische Gesellschaft Bern, metadata in Pfister et al. (2019)
April	Lake Constance	abundant rain, snowfall, hay prices increase	Paffrath (1915)
April/May	Appenzell Innerrhoden	late snowmelt	Walser (1731) as cited in the EuroClimhist (Pfister et al., 2017)
May	Uri	abundant snow	Schaller-Donauer (1937)
June/July	Gurzelen (BE)	fresh snow at higher elevations	quoted in Zumbühl (1980)
July	Lake Constance	abundant rain, hail, rain impact	Paffrath (1915)
August	Lake Constance	abundant rain, impacts of floods and high water level	Paffrath (1915)
September	Gurzelen (BE)	fresh snow at higher elevations	Oekonomische Gesellschaft Bern, Metadata in Pfister et al. (2019)
Summer	Glarus	pasture yield poor: most mountain snow cover does not melt	Trümpi (1774)
Summer	Grindelwald (BE)	permanent snow cover	Strasser (1890)
Summer	Stockhorn Massif (BE)	permanent snow cover	quoted in Pfister (1975)
Summer	Rhine Valley (SG)	high water level	Walser (1731) as cited in the EuroClimhist (Pfister et al., 2017)
Summer	Erguel (BE)	grain harvest poor	Kohler (1871)

The area mean of the Swiss reconstruction does indeed show monthly precipitation anomalies (with respect to the 1763 to 1812 climatology) which are constantly above average for a period from 1769 to the end of 1771 (Fig. 2.9a). Two other data sets EKF400v2, (Valler et al., 2022) and Casty (Casty et al., 2005), show peaks in 1770 and 1771 but not the persistent positive precipitation anomalies. Note that we use a 12-month running mean for the time series shown and that we select the closest grid cells in EKF400v2 and Casty. Thus, the data are not representative of exactly the same area. Temperature anomalies are negative, especially for the first half year of 1770 but also for the beginning of 1771 (Fig. 2.9b). For temperature, the three data sets agree well, which is not the case for precipitation. For precipitation, however, the data sets agree better starting in the 19th century (not shown).

Crop failure mainly relates to adverse weather conditions during the growing seasons. To track these adverse weather conditions, we exemplarily have a look at the summer half year 1770. Several sources report on abundant snowfall for the month of April 1770 (Table 2.3) which may have delayed the start of the growing season. Days with snowfall were calculated using a threshold of 2° C for daily mean temperature and 1 mm for precipitation as it has been derived by Zubler et al. (2014). Optimal temperature thresholds for distinguishing snow from rain, however, depend heavily on the relative humidity of the air, which we do not have as a parameter for the historical time period, and they depend on the season (Jennings et al., 2018; Kienzle, 2008). Large parts of Switzerland show an above-average number of days with snowfall with respect to the 1763 to 1812 April climatology (Fig. 2.10a). In the pre-Alps and the Jura, up to 12 d more snowfall occurred than on average. For the surrounding hills of Bern and Gurzelen, for which historical sources reported snowfall, up to 3 snowfall days more occurred than usual, which, in relative terms, is almost a doubling with respect to the April climatology. In lower elevation areas in the Swiss Plateau, low-elevation mountain valleys, and the Ticino no snow days were registered in the reconstruction. For example, for Basel, weather notes by d'Annone (Brönnimann and Brugnara, 2020a) note snowfall for 4 d, but from our reconstruction no snowfall can be inferred. However, using daily data for snow detection is difficult, as the threshold for snow to occur may be reached at some point during the day, whereas it is not reached based on the daily mean; this is particularly the case in spring. Indeed, daily temperature values in Basel by d'Annone never reached values below 2.5° C. However, the early morning measurements, for example, reached 1.6 and 1.9° C on the days when snowfall was reported.

Crops require a certain amount of accumulated heat to reach their different phenological stages. The growing degree day (GDD) index can be used to express the heat accumulation needed until a phenological stage is reached (Wypych et al., 2017). The index is calculated as the sum of daily mean temperature above a certain threshold of daily mean temperature

(e.g. Bonhomme, 2000). Here, we set this threshold to 5° C. At a GDD of 1000° C, various cereals, such as oat, barley and wheat, reach their seed-filling phase (Miller et al., 2001). In the summer of 1770, a GDD of 1000 ° C was reached around 15 da later in the Swiss Plateau than what would be expected on average for the period from 1763 to 1812. For higher-altitude locations, it was even reached up to 30 d later. This growth stage was therefore delayed by around half a month in the year 1770 (Fig. 2.10a). However, the weather conditions at later stages are also relevant for plant development and harvest. In the summer half year of 1770, the number of cold days was increased, which can be seen in the anomaly of a cold-day index, i.e. the number of days below the 20th quantile calculated for each day of the year. It shows above-average cold days ranging from $+5$ to $+30$ d (Fig. 2.10b) mainly for the area north of the Alps. In southern Switzerland, this was less pronounced, and only between 0 and 10 more cold days were registered.

Historical sources also reported wet conditions throughout the summer, for example for Lake Constance and the Rhine Valley (see Table 2.3, Paffrath (1915) and Walser (1731)). For the summer season from April to September 1770, in most of northern Switzerland above-average wet days were recorded with areas reaching up to 125 % wet days compared to the climatology of 1763 to 1812 (Fig.2.10c). In the very south of southern Switzerland, an above-average number of wet days was also recorded, although some areas also show an around average number of wet days. These values thus confirm the reports of wetter than usual weather.

However, if we compare the summer of 1770 to the summer of 1816 in our reconstruction, which is known as "the year without a summer" because of its very wet and cold conditions (Flückiger et al., 2017; Luterbacher and Pfister, 2015), these anomalies become small (see Appendix, Fig. A.5). In 1816, a GDD of 1000 was reached in the Swiss Plateau on average 20 to 25 d later. The area where a GDD of 1000 is never reached is much larger, meaning that some cereals never fully developed. Up to 50 more cold days were registered during the summer of 1816, and wet days increased to up to 150 % compared to the 1763 to 1812 climatology. The summer of 1816 was, therefore, considerably more extreme. Our reconstruction might also be more accurate for the summer of 1816, particularly for precipitation, as up to four precipitation/precipitation occurrence time series and also considerably more temperature measurements were available in 1816.

With the reconstruction, we are nevertheless able to reproduce the wet and cold weather during 1769 to 1771 in Switzerland, which caused severe famines in parts of central Europe. Studies showed that, based on such gridded data sets, crop yields (Flückiger et al., 2017), for example, can be simulated. Such follow-up studies could also be applied to quantitatively reproduce crop losses for this famine for Switzerland based on the reconstruction presented here, or even for the all of Europe.
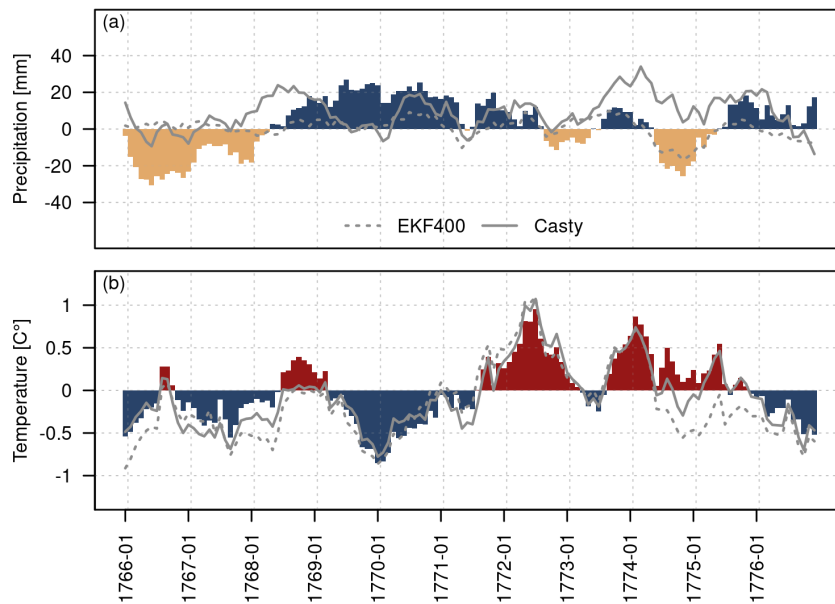
Figure 2.9: a) Area mean of monthly precipitation anomalies with respect to the monthly 1763 to 1812 means for the precipitation reconstruction (coloured bars); lines show the closest grid point of EKF400v2 (dashed) and of the reconstruction from Casty (solid). b) Area mean of monthly temperature anomalies with respect to 1763 to 1812 for the temperature reconstruction; lines show the closest grid point of EKF400v2 (dashed) and the reconstruction from Casty (solid). All values are a mean over a 12-month window.
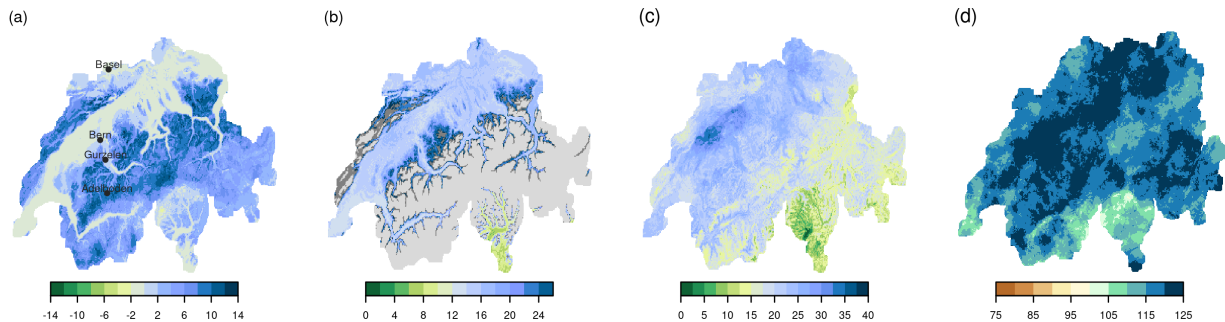

Figure 2.10: a) Anomaly of the number of days with snowfall for April 1770. Black dots denote areas where abundant snowfall was reported in historical sources. b) Anomaly in days for the year 1770 when the threshold of 1000 GDDs was reached. Light-grey areas denote values where no climatology of a 1000 GDD threshold was calculated because the threshold was reached in less than 75 % of the years between 1763 and 1812. Dark grey denotes areas where the threshold of 1000 GDDs was not reached in the year 1770. c) Anomaly of the number of cold days (days below the 20th percentile of daily mean temperature) for April to September 1770. d) Wet-day anomaly in percentage for April to September 1770. All anomalies are calculated with respect to the 1763 to 1812 climatology.

2.6   Conclusion

In this study, we present a reconstruction of 258 years of high-resolution daily temperature and precipitation fields for Switzerland covering the period of 1763 to 2020. The data set is available in the open-access repository PANGAEA (https://doi.pangaea.de/10.1594/PANGAEA.950236) (Imfeld et al., 2022). Meteorological fields were resampled based on the most similar days in a reference period calculated from station measurements. The resampled temperature fields were further improved with data assimilation and the resampled precipitation fields were bias corrected with quantile mapping. Extending a daily reconstruction for Switzerland as far back as the end of the 18th century was possible because of the data rescue efforts of CHIMES and follow-up projects (Brugnara et al., 2020b; Pfister et al., 2019; Brugnara et al., 2022).

Despite the considerable decrease in observations before 1864, the reconstruction still shows good results. Pearson correlations from a cross-validation of de-seasonalized temperature are between 0.58 and 0.99 and RMSEs are as high as 5° C including the very sparse network set-ups. Because very few or no station observations are available for the Alps and the south side of the Alps, the performance is considerably reduced in these regions. Cross-validation results for precipitation show lower performance than for temperature because few precipitation data were available and because precipitation is highly heterogeneous in space. The use of weather notes transformed to precipitation occurrence, however, increased the Spearman correlation and Brier score, especially around the measurement locations, but it decreased rapidly with increasing distance from the observations.

The validation with independent station data confirmed the better reconstruction skills for temperature for stations in the Plateau region and worse results for stations in the Alps. A comparison with an independent time series of precipitation occurrence showed that around 76 % of the days are assigned to wet or dry days correctly and that the reconstruction was able to reproduce the monthly wet-day frequencies, indicating that the few observations of precipitation occurrence helped to reconstruct the monthly signal.

However, several limitations have to be considered, when working with the data set. The results of the cross-validation cannot be used directly to infer the reconstruction skill in the historical period because the data quality differs and data gaps in the historical period have not been filled. Early instrumental data are a valuable source of information on daily weather in the 17th, 18th, and 19th centuries, but they come with uncertainties that are often hard to correct. A reconstruction based on such data inherits these errors and uncertainties. Also, the method assumes that our analogue pool represents the weather of the previous 200 years, but the 60 years of our analogue pool may not cover enough extreme events, which we are thus not able to reconstruct. Furthermore, the lack of

stations south of the Alps and in the Alps considerably lowers the reconstruction quality in these areas. Reconstruction errors were large in the south of Switzerland especially for precipitation, because the Alps act as a climatological barrier. Measurements would be needed to create a valid reconstruction for this area. Lastly, the changes in the network introduce inhomogeneities that need to be considered when working with long-term data.

Nevertheless, our case study on the famine years 1769 to 1772 shows that the wet and cold weather described in various documentary sources is reproduced in the reconstruction. The summer of 1770 was, for example, wetter and cooler than average, but it did not by far reach the wet and cold conditions of the summer of 1816 in Switzerland. The new reconstruction also opens up options of studying similar events in more detail, for example by feeding the reconstructed fields into crop models or hydrological models.

Further improvements in the data set could be obtained by incorporating more and better-corrected data. In particular, the long time series such as they have been created for Bern, Basel, Geneva, and Zurich (Brugnara et al., 2022) are very valuable. Despite being very tedious work, the precipitation reconstruction could profit substantially if more weather notes were digitized. Other reconstruction approaches have been and are being explored that could also contribute to improved reconstructions, for example machine learning techniques and data assimilation for precipitation as well as methods including temporal information in the reconstruction. Furthermore, for some applications, not only daily mean temperature but also minimum and maximum temperature, and sunshine duration are needed and could be reconstructed in a similar manner since gridded data for a reference period are available.

Code availability

The code for the data preparation and the temperature and precipitation reconstruction is available in the Supplement.

Data availability

Reconstructed daily precipitation and temperature data sets over the period 1763-01-02 to 2020-12-31 are published in the open-access repository PANGAEA https://doi.pangaea.de/10.1594/PANGAEA.950236) (Imfeld et al., 2022). Station data used for the reconstruction are referenced in the sources of the article.

Author contribution

NI performed the reconstruction and the case studies and wrote the paper. LP created the first version of the data set for the period of 1864 to 2017. YB provided the historical observations. SB provided the idea for the reconstruction and supervised the process. LP, YB, and SB contributed to the paper.

Acknowledgements

Appendix

Figure A.1: Cross-validation results of all networks shown in Figure 1a-e with 11, 21, 32, 43, and 108 time series used for reconstructing the temperature fields. The cross-validation results are based on annual de-seasonalized temperature anomalies during 1961-2020. a-e) Pearson correlation, f-j) RMSE, k-o) MSESS, and p-t) mean bias.
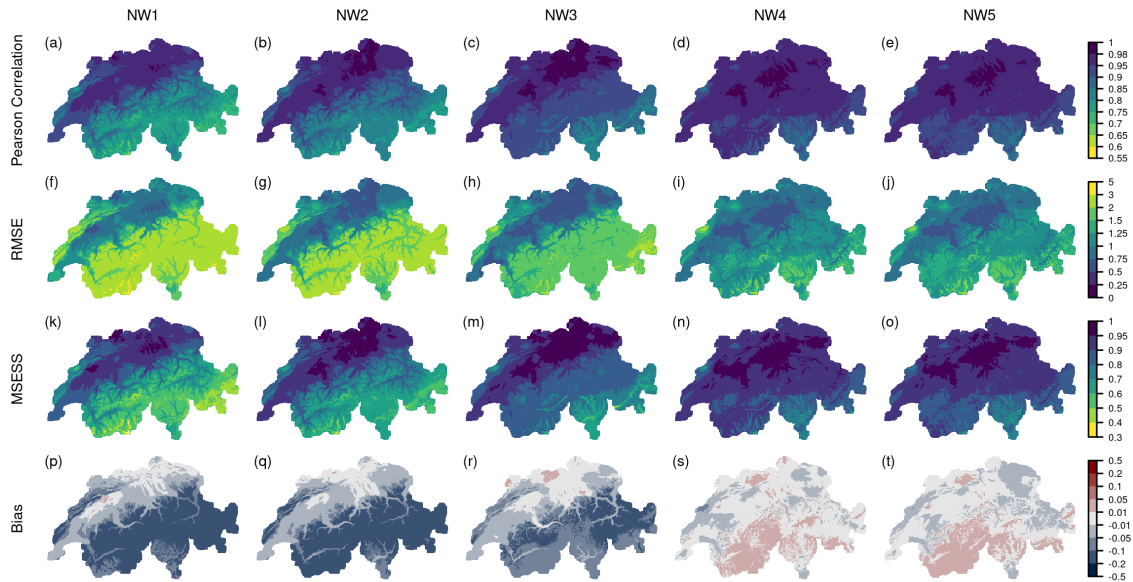
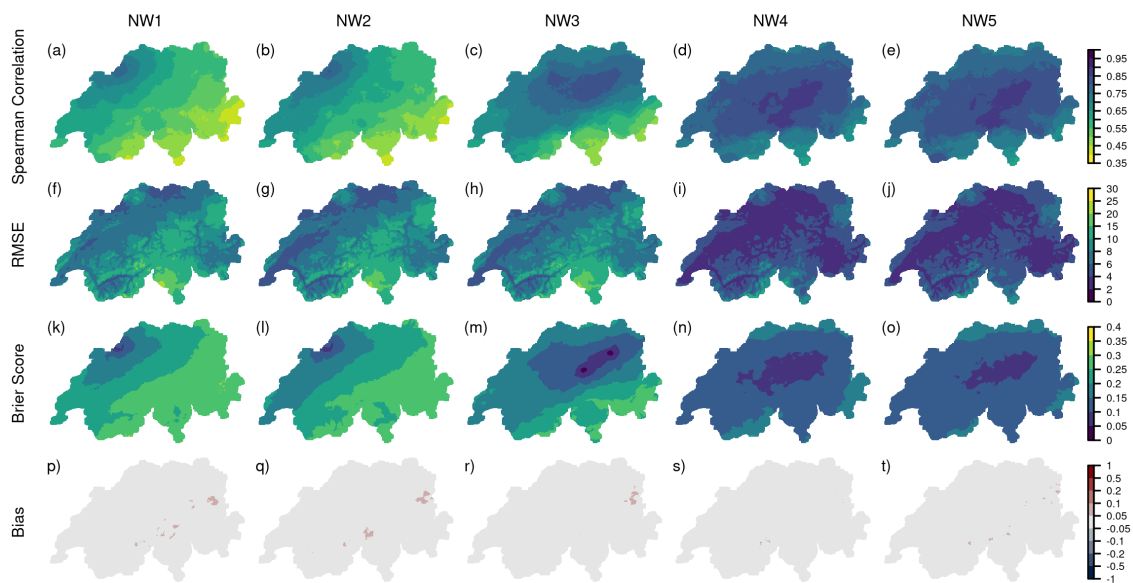*Figure A.2: Cross-validation results of all networks shown in Figure 1a-e with 11, 21, 32, 43, and 108 time series used for reconstructing the precipitation fields. The cross-validation results are based on annual daily precipitation during 1961-2020. a-e) Spearman correlation, f-j) RMSE, k-o) Brier score, and p-t) mean bias. The RhiresD data set also contains the northern catchments that drain into Switzerland.*
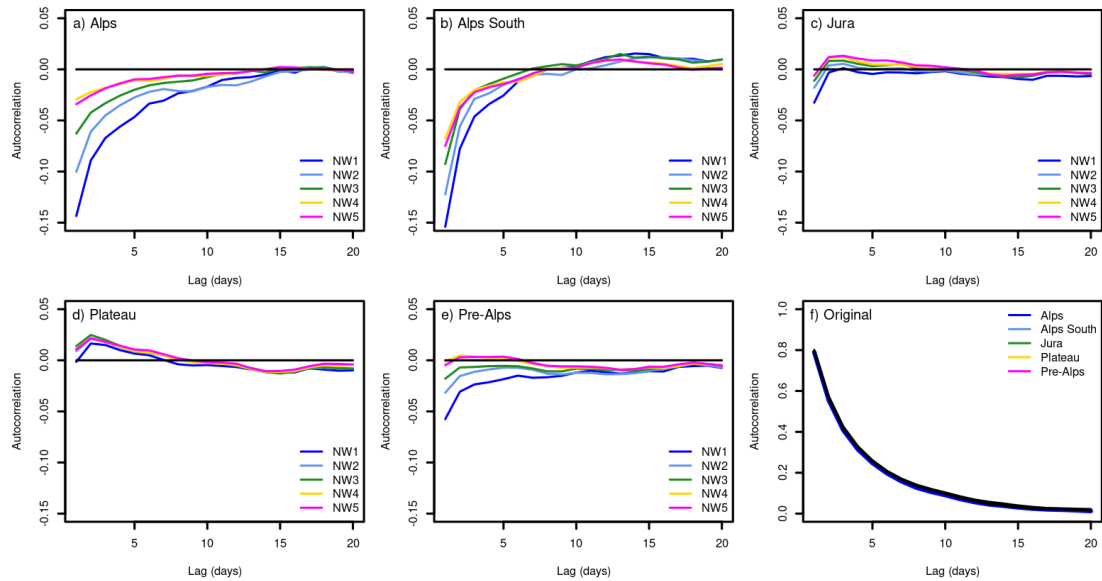
Figure A.3: a-e) Differences between the area mean autocorrelation of the original grid and the reconstructed grid for the five different networks and for five regions of Switzerland. f) Autocorrelation at lag day 1 to 20 for the original grid and for five regions covering Switzerland. The analysis is performed on the cross-validation results for the period of 1961 to 2020. See Fig. 2.1 for the network set-ups. The regions correspond to the major regions used for the national climate scenarios (NCCS, 2018).

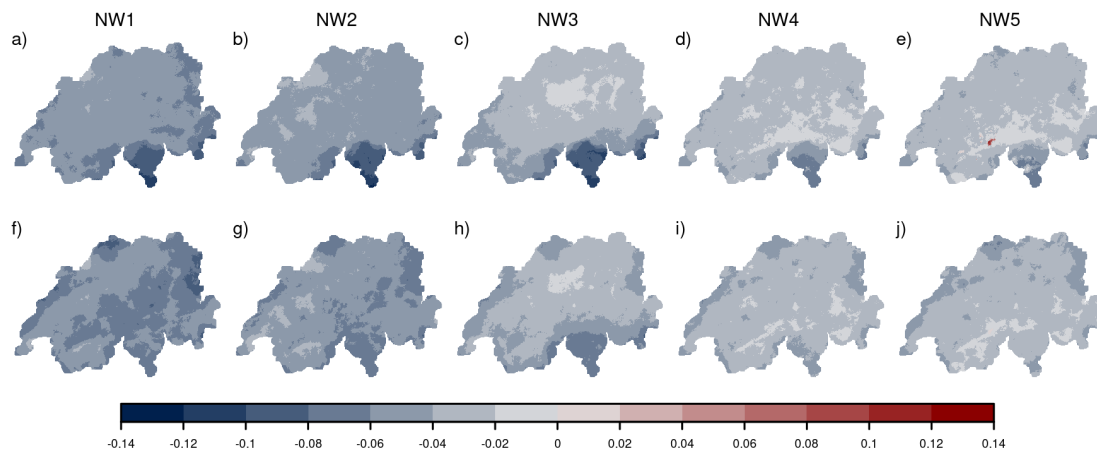*Figure A.4: a-e) Differences in the fraction of wet days followed by wet days for the cross-validations of the five networks (see Fig. 2.1) compared to the original data set (cross-validation minus original). f-j) Same but for the fraction of dry days followed by dry days. A wet day is defined as a day above 0.1 mm. The fractions are calculated across the entire cross-validation period of 1961 to 2020.*
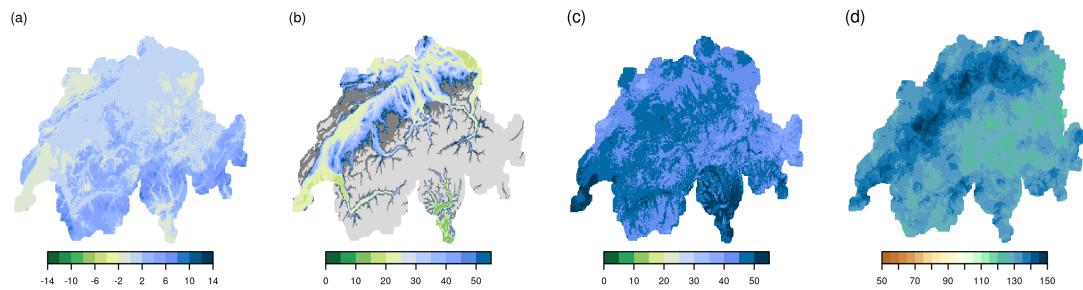
Figure A.5: a) Anomaly of the number of days with snowfall for April 1816. b) Anomaly in days for the year 1816 when the threshold of 1000 GDDs was reached. Light-grey areas denote values where no climatology of a 1000 GDD threshold was calculated because the threshold was reached in less than 75% of the years between 1763 and 1812. Dark grey denotes areas where the threshold of 1000 GDDs was not reached in the year 1816. c) Anomaly of the number of cold days (days below the 20th percentile of daily mean temperature) for April to September 1816. d) Wet-day anomaly in percentage for April to September 1816. For comparison with the summer of 1770, all anomalies are calculated with respect to the 1763 to 1812 climatology, which does not include the year 1816. Note that the colour scales are different from Fig. 2.10.

Bibliography

Baertschi, A.: Wetterberichte einer Oberländischen Gemeinde vom 15.-19. Jahrhundert, Hardermannli. Illlustrierte Sonntagsbeilage zum Oberländer Volksblatt, 16, 1916.

Begert, M., Schlegel, T., and Kirchhofer, W.: Homogeneous temperature and precipitation series of Switzerland from 1864 to 2000, International Journal of Climatology, 25, 65–80, doi:10.1002/joc.1118, 2005.

Begert, M., Seiz, G., Foppa, N., Schlegel, T., Appenzeller, C., and Müller, G.: Die Überführung der klimatologischen Referenzstationen der Schweiz in das Swiss National Basic Climatological Network (Swiss NBCN), Arbeitsberichte der MeteoSchweiz, 215, URL https://www.meteoschweiz.admin.ch/dam/jcr:07db700e-0e10-4b75-b17a-39febbeb3fa1/arbeitsbericht215.pdf, 2007.

Bhend, J., Franke, J., Folini, D., Wild, M., and Brönnimann, S.: An ensemble-based approach to climate reconstructions, Climate of the Past, 8, 963–976, doi:10.5194/cp-8-963-2012, 2012.

Böhm, R., Jones, P. D., Hiebl, J., Frank, D., Brunetti, M., and Maugeri, M.: The early instrumental warm-bias: a solution for long central European temperature series 1760–2007, Climatic Change, 101, 41–67, doi:10.1007/s10584-009-9649-4, 2010.

Bonhomme, R.: Bases and limits to using 'degree day' units, European Journal of Agronomy, 13, 1–10, 2000.

Brönnimann, S., ed.: Swiss Early Instrumental Meteorological Series, Geographica Bernensia G96, Bern, doi:10.4480/GB2022.G96, 2020.

Brönnimann, S.: From climate to weather reconstructions, PLOS Climate, 1, e0000 034, doi:10.1371/journal.pclm.0000034, 2022.

Brönnimann, S. and Brugnara, Y.: D'Annone's Meteorological Series from Basel, 1755–1804. Swiss Early Instrumental Meteorological Series, Bern: Geographica Bernensia, G96, 119–126, doi:10.4480/GB2020.G96.11, 2020a.

Brönnimann, S. and Brugnara, Y.: The meteorological series from the Great St. Bernard, 1817-1863. Swiss Early Instrumental Meteorological Series, Bern: Geographica Bernensia, G96, 109–117, doi:10.4480/GB2020.G96.10, 2020b.

Brönnimann, S. and Brugnara, Y.: Meteorological Series from Basel, 1825–1863. Swiss Early Instrumental Meteorological Series, Bern: Geographica Bernensia, G96, 127–138, doi:10.4480/GB2020.G96.12, 2021.

Brönnimann, S. and Brugnara, Y.: Nineteenth century meteorological records from Vevey, Einsiedeln,Bellinzona, Lucerne, Fribourg, and Zug. Swiss Early Instrumental Meteorological Series, Bern: Geographica Bernensia, G96, 245–259, doi:10.4480/GB2020.G96.22, 2022.

Brönnimann, S., Bühler, M., and Brugnara, Y.: The series from Geneva, 1799–1863. Swiss Early Instrumental Meteorological Series, Bern: Geographica Bernensia, G96, 47–59, doi:10.4480/GB2020.G96.04, 2020.

Brugnara, Y.: Early Instrumental Temperature Records for Basel, Bern, Geneva, and Zurich, Bern Open Repository and Information System (BORIS) [data set], doi:10.48620/74, 2022.

Brugnara, Y., Brönnimann, S., Zamuriano Carbajal, J. M., Schild, J., Rohr, C., and Segesser, D.: Reanalysis sheds lights on 1916 avalanche disaster, ECMWF Newsletter, pp. 28–34, doi:10.21957/h9b197, 2017.

Brugnara, Y., Gilabert, A., Ventura, C., and Hunziker, S.: dataresqc: Quality control tools for climate data developed by the C3S Data Rescue Service, 2019.

Brugnara, Y., Flückiger, J., and Brönnimann, S.: Instruments, procedures, processing, and analyses. Swiss Early Instrumental Meteorological Series., Bern: Geographica Bernensia, G96, 17–32, doi:10.4480/GB2020.G96.02, 2020a.

Brugnara, Y., Pfister, L., Villiger, L., Rohr, C., Isotta, F. A., and Brönnimann, S.: Early instrumental meteorological observations in Switzerland: 1708–1873, Earth System Science Data, 12, 1179–1190, doi:10.5194/essd-12-1179-2020, 2020b.

Brugnara, Y., Hari, C., Pfister, L., Valler, V., and Brönnimann, S.: Pre-industrial Temperature Variability on the Swiss Plateau Derived from the Instrumental Daily Series of Bern and Zurich, Climate of the Past Discussions, pp. 1–34, doi:10.5194/cp-2022-34, 2022.

Brönnimann, S., Allan, R., Ashcroft, L., Baer, S., Barriendos, M., Brázdil, R., Brugnara, Y., Brunet, M., Brunetti, M., Chimani, B., Cornes, R., Domínguez-Castro, F., Filipiak, J., Founda, D., Herrera, R. G., Gergis, J., Grab, S., Hannak, L., Huhtamaa, H., Jacobsen, K. S., Jones, P., Jourdain, S., Kiss, A., Lin, K. E., Lorrey, A., Lundstad, E., Luterbacher, J., Mauelshagen, F., Maugeri, M., Maughan, N., Moberg, A., Neukom, R., Nicholson, S., Noone, S., Øyvind Nordli, Ólafsdóttir, K. B., Pearce, P. R., Pfister, L., Pribyl, K., Przybylak, R., Pudmenzky, C., Rasol, D., Reichenbach, D., Řezníčková, L., Rodrigo, F. S., Rohr, C., Skrynyk, O., Slonosky, V., Thorne, P., Valente, M. A., Vaquero, J. M., Westcottt, N. E., Williamson, F., and Wyszyński", P.: Unlocking Pre-1850

Instrumental Meteorological Records: A Global Inventory, Bulletin of the American Meteorological Society, 100, ES389 – ES413, doi:10.1175/BAMS-D-19-0040.1, 2019.

Caillouet, L., Vidal, J.-P., Sauquet, E., Graff, B., and Soubeyroux, J.-M.: SCOPE Climate: a 142-year daily high-resolution ensemble meteorological reconstruction dataset over France, Earth System Science Data, 11, 241–260, doi:10.5194/essd-11-241-2019, 2019.

Camuffo, D. and Jones, P.: Improved understanding of past climatic variability from early daily European instrumental sources, Springer Dordrecht, doi:10.1007/978-94-010-0371-1, 2002.

Casty, C., Wanner, H., Luterbacher, J., Esper, J., and Böhm, R.: Temperature and precipitation variability in the European Alps since 1500, International Journal of Climatology, 25, 1855–1880, doi:10.1002/joc.1216, 2005.

Casty, C., Raible, C. C., Stocker, T. F., Wanner, H., and Luterbacher, J.: A European pattern climatology 1766–2000, Climate Dynamics, 29, 791–805, doi:10.1007/s00382-007-0257-6, 2007.

Collet, D.: Die doppelte Katastrophe: Klima und Kultur in der europäischen Hungerkrise 1770–1772., vol. 18 of *Umwelt und Gesellschaft*, Vandenhoeck & Ruprecht, doi:10.13109/9783666355929, 2018.

Cook, E. R., Seager, R., Kushnir, Y., Briffa, K. R., Büntgen, U., Frank, D., Krusic, P. J., Tegel, W., van der Schrier, G., Andreu-Hayles, L., et al.: Old World megadroughts and pluvials during the Common Era, Science Advances, 1, e1500 561, 2015.

Cornes, R. C., van der Schrier, G., van den Besselaar, E. J., and Jones, P. D.: An ensemble version of the E-OBS temperature and precipitation data sets, Journal of Geophysical Research: Atmospheres, 123, 9391–9409, doi:10.1029/2017JD028200, 2018.

Devers, A., Vidal, J.-P., Lauvernet, C., and Vannier, O.: FYRE Climate: a high-resolution reanalysis of daily precipitation and temperature in France from 1871 to 2012, Climate of the Past, 17, 1857–1879, doi:10.5194/cp-17-1857-2021, 2021.

Dobrovolnỳ, P., Moberg, A., Brázdil, R., Pfister, C., Glaser, R., Wilson, R., van Engelen, A., Limanówka, D., Kiss, A., Halíčková, M., et al.: Monthly, seasonal and annual temperature reconstructions for Central Europe derived from documentary evidence and instrumental records since AD 1500, Climatic Change, 101, 69–107, doi:10.1007/s10584-009-9724-x, 2010.

Estévez, J., Gavilán, P., and García-Marín, A.: Spatial regression test for ensuring temperature data quality in southern Spain, Theoretical and Applied Climatology, 131, 309–318, doi:10.1007/s00704-016-1982-8, 2018.

Faden, M., Villiger, L., Brugnara, Y., and Brönnimann, S.: The meteorological series from Aarau, 1807–1865. Swiss Early Instrumental Meteorological Series, Bern: Geographica Bernensia, G96, 61–72, doi:10.4480/GB2020.G96.05, 2020.

Feigenwinter, I., Kotlarski, S., Casanueva, A., Schwierz, C., and Liniger, M.: Exploring quantile mapping as a tool to produce user-tailored climate scenarios for Switzerland, MeteoSchweiz, URL https://www.meteoswiss.admin.ch/dam/jcr:1b810050-11a2-415d-b439-3b2eb75f9693/MeteoSchweiz_Fachbericht_270_final.pdf, (last access: 23 March 2023), 2018.

Flückiger, S., Brönnimann, S., Holzkämper, A., Fuhrer, J., Krämer, D., Pfister, C., and Rohr, C.: Simulating crop yield losses in Switzerland for historical and present Tambora climate scenarios, Environmental Research Letters, 12, 074 026, doi:10.1088/1748-9326/aa7246, 2017.

Franke, J., Brönnimann, S., Bhend, J., and Brugnara, Y.: A monthly global paleo-reanalysis of the atmosphere from 1600 to 2005 for studying past climatic variations, Scientific Data, 4, 1–19, doi:10.1038/sdata.2017.76, 2017.

Frei, C.: Interpolation of temperature in a mountainous region using nonlinear profiles and non-Euclidean distances, International Journal of Climatology, 34, 1585–1605, doi:10.1002/joc.3786, 2014.

Füllemann, C., Begert, M., Croci-Maspoli, M., and Bönnimann, S.: Digitalisieren und Homogenisieren von historischen Klimadaten des Swiss NBCN: Resultate aus DigiHom, Arbeitsberichte der MeteoSchweiz, 236, URL https://www.meteoswiss.admin.ch/dam/jcr:c0d90a48-a05d-4ac9-9cf3-10769270d75e/ab236.pdf, (last access: 23 March 2023), 2011.

Gómez-Navarro, J. J., Zorita, E., Raible, C. C., and Neukom, R.: Pseudo-proxy tests of the analogue method to reconstruct spatially resolved global temperature during the Common Era, Climate of the Past, 13, 629–648, doi:10.5194/cp-13-629-2017, 2017.

Gower, J. C.: A general coefficient of similarity and some of its properties, Biometrics, pp. 857–871, doi:10.2307/2528823, 1971.

Gudmundsson, L., Bremnes, J. B., Haugen, J. E., and Engen-Skaugen, T.: Downscaling RCM precipitation to the station scale using statistical transformations–a comparison of methods, Hydrology and Earth System Sciences, 16, 3383–3390, doi:10.5194/hessd-9-6185-2012, 2012.

Häderli, S., Pfister, S. M., Villiger, L., Brugnara, Y., and Brönnimann, S.: Two meteorological series from Geneva, 1782–1791. Swiss Early Instrumental Meteorological Series, Bern: Geographica Bernensia, G96, 33–46, doi:10.4480/GB2020.G96.03, 2020.

Hari, C., Brugnara, Y., Rohr, C., and Brönnimann, S.: Meteorological Observations in Bern and Vicinity, 1777-1834. Swiss Early Instrumental Meteorological Series, Bern: Geographica Bernensia, G96, 199–211, doi:10.4480/GB2020.G96.19, 2022.

Harvey-Fishenden, A. and Macdonald, N.: Evaluating the utility of qualitative personal diaries in precipitation reconstruction in the eighteenth and nineteenth centuries, Climate of the Past, 17, 133–149, doi:10.5194/cp-17-133-2021, 2021.

Hersbach, H., Bell, B., Berrisford, P., Hirahara, S., Horányi, A., Muñoz-Sabater, J., Nicolas, J., Peubey, C., Radu, R., Schepers, D., et al.: The ERA5 global reanalysis, Quarterly Journal of the Royal Meteorological Society, 146, 1999–2049, doi:10.1002/qj.3803, 2020.

Hupfer, F.: Das Wetter der Nation: Meteorologie, Klimatologie und der schweizerische Bundesstaat, 1860–1914, Chronos Verlag, 2019.

Hürzeler, A., Brugnara, Y., and Brönnimann, S.: The meteorological record from St. Gall, 1812–1853. Swiss Early Instrumental Meteorological Series, Bern: Geographica Bernensia, G96, 87–95, doi:10.4480/GB2020.G96.07, 2020.

Imfeld, N., Pfister, L., Brugnara, Y., , and Brönnimann, S.: Daily high-resolution temperature and precipitation fields for Switzerland from 1763 to 2020, PANGAEA [data set], doi:10.1594/PANGAEA.950236, 2022.

Isotta, F. A., Begert, M., and Frei, C.: Long-term consistent monthly temperature and precipitation grid data sets for Switzerland over the past 150 years, Journal of Geophysical Research: Atmospheres, 124, 3783–3799, doi:10.1029/2018JD029910, 2019.

Jennings, K. S., Winchell, T. S., Livneh, B., and Molotch, N. P.: Spatial variation of the rain–snow temperature threshold across the Northern Hemisphere, Nature communications, 9, 1–9, doi:10.1038/s41467-018-03629-7, 2018.

Keller, V., Tanguy, M., Prosdocimi, I., Terry, J., Hitt, O., Cole, S., Fry, M., Morris, D., and Dixon, H.: CEH-GEAR: 1 km resolution daily and monthly areal rainfall estimates for the UK for hydrological and other applications, Earth System Science Data, 7, 143–155, doi:10.5194/essd-7-143-2015, 2015.

Kienzle, S. W.: A new temperature based method to separate rain and snow, Hydrological Processes, 22, 5067–5085, doi:10.1002/hyp.7131, 2008.

Klein Tank, A., Wijngaard, J., Können, G., Böhm, R., Demarée, G., Gocheva, A., Mileta, M., Pashiardis, S., Hejkrlik, L., Kern-Hansen, C., et al.: Daily dataset of 20th-century surface air temperature and precipitation series for the European Climate Assessment, International Journal of Climatology, 22, 1441–1453, doi:10.1002/joc.773, 2002.

Kohler, X.: Observations Météorologiques, Économiques et Rurales dans l'Erguel et la Prévôté de Moutier de 1747 à 1804 par le pasteur T. Frêne, in: Actes de la Société Jurassienne d' Émulation, 22, pp. 213–267, doi:10.5169/seals-684289, 1871.

Kuhn, M. and Johnson, K.: Feature engineering and selection: A practical approach for predictive models, CRC Press, 2019.

Luterbacher, J. and Pfister, C.: The year without a summer, Nature Geoscience, 8, 246–248, doi:10.1038/ngeo2404, 2015.

Luterbacher, J., Dietrich, D., Xoplaki, E., Grosjean, M., and Wanner, H.: European Seasonal and Annual Temperature Variability, Trends, and Extremes Since 1500, Science, 303, 1499–1503, doi:10.1126/science.1093877, 2004.

MeteoSwiss: Documentation of MeteoSwiss Grid-Data Products. Daily Precipitation (final analysis): RhiresD, https://www.meteoswiss.admin.ch/content/dam/meteoswiss/de/service-und-publikationen/produkt/raeumliche-daten-niederschlag/doc/ProdDoc_RhiresD.pdf, (last access: 30 June 2022), 2021a.

MeteoSwiss: Documentation of MeteoSwiss Grid-Data Products. Daily Mean, Minimum and Maximum Temperature: TabsD, TminD, TmaxD, https://www.meteoswiss.admin.ch/content/dam/meteoswiss/de/service-und-publikationen/produkt/raeumliche-daten-temperatur/doc/ProdDoc_TabsD.pdf, (last access: 30 June 2022), 2021b.

MeteoSwiss: Documentation of MeteoSwiss Grid-Data Products. Monthly Temperature and Precipitation Reconstructions, https://www.meteoschweiz.admin.ch/dam/jcr:98a965e5-30dd-4fdf-a42b-74c414a4a731/ProdDoc_rec.pdf, (last access: 23 February 2023), 2021c.

Miller, P., Lanier, W., and Brandt, S.: Using growing degree days to predict plant stages, Montguide MT200103 AG, URL https://landresources.montana.edu/soilfertility/documents/PDF/pub/GDDPlantStagesMT200103AG.pdf, (last access: 23 March 2023), 2001.

Moon, H., Gudmundsson, L., Guillod, B. P., Venugopal, V., and Seneviratne, S. I.: Intercomparison of daily precipitation persistence in multiple global observations and climate models, Environmental Research Letters, 14, 105 009, doi:10.1088/1748-9326/ab4169, 2019.

Muñoz-Sabater, J., Dutra, E., Agustí-Panareda, A., Albergel, C., Arduini, G., Balsamo, G., Boussetta, S., Choulga, M., Harrigan, S., Hersbach, H., et al.: ERA5-Land: A state-

of-the-art global reanalysis dataset for land applications, Earth System Science Data, 13, 4349–4383, doi:10.5194/essd-13-4349-2021, 2021.

Murphy, C., Wilby, R. L., Matthews, T., Horvath, C., Crampsie, A., Ludlow, F., Noone, S., Brannigan, J., Hannaford, J., McLeman, R., et al.: The forgotten drought of 1765–1768: Reconstructing and re-evaluating historical droughts in the British and Irish Isles, International Journal of Climatology, 40, 5329–5351, doi:10.1002/joc.6521, 2020.

NCCS: Major regions, URL https://www.nccs.admin.ch/nccs/en/home/regions/grossregionen.html, (last access: 01 February 2023), 2018.

Paffrath, J.: Schriften des Vereins für die Geschichte des Bodensees und seiner Umgebung, chap. Zum Wetterverlauf am Bodensee, Kommissionsverlag von Joh. Thom. Stettner, Lindau, 1915.

PAGES2kConsortium: Continental-scale temperature variability during the past two millennia, Nature Geoscience, 6, 339–346, doi:10.1038/ngeo1797, 2013.

Pappert, D., Barriendos, M., Brugnara, Y., Imfeld, N., Jourdain, S., Przybylak, R., Rohr, C., and Brönnimann, S.: Statistical reconstruction of daily temperature and sea-level pressure in Europe for the severe winter 1788/9, Climate of the Past Discussions, pp. 1–35, doi:10.5194/cp-18-2545-2022, 2022.

Pauling, A., Luterbacher, J., Casty, C., and Wanner, H.: Five hundred years of gridded high-resolution precipitation reconstructions over Europe and the connection to large-scale circulation, Climate Dynamics, 26, 387–405, doi:10.1007/s00382-005-0090-8, 2006.

Pfister, C.: Agrarkonjunktur und Witterungsverlauf im westlichen schweizer Mittelland zur Zeit der ökonomischen Patrioten, 1755-1797: ein Beitrag zur Umwelt-u. Wirtschaftsgeschichte des 18. Jahrhunderts, PhD Thesis, vol. 2, Lang Druck AG, 1975.

Pfister, C.: Das Klima der Schweiz von 1525-1860 und seine Bedeutung in der Geschichte von Bevölkerung und Landwirtschaft, vol. 1, Haupt, 1988.

Pfister, C. and Brázdil, R.: Social vulnerability to climate in the" Little Ice Age": an example from Central Europe in the early 1770s, Climate of the Past, 2, 115–129, doi:10.5194/cp-2-115-2006, 2006.

Pfister, C. and Wanner, H.: Klima und Gesellschaft in Europa. Die letzten tausend Jahre, Haupt Verlag, 2021.

Pfister, C., Rohr, C., and Jover, A. C. C.: Euro-Climhist: eine Datenplattform der Universität Bern zur Witterungs-, Klima-und Katastrophengeschichte, Wasser Energie Luft, 109, doi:10.7892/boris.97013, 2017.

Pfister, L., Hupfer, F., Brugnara, Y., Munz, L., Villiger, L., Meyer, L., Schwander, M., Isotta, F. A., Rohr, C., and Brönnimann, S.: Early instrumental meteorological measurements in Switzerland, Climate of the Past, 15, 1345–1361, doi:10.5194/cp-15-1345-2019, 2019.

Pfister, L., Brönnimann, S., Schwander, M., Isotta, F. A., Horton, P., and Rohr, C.: Statistical reconstruction of daily precipitation and temperature fields in Switzerland back to 1864, Climate of the Past, 16, 663–678, doi:10.5194/cp-16-663-2020, 2020.

Piuz, A.-M.: Climat, récoltes et vie des hommes à Genève, XVIe-XVIIIe siècle, Annales. Histoire, Sciences Sociales, 29, 599–618, doi:10.3406/ahess.1974.293496, 1974.

Rajczak, J., Kotlarski, S., and Schär, C.: Does quantile mapping of simulated precipitation correct for biases in transition probabilities and spell lengths?, Journal of Climate, 29, 1605–1615, doi:10.1175/JCLI-D-15-0162.1, 2016.

Rössler, O. and Brönnimann, S.: The effect of the Tambora eruption on Swiss flood generation in 1816/1817, Science of The Total Environment, 627, 1218–1227, doi:10.1016/j.scitotenv.2018.01.254, 2018.

Rutishauser, T., Brönnimann, S., Gehrig, R., Pietragalla, B., Baumgarten, F., Vitasse, Y., Stöckli, S., Pfister, C., Holzkämper, A., Hund, A., Fossati, D., Meier, M., Weingartner, R., and Buchmann, M.: Klimawandel und Jahreszeiten (Reihe G Grundlagenforschung G97), Geographica Bernensia, doi:10.4480/GB2020.G97.01, 2020.

Schaller-Donauer, A.: Chronik der Naturereignisse im Urnerland 1000-1800, Gotthardpost, 1937.

Schenk, F. and Zorita, E.: Reconstruction of high resolution atmospheric fields for Northern Europe using analog-upscaling, Climate of the Past, 8, 1681–1703, doi:10.5194/cp-8-1681-2012, 2012.

Scherrer, S. C. and Appenzeller, C.: Fog and low stratus over the Swiss Plateau- a climatological study, International Journal of Climatology, 34, 678–686, doi:10.1002/joc.3714, 2014.

Schwander, M., Brönnimann, S., Delaygue, G., Rohrer, M., Auchmann, R., and Brugnara, Y.: Reconstruction of Central European daily weather types back to 1763, International Journal of Climatology, 37, 30–44, doi:10.1002/joc.4974, 2017.

Slivinski, L. C., Compo, G. P., Whitaker, J. S., Sardeshmukh, P. D., Giese, B. S., McColl, C., Allan, R., Yin, X., Vose, R., Titchner, H., et al.: Towards a more reliable

historical reanalysis: Improvements for version 3 of the Twentieth Century Reanalysis system, Quarterly Journal of the Royal Meteorological Society, 145, 2876–2908, doi:10.1002/qj.3598, 2019.

Strasser, G.: Grindelwaldner Chroniken, Gletschermann. Familienblatt für Grindelwald, doi:10.3931/e-rara-78062, 1890.

Stucki, P., Brönnimann, S., Martius, O., Welker, C., Rickli, R., Dierer, S., Bresch, D. N., Compo, G. P., and Sardeshmukh, P. D.: Dynamical downscaling and loss modeling for the reconstruction of historical weather extremes and their impacts: a severe Foehn storm in 1925, Bulletin of the American Meteorological Society, 96, 1233–1241, doi:10.1175/BAMS-D-14-00041.1, 2015.

Trümpi, C.: Neuere Glarner Chronik, Verlag Heinrich Steiners und Comp. und der Herren Buchbinder, doi:10.3931/e-rara-18988, 1774.

Valler, V., Franke, J., Brugnara, Y., and Brönnimann, S.: An updated global atmospheric paleo-reanalysis covering the last 400 years, Geoscience Data Journal, p. 89–107, doi:10.1002/gdj3.121, 2022.

Walser, G.: Neue Appenzeller Chronik oder Geschichte des Landes Appenzell der Innern und Aussern Rhoden, vol. 1-2, doi:10.3931/e-rara-24883, 1731.

Wang, X., Toride, K., and Yoshimura, K.: Impact of Gaussian Transformation on Cloud Cover Data Assimilation for Historical Weather Reconstruction, Earth and Space Science Open Archive ESSOAr, doi:10.1002/essoar.10506932.2, 2021.

Wang, X. L.: Penalized maximal F test for detecting undocumented mean shift without trend change, Journal of Atmospheric and Oceanic Technology, 25, 368–384, doi:10.1175/2007JTECHA982.1, 2008.

Wang, X. L. and Feng, Y.: RHtestsV4 user manual, Climate Research Division, Atmospheric Science and Technology Directorate, Science and Technology Branch, Environment Canada, 28, 2013.

Wang, X. L., Wen, Q. H., and Wu, Y.: Penalized maximal t test for detecting undocumented mean change in climate data series, Journal of Applied Meteorology and Climatology, 46, 916–931, doi:10.1175/JAM2504.1, 2007.

Wartenburger, R., Brönnimann, S., and Stickler, A.: Observation errors in early historical upper-air observations, Journal of Geophysical Research: Atmospheres, 118, 12–012, doi:10.1002/2013JD020156, 2013.

Weber, J., Brugnara, Y., and Brönnimann, S.: Two meteorological series from Herisau, 1821–1844. Swiss Early Instrumental Meteorological Series, Bern: Geographica Bernensia, G96, 73–85, doi:10.4480/GB2020.G96.06, 2020.

Weusthoff, T.: Weather Type Classification at MeteoSwiss-Introduction of new automatic classification schemes. Arbeitsberichte der MeteoSchweiz, 235, 46, URL https://www.meteoswiss.admin.ch/dam/jcr:ca090643-2407-49f3-9737-a3e55645cfb4/ab235.pdf, (last access: 24 March 2023), 2011.

Whitaker, J. S. and Hamill, T. M.: Ensemble data assimilation without perturbed observations, Monthly Weather Review, 130, 1913–1924, doi:10.1175/1520-0493(2002)130%3C1913:EDAWPO%3E2.0.CO;2, 2002.

Wilks, D. S.: Statistical methods in the atmospheric sciences, vol. 100, Academic press, doi:10.1016/C2017-0-03921-6, 2011.

Winkler, P.: Hohenpeißenberg: 1781-2006; das älteste Bergobservatorium der Welt; 225 Jahre Meteorologisches Observatorium Hohenpeißenberg, Deutscher Wetterdienst, 2006.

Wyer, V., Brugnara, Y., and Brönnimann, S.: Meteorological Series from Neuchâtel, Bern, and Gurzelen from the 18th Century. Swiss Early Instrumental Meteorological Series, Bern: Geographica Bernensia, G96, 169–182, doi:10.4480/GB2020.G96.16, 2021.

Wypych, A., Sulikowska, A., Ustrnul, Z., and Czekierda, D.: Variability of growing degree days in Poland in response to ongoing climate changes in Europe, International Journal of Biometeorology, 61, 49–59, doi:10.1007/s00484-016-1190-3, 2017.

Zubler, E. M., Scherrer, S. C., Croci-Maspoli, M., Liniger, M. A., and Appenzeller, C.: Key climate indices in Switzerland; expected changes in a future climate, Climatic change, 123, 255–271, doi:10.1007/s10584-013-1041-8, 2014.

Zumbühl, H. J.: Die Schwankungen des Unteren Grindelwaldgletschers, in: Die Schwankungen der Grindelwaldgletscher in den historischen Bild-und Schriftquellen des 12. bis 19. Jahrhunderts, pp. 15–55, Springer, doi:10.1007/978-3-0348-6546-3_2, 1980.

Chapter 3

Extreme springs in Switzerland since 1763 in climate and phenological indices

Noemi Imfeld[1,2], Koen Hufkens[1,2], and Stefan Brönnimann[1,2]

1. Oeschger Center for Climate Change Research, University of Bern, Switzerland.
2. Institute of Geography, University of Bern, Switzerland.

Abstract

Historical sources report manifold on hazardous past climate and weather events that had considerable impacts on society. Studying changes in the occurrence or mechanisms behind such events is, however, hampered by a lack of spatially and temporally complete weather data. Especially, the spring season has received less attention in comparison to summer and winter, but is nevertheless relevant since weather conditions in spring can delay vegetation and create substantial damage due to for example late frost events. For Switzerland, we created a daily high-resolution (1x1 km^2) reconstruction of temperature and precipitation fields from 1763 to 1960, that forms together with present-day meteorological fields a 258-year-long gridded data set. With this data set, we study changes in longer-term climate and historical weather events based on climate and phenological indices focusing on the spring season.

Climate and phenological indices show few changes in the mean during the first 200 years, but climate change signals clearly emerge in all indices in the most recent period. We evaluate the climate and phenological indices for three cases of extreme spring weather conditions, an unusually warm spring, two late frost events, and three cold springs. Warm springs are much more frequent in the 21st century, but also in 1862 a very warm and early spring occurred. Spring temperatures, however, do not agree on how anomalously warm the spring was when comparing the Swiss reconstruction with reanalyses that extend back to 1868. The three springs of 1785, 1837, and 1853, were particularly cold with historical sources reporting for example prolonged lake freezing and abundant snowfall. Whereas the springs of 1837 and 1853 were characterized by cold and wet conditions, in the spring of 1785 wet days were below average, and, in particular, in the Swiss Plateau, frost days reached an all-time maximum. Such inversion conditions are confirmed by mostly north-easterly and high pressure weather types and historical sources describing prolonged Bise conditions. Studying such historical events is valuable since similar atmospheric conditions can also nowadays lead to cold springs affecting vegetation growth and agricultural production.

3.1 Introduction

Studies of long-term climate variability often focus on the summer or winter season. However, climate in spring is equally important, for example, for plant growth, and may have far reaching impacts. Cold spells in spring can delay crop growth considerably, late frost events can destroy harvests, and spring snowfall may put trees at risk. Moreover, late beech leaf unfolding may prolong the spring wildfire season as sunlight penetrates to the ground and dries the litter layer. Studying such adverse weather conditions in spring requires daily data, from which targeted climate indices can be calculated. Studies have evaluated changes in climate indices over the last few decades (e.g. Brown et al., 2010; Domínguez-Castro et al., 2020; Zhang et al., 2011), also focusing specifically on spring conditions, such as changes in late frost occurrence and safety margins of plants (e.g. Wypych et al., 2017; Vitasse et al., 2018). Only very few studies, however, extended analyses of daily-based climate indices across several centuries because the temporally complete daily data that is needed is scarcely available (Brugnara et al., 2022; Parker et al., 1992; Diodato et al., 2020). In particular from a historical perspective evaluating daily-based indices, such as the occurrence of frost days or the occurrence of the last frost day in spring can be relevant as they are often reported in historical documents (Zhang et al., 2011; Pfister et al., 2017). Studying historical weather conditions in spring may also contribute to our understanding of adverse spring weather since it extends the sample of extreme events.

For Switzerland, we created a daily high-resolution (1x1 km^2) reconstruction of temperature and precipitation fields from 1763 to 1960 (Imfeld et al., 2023), that forms together with present-day meteorological fields a 258-year-long gridded data (MeteoSwiss, 2021a,b). This data set allows us to calculate impact-relevant climate and phenological indices for the 258-year-long period and to study longer-term climate and past extreme springs since 1763. A dense network of phenological observations exists in Switzerland starting in 1951 (Auchmann et al., 2018; Brugnara et al., 2020a), but for earlier periods, historical phenological observations are sparse. Thus, we used numerical approaches to model phenology from the gridded daily meteorological data.

This article is organized as follows. In Sect. 2, we describe the meteorological data used to calculate climate and phenological indices. In Sect. 3, we describe the calculation of the climate indices and the phenological application. In Sect. 4, we describe the long-term changes in the climate and phenological indices, and analyze these indices for three different extreme spring cases, a warm spring, two frost events, and three cold springs. These results are discussed in Sect. 5. In Sect. 6, we conclude our article.

3.2 Data

3.2.1 Meteorological data

For the calculation of climate and phenological indices, we used a reconstruction of 258 years of daily mean temperature and daily precipitation sums for Switzerland covering a period from 2 January 1763 to 31 December 2020 with a resolution of 1 km (Imfeld et al., 2023). For precipitation, the gridded dataset also covers catchment areas outside Switzerland. These meteorological fields were reconstructed with the analog resampling method, quantile mapping, and data assimilation. The analog resampling and data assimilation are performed using a large number of instrumental measurement series from Switzerland and neighbouring regions. The data sets consist of two main sub-periods with different reconstruction skills due to the availability and quality of the input data. From 1763 to 1864, the reconstruction shows good skills for daily temperature with correlations on average between 0.80 and 0.96 (calculated from the anomalies of a climatological annual cycle) and root mean squared errors on average between 1 and 2.6 °C depending on the input station network and season. For precipitation, the reconstruction skill for the period from 1763 to 1864 is considerably lower with correlations on average between 0.6 and 0.8 and root mean squared errors between 6 and 10 mm depending on station network and season. However, the number of monthly wet days compares well to independent observations. After 1864, reconstruction skills are much improved across Switzerland for both temperature and precipitation data. Despite the drawbacks in the early period, we used this novel data set, since it is the first one offering daily data at a high spatial resolution. A detailed description of the reconstruction is found in Imfeld et al. (2023).

3.2.2 Reanalyses and weather types

In addition, we used the station-based daily temperature time series for the Swiss Plateau derived from the series of Bern and Zurich (Brugnara et al., 2022), further denoted as the "Swiss series", the reanalysis 20CRv3 starting in 1807 (Slivinski et al., 2019), and the Modern Era Reanalysis ModE-RA (Valler et al., in review) to calculate the same indices. Note that these data sets are not fully independent of the Swiss reconstruction since they all rely partly on the same input data. From the reanalysis 20CRv3, we selected out of the four closest grid cells, the cell that correlates well and had a low bias compare to the Swiss Plateau area mean value. For ModE-RA, we used the grid cell in the northwest of Switzerland because it had a low biases in comparison to the Swiss Plateau area mean. 20CRv3 assimilates pressure observations from Hohenpeissenberg, Torino, and Geneva, which are also used in the Swiss reconstruction (Imfeld et al., 2023), whereas ModE-RA assimilates pressure, temperature, and wet days, but on a monthly resolution. 20CRv3

and ModE-RA were further used to analyze similar atmospheric conditions during the extreme spring examples. To evaluate the occurrence of weather types, we considered the reconstruction of Schwander et al. (2017) starting in 1763.

3.3 Methods

3.3.1 Climate indices

We selected eight different climate indices for daily mean temperature and precipitation (Tab. 3.1, upper row) which have been suggested by the Expert Team on Climate Change Detection and Indices (ETCCDI) (e.g. Zhang et al., 2011). They are not exclusively based on spring weather, i.e. some are influenced already by winter temperatures, but they generally relate to conditions in spring. Because only daily mean temperature is available for the period since 1763, we adjusted the indices to daily mean temperature. A frost day was defined as a day with a daily mean temperature below 0 °C. Such a day is thus colder than what is normally considered a frost day. The warm and cold spell indices were calculated for the 10th and 90th percentile thresholds in the reference period of 1871 to 1900 for daily mean temperature and not minimum and maximum temperature. Snowfall days were calculated according to Zubler et al. (2014) using a threshold of at least 1 mm for precipitation and less than 2 °C for daily mean temperature. Further, we calculated the growing season start based on the first 6 d with daily mean temperature above 5 °C in a year. The growing season length index, which is based on the growing season start, has been criticized for a high inter-annual variability related to the fact that the index operates on synoptic time scales (Cornes et al., 2019), rather than representing the conditions within a whole season. Thus, we also used the growing degree days index that can be seen as a starting point for spring vegetation based on different thresholds (Wypych et al., 2017).

All indices were calculated for the entire available period from 1763 to 2020 and for the months of March to May for aggregated indices. Long-term changes in the indices were discussed based on 30-year mean values for eight climatological periods from 1781 to 1810, 1811 to 1840, 1841 to 1870, 1871 to 1900, 1901 to 1930, 1931 to 1960, 1961 to 1990, and 1991 to 2020. Anomalies are shown as a deviation from the pre-industrial reference period of 1871 to 1900 as it is defined in Begert et al. (2019). For the calculation of indices based on the Swiss Plateau series (Brugnara et al., 2022), the entire year/season was set to missing for growing season start and growing degree days if a missing value occurred. For aggregated indices (e.g. frost days, wet days), a value was set to missing if more than 10 % of the values in an aggregation period were missing. Further definitions can be found in Table 3.1.

All calculated indices for a monthly, seasonal, and annual time aggregation for the period

1763 to 2020 are published at the open-access repository PANGAEA (Imfeld et al., in review).

Table 3.1: Climate and phenological indices. The phenological model descriptions are found in Appendix 3.6

Climate index (Abbr.)	Definition	Units
Growing season start (GSS)	First day of at least 6 d with daily mean temperature > 5 °C	day-of-year
Growing degree days (GDD)	Accumulated temperature > 5 °C reaching 200 GDD	day-of-year
Frost days (FD)	Number of frost days with daily mean temperature $\leq$ 0 °C	days
Last frost day (LFD)	Last day of the first half of the year with daily mean temperature $\leq$ 0 °C	day-of-year
Cold spell index (CSDI)	Number of 5 consecutive days with daily mean temperature > 20th percentile	days
Warm spell index (WSDI)	Number of 5 consecutive days with daily mean temperature < 80th percentile	days
Wet days (WD)	Number of days with daily precipitation $\geq$ 1 mm	days
Snowfall days (SD)	Number of days with daily mean temperature < 2 °C and daily precipitation sum $\geq$ 1 mm	days
Phenological index	**Description and scientific name**	**Model**
Cherry full flowering	Prunus avium - flowering (50 %)	PTT
Beech leaf unfolding	Fagus sylvatica - leaf unfolding (50 %)	TT
Frost index	Accumulated temperature below 0 °C after phenological phase	-

3.3.2 Phenological application

To study the impacts of past weather on the spring vegetation, we calculated the cherry full flowering and beech leaf unfolding day-of-year from daily mean temperature data. Cherry flowering occurs around mid April in the Swiss Plateau and can thus serve as a good indication for the state of the spring vegetation. Beech leaf unfolding occurs around the beginning of May in the Swiss Plateau and is thus representative of later spring vegetation. The phenological phases refer to the day of the year when 50 % of the cherry tree is blooming, resp. 50 % of the beech leafs are unfolding. We used the phenological observations of the Swiss phenological network (SPN) between 1951 and 2020 for calibrating and reconstructing the phenological phases during the 258-year long period. Only series with a quality class of at least 3 were used leading to a total of 68 (56) time

series for cherry flowering (beech leaf unfolding) with record lengths between 35 and 71 years distributed across Switzerland (Auchmann et al., 2018; Brugnara et al., 2020a). For cherry full flowering only grid cells below 1600 m a.s.l. where considered because the observational network only includes observations below this altitude.

The cherry full flowering time was estimated using a photo thermal time model (PTT) as implemented in the phenor R package (Hufkens et al., 2018) for which 3 parameters needed to be calibrated (Appendix 3.6, Eq. 3.1 and Eq. 3.2). Beech leaf unfolding was estimated using a thermal time model (TT) which also is based on 3 parameters but no term accounting for daylength, i.e. photoperiod (Appendix 3.6, Eq. 3.1 and Eq. 3.3). The model parameters were calibrated with a Markov Chain Monte Carlo differential evolution sampler with snooker update (Ter Braak and Vrugt, 2008; Hartig et al., 2023) and run with 18000 iteration across 3 chains. Bayesian model calibration has been shown to perform well for the calibration of phenological models (e.g. Meier and Bigler, 2023; Fu et al., 2012) and it further allows for assessing the uncertainty and convergence of model parameters. For the prior distributions of the parameters a uniform distribution with pre-set bounds as defined in Hufkens et al. (2018) were used. The model calibration converged with a potential scale reduction factors of 1.02 or below (Gelman and Rubin, 1992). Figure A.1 in Appendix A shows the trace of the calibrated parameters for the 6000 iterations and the marginal densities thereof. Figure A.2b shows the root mean square error from a cross-validation based on station data. We added both phenological phases to the provided indices on PANGAEA (Imfeld et al., in review), but in the following only discuss cherry full flowering.

For comparing the phenological reconstructions to independent historical observations, we used the time series for full flowering of cherry in Liestal (Canton of Baselland) starting in 1894 (Defila and Clot, 2001) and a composite time series of cherry flowering from different historical sources representative of the Swiss Plateau by (Rutishauser et al., 2003; Burgdorf et al., 2023).

The cherry full flowering was further used to study the frost occurrence after flowering that could cause damage to trees. A frost index was calculated following Lhotka and Brönnimann (2020) by accumulating daily mean temperature below 0 °C from the onset of cherry flowering (minus 3 d) until the 30th June. This yielded an estimate of the area affected by late frost and the intensity of the frost occurring.

3.4 Results

3.4.1 Longterm changes in climate and phenological indices

Most climate indices showed few differences in their climatological mean in the first five periods from 1781 to 1900 (Fig. 3.1). The Swiss climatological reference period from 1871 to 1900 showed slightly colder conditions in some of the indices compared to the earlier periods. Growing degree days were up to 5 d earlier in the Swiss Plateau in the periods between 1781 to 1870 compared to the 1871 to 1900 period, up to 4 frost days less were registered in these periods, and up to 8 warm spell days more. Figure A.3 in Appendix B shows the anomalies of the seven periods with respect to the pre-industrial mean period from 1871 to 1900 (Begert et al., 2019).
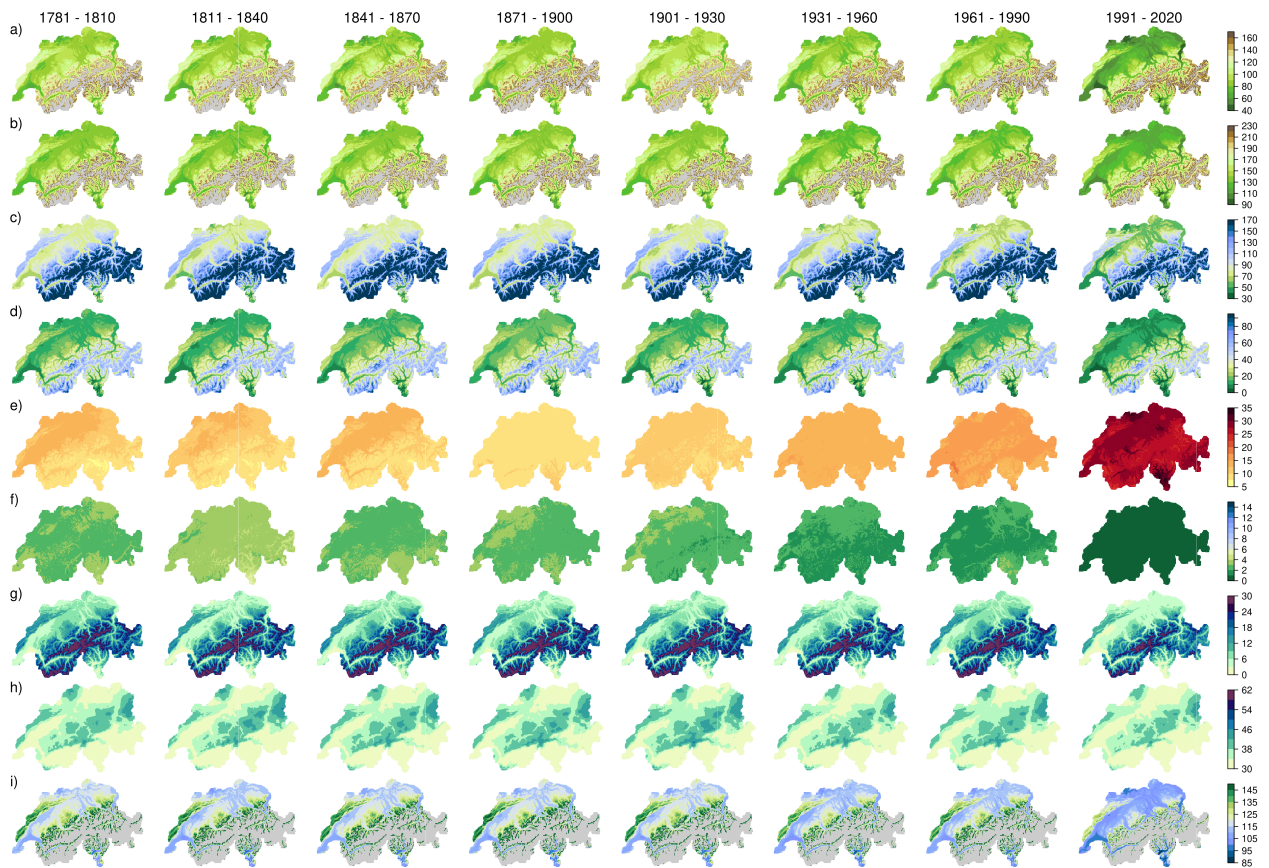
Figure 3.1: 30-year climatological mean for climate indices for the eight periods between 1781 to 2020. a) Growing season start, b) growing degree days, c) last frost day, d) frost days, e) warm spell duration index, f) cold spell duration index, g) snowfall days, h) wet days, and i) cherry full flowering day-of-year. Light grey areas depict areas, where the indices was not reached in more than 75 % of the years in a period or we did not calculate the index because the grid cells are above 1600 m a.s.l. (last row).

Warmer conditions emerged in all indices for the three periods from 1931 onward. The 1931 to 1960 period showed earlier growing season start and earlier growing degree days compared to the period from 1961 to 1900, but few differences in frost days, last frost days, and warm and cold spells. Very clear differences emerged in the last period of 1991 to 2020 (Fig. 3.1, last column). Across Switzerland, the growing season started up to 24 d earlier than in the pre-industrial period 1871 to 1900. The 200 GDD was reached up to 25 d earlier, and the last frost days occurred up to 25 d earlier compared to the pre-industrial period 1871 to 1900. Warm spell days increased by up to 20 d, whereas cold spell days decreased by up to 10 d. P values from the comparison of the climatological mean and the pre-industrial mean with a Student's t test show that for most indices the last period significantly differs at a 0.05 confidence level (not shown).

For the precipitation-related indices snowfall days and wet days, differences only ranged between -5 to +5 d throughout all periods (Fig. 3.1 and A.3g and h). The first two periods showed a north-south precipitation difference compared to the pre-industrial mean, which is likely an artifact of the dataset due to the lack of precipitation data before 1864 in southern Switzerland. The 1931 to 1960 period showed fewer snowfall days and wet days than the pre-industrial reference period. This period also included a prolonged episode of warm and dry years between 1945 to 1952 in Switzerland and Western Europe (Imfeld et al., 2022). The period from 1961 to 1990 showed no differences in snowfall days compared to the pre-industrial period, whereas the 1991 to 2020 period showed up to 5 d fewer snowfall days. Similarly, wet days did not show any difference in the 1961 to 1990 period, whereas they decreased in the last period. For snowfall days, the differences in the mean value became significant at a 0.05 level for the last period compared to the pre-industrial reference period (not shown).

Based on our reconstruction, cherry flowering occurred on average between mid and end of April in the Swiss Plateau during the pre-industrial period from 1871 to 1900 (Fig. 3.1 i). The flowering phase did not show considerable changes in the mean in the first five periods until 1930. Changes become apparent in the period of 1931 to 1960 at higher locations, and much more pronounced again in 1991 to 2020 with between 5 and 15 d earlier than in the pre-industrial reference period (see also Appendix Fig. A.3). The Student's t test showed significant differences at a level of 0.05 in parts of Switzerland already in the 1931 to 1960 period (not shown).

Time series for the area-mean of the Swiss Plateau region (Swiss recon), for the 20CRv3 reanalysis, the merged time series from Zurich and Bern (Swiss series), and the ensemble mean of ModE-RA depict a steep trend of the indices in the late 1980s for daily mean temperature and GDD (Fig. 3.2a and b). 20CRv3 shows lower temperatures, e.g. leading to later GDD, in the period from 1806 to around 1835, which is also a period where few
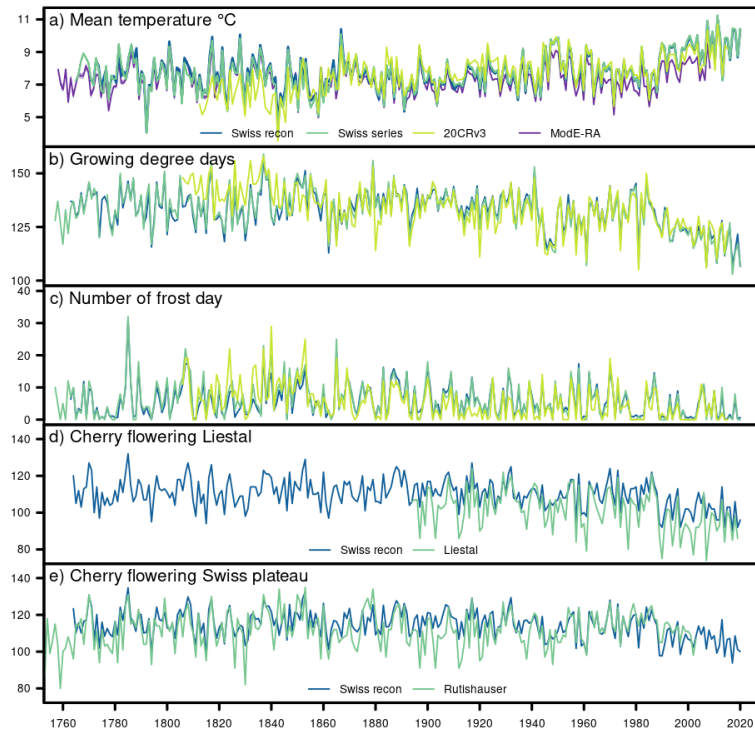
Figure 3.2: a) Mean temperature, b) growing degree days, c) number of frost days, d) cherry flowering in Liestal for the reconstruction and the observations of Liestal (Defila and Clot, 2001), and f) mean cherry flowering in the Swiss Plateau for the reconstruction and the composite series of Rutishauser et al. (2003). Note that for the Swiss series, NA values are removed. The time series of the Swiss gridded reconstruction set cover the area of the Swiss Plateau. ModE-RA shows the ensemble mean, and the minimum and maximum member. 20CRv3 shows the ensemble mean and the spread.

observations were assimilated into 20CRv3 (Slivinski et al., 2021, 2019). ModE-RA agrees well with the Swiss reconstruction and the Swiss series in the 18th and 19th century, whereas it is on average colder than the other data sets in the 20th century. Notably cold springs in the time series are 1785, which also showed a much higher number of frost days in the Swiss Plateau than any other year, and 1837, which is together with 1785 the coldest spring in the 258-year-long time series. On the other hand, several springs showed quite high temperatures, comparable to the beginning of the 21st century. The most prominent among these is the spring of 1862.

The trend towards earlier flowering is also seen in the cherry flowering time series, with much earlier dates after 1989. For the cherry tree in Liestal, the Pearson correlation between the reconstruction and the observation was 0.85, but the reconstruction showed a mean bias of 7.36 d (Fig. 3.2d). For the composite cherry flowering from Rutishauser et al. (2003), Pearson correlation was 0.67 and the mean bias 2.97 d (Fig. 3.2e). Despite

the biases between the reconstruction and the historical observations, the phenological reconstruction reproduced the overall variability throughout the years. Thus, the reconstruction offers an estimate to study cherry flowering in the past across Switzerland. The earliest flowering occurred in 2017 (4th April), which was related to a damaging frost event in Switzerland (Vitasse and Rebetez, 2018). The latest flowering happened in 1785 (15th May), followed by 1853 (12th May), and other late years with cherry flowering between 9 and 10 of May were for example 1770 (a prolonged cold and wet period; see Collet 2018 and Imfeld et al. 2023), 1817 (after the year without a summer; see Flückiger et al. 2017), 1808, 1932, and 1837.

3.4.2 Examples of extreme springs

Based on these climate and phenological indices, we studied three examples of extreme spring conditions, that may affect for example vegetation growth in spring. Namely, we considered the early warm spring in 1862, the occurrence of late frost events in 1873 and 1957, and the three years 1785, 1837, and 1853 with especially cold springs and late cherry flowering. In addition to the presented indices, we analyzed atmospheric variables for illustration of the weather conditions during the extreme spring cases, and we qualitatively evaluated historical sources reporting the weather conditions and weather-related impacts.

3.4.2.1 The warm spring in 1862

Very warm springs considerably increased after the 1980s (Fig. 3.2a). However, also in the late 18th and early 19th century several warm springs with high daily mean temperature and for example, early reach of 200 GDD occurred (Fig. 3.2). The spring of 1862 in particular, stands out with a mean temperature of 10.4 °C between March and May in the Swiss Plateau and based on the gridded reconstruction. It ranks as the third warmest spring since 1763 after the two warmest springs 2011 (11 °C) and 2007 (10.9 °C). With respect to the climatological period 1841 to 1870, 1862 was exceptionally warm with an anomaly of 2.9 °C for the Swiss Plateau area mean. In contrast, the second (1841) and third (1846) warmest springs in the 1841 to 1870 period showed less pronounced anomalies of 1.8 and 1.1 °C. The warmest spring in 2011 had an anomaly of only 1.8°C with respect to its mean climate from 1991 to 2020. We also considered the Swiss series of Bern and Zurich (Brugnara et al., 2022) and 2 m temperature from 20CRv3 (Slivinski et al., 2019). In the Swiss series, the spring of 1862 ranks seventh with a mean temperature of 10.09 °C between March and May. It had an anomaly of 2.8 °C considering the mean of the period from 1841 to 1870, whereas 2011 it had an anomaly of 1.8 °C considering its mean climate from 1991 to 2020. Thus, the anomalies were very similar and the spring of 1862 seemed to be unusually warm for this period. In 20CRv3, the anomaly of the spring 1862 was lower with 1.9 °C with respect to the 1841 to 1870 period. Across all years, the spring of
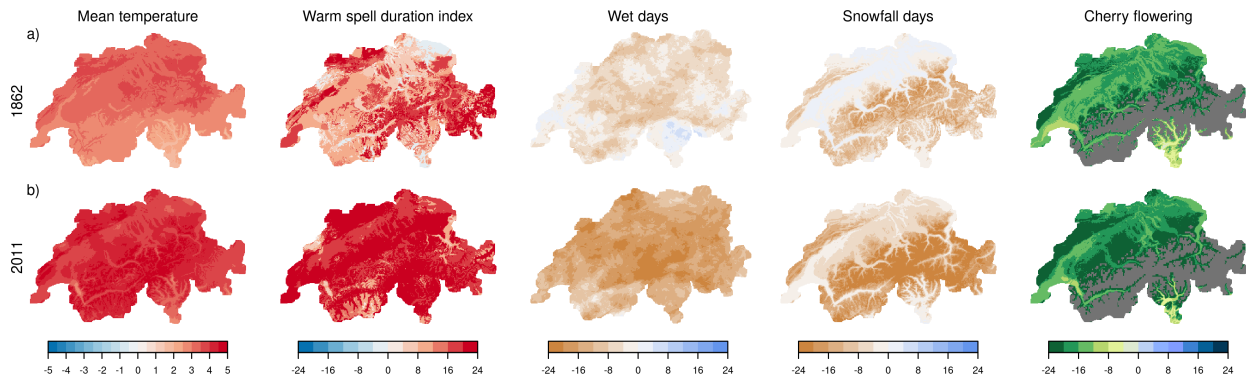
Figure 3.3: *Anomalies of mean seasonal temperature, warm spell duration index, wet days, snowfall days, and cherry flowering date for the two warm springs of a) 1862 and b) 2011. All anomalies are calculated with respect to March to May for the period 1871 to 1900.*
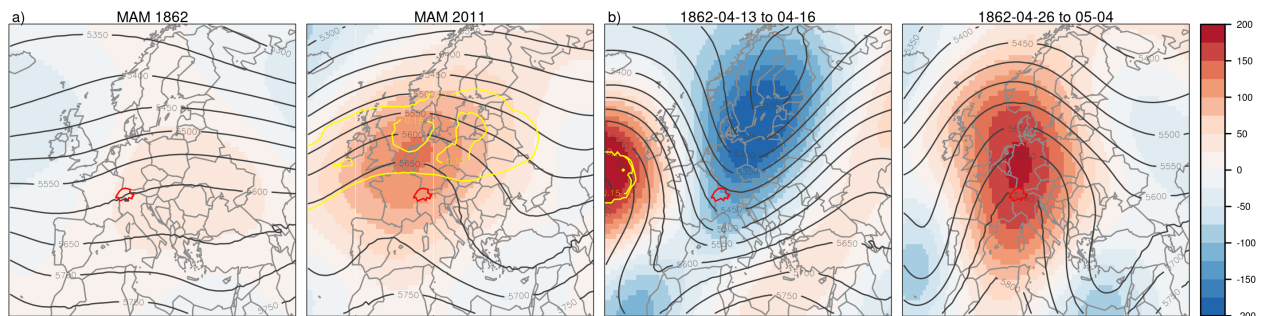
Figure 3.4: *a) Geopotential height field (gpm) at the 500 hPa level (contours) and its anomalies (shading) for the March to May mean in 1862 and 2011. b) The period during and after a cold air outbreak in April 1862. Anomalies are calculated with respect to 1871 to 1900. Yellow lines show the blocking frequencies (0.05 and 0.1) across all time steps and all members. The data is from 20CRv3 (Slivinski et al., 2019).*

1862 only ranks 17th in 20CRv3. In contrast, in ModE-RA, which ends in 2008, the spring of 1862 showed the highest temperature across the period from 1763 to 2008 and had an anomaly of 2.6 °C concerning the 1841 to 1870 mean. The spring of 2007 was the second warmest, but 2011 is missing for comparison. The number of assimilated observations in ModE-RA, however, gradually reduces towards the 21st century affecting the temperature analysis (Valler et al., in review).

For both, the warmest spring of 2011 and the warm pre-industrial spring of 1862, climate indices showed above-average temperatures and an above-average number of warm spell days across the entire Switzerland, though much more pronounced in 2011 (Fig. 3.3). Both springs showed mostly fewer wet days and fewer snowfall days than on average between 1871 and 1900. Cherry flowering was in certain areas up to 24 d advanced, in particular

at higher altitudes.

Over eastern Europe, 20CRv3 showed only a very weak positive geopotential height anomaly at the 500 hPa level for the mean of the spring months March to May 1862 (Fig. 3.4a). For the spring of 2011, a more pronounced positive geopotential height anomaly at the 500 hPa level was present over western Europe indicating that Switzerland was affected by the warmer and drier conditions (Fig. 3.4b). In the spring of 1862, a cold anomaly in mid-April interrupted the warm weather (Fig. 3.4c) leading to frost and snowfall over Switzerland, but, for example, for Aarau as mentioned above no reports on vegetation damage were found (Zschokke, 1865). After the cold spell, a pronounced ridge established again over Western Europe leading to the warm spring weather (Fig. 3.4d). In ModE-RA, for which 1862 is the warmest spring in the 1763 to 2008 period, the geopotential height field of March to May was comparable to 20CRv3. Still, the respective temperature anomalies were more pronounced than in 20CRv3 (see e.g. Fig. 3.2 and anomalies in the text above) (Appendix, Fig. A.4).

Historical sources indeed reported an unusual early snow-free period in spring 1862 in Ursern, a valley in the Canton of Uri (Ambühl, 1961). Already very early in the year the Gotthard was passed by carriage and not sled (Zschokke, 1865) which could point to warm weather leading to early snow-melting, but also to less snowfall in the months before. For Aarau, Theodor Zschokke reported unusual advances in the vegetation, for example, a start of the cherry flowering as early as the 6th of April. In our reconstruction the cherry flowering happened on the 8th April in Aarau and on average on the 11th April in the Swiss Plateau. The snowfall and frost that occurred in mid-April did not lead to damage in lower-lying areas (Zschokke, 1865). An official weather report from the weather service for the year 1862, however, did not mention an unusually warm spring (MeteoSwiss, 2016), but more qualitative sources describing the spring weather might be available.

3.4.2.2 The late frost events in 1873 and 1957

Combining the cherry flowering reconstruction with climate indices allows us to look at climate events that affected vegetation directly, such as the occurrence of late frost in spring that can lead to considerable damage to vegetation. Two events stand out when considering the affected area and the intensity of the frost events. In 1873, frost conditions after the cherry flowering affected large parts of Switzerland, however, the temperature did not fall much below 0 °C (daily mean temperature). The frost index based on the accumulated negative temperature reached at most -6 °C in the Swiss Plateau (Fig. 3.5a). The last frost day occurred between the 26th and 28th of April across northern Switzerland, which is more than half a month later than it occurred on average between 1871 and 1900. In contrast, cherry trees reached their full bloom up to 10 d early. In the spring of 1957,
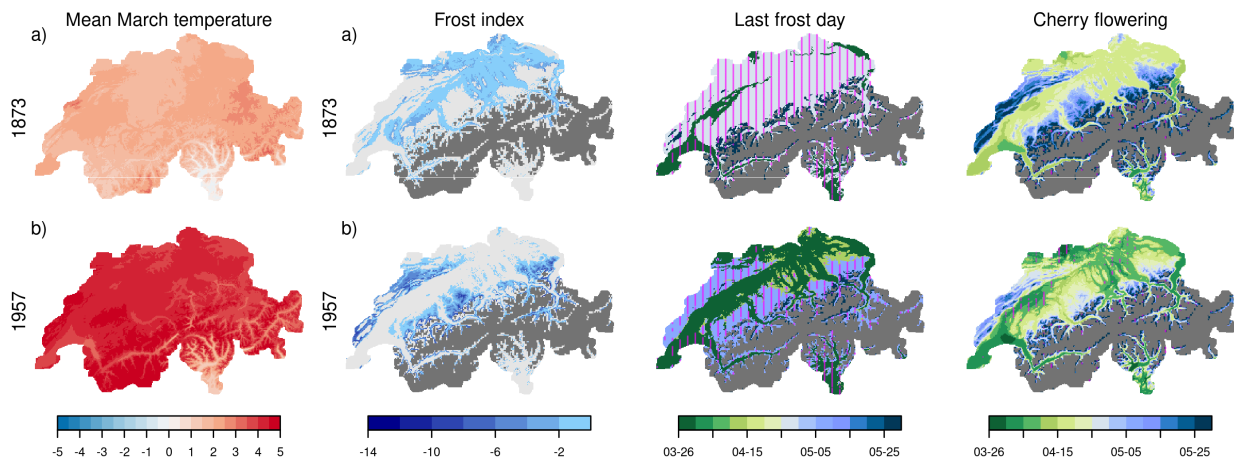
Figure 3.5: Two frost events causing damage to fruit trees in Switzerland. Temperature anomaly in March with respect to 1871 to 1900, frost index, last frost day, and day of cherry flowering for the two events of a) 1873 and b) 1957. The vertical purple lines indicate areas where frost (cherry flowering) occurred 15 d later (earlier) than the 1871 to 1900 average. The dark grey area denotes grid cells above 1600 m a.s.l.

a frost event occurred with very low temperatures, but the affected area was smaller (Fig. 3.5b). The frost index showed much higher values but affected only areas above 800 m a.s.l. For these areas, the last frost days, which occurred between the 6th and 8th of May, were also more than half a month later than between 1871 and 1900, and the cherry tree flowering was considerably earlier.

For both springs, March was characterized by average or above-average temperature conditions across Central Europe, though more pronounced for March 1957 (Fig. 3.5a). These high temperatures in March might have led to an early start of the cherry flowering. In March 1873, temperature anomalies were positive, but the geopotential field shows a more zonal configuration. On the 26th of April 1873, a large trough extended over Switzerland from the Northeast leading to the temperature drop. In 1957, temperatures reached their lowest values on the 8th May when a large trough was located above Switzerland.

For both events, damage caused by the late frost events was reported. In 1873, frost damage was reported for Sursee, Marschlins, Bad-Ragaz, and Appenzell-Innerrhoden, whereas many locations registered snowfall during the 26th to 28th April leading to further damage to the vegetation (Tab. 3.2). For the frost event of 1957, the Swiss farmer association calculated a reduction of yield in pear and apple trees of 75 % and for cherries of 44 % compared to the six preceding years indicating considerable loss in harvests (Tab. 3.2).
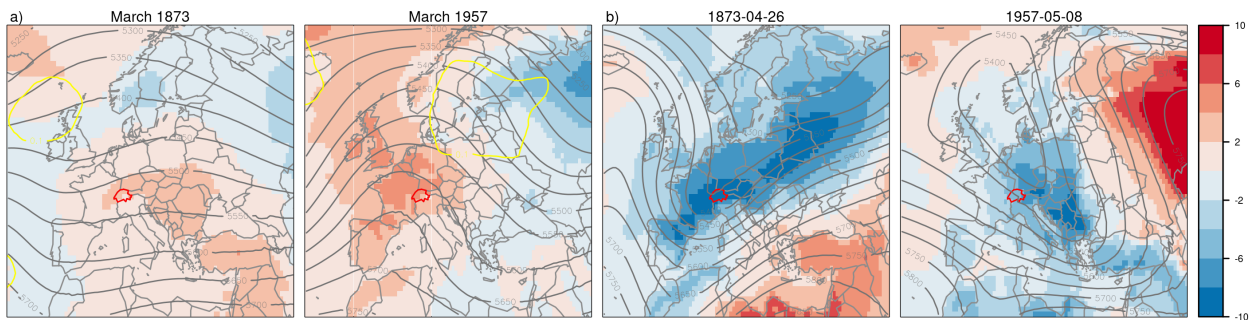
Figure 3.6: a) 2 m temperature anomalies and geopotential height fields at the 500 hPa level for March of 1873 and 1957. b) Daily 2 m temperature anomalies and daily geopotential height field of the coldest day during the late frost in Bern. Anomalies are calculated with respect to 1871 to 1900. The boundaries of Switzerland are marked in red. The data is from 20CRv3 (Slivinski et al., 2019).

3.4.2.3 The cold springs of 1785, 1837, and 1853

The three springs, 1785, 1837, and 1853 registered the lowest temperatures of the entire time series of 258 years and lie below the 1% quantile of all springs temperatures. Their mean temperature in the Swiss Plateau from March to May reached only between 4.1 to 5.1 °C (Fig. 3.2) which is up to 3 °C degrees colder than the 1871 to 1900 average (Fig. 3.7). In the Swiss series, the coldest spring was in 1837 with a mean temperature of only 3.8 °C and an anomaly of -3.4 °C followed by 1785 with a mean temperature of 4.1 °C and 1853 with a mean temperature of 5.1 °C. In 20CRv3, the spring of 1837 ranks the coldest with an anomaly of -4.0 °C with respect to 1871 to 1900, but 1785 is not available. In ModE-RA, the coldest spring was registered in 1837, followed by 1785, 1970, and 1853 with anomalies between -2.24 and -1.84 °C with respect to 1871 to 1900.

Indices show, that during the three springs, the cherry flowering was up to 20 d later than the average of 1871 to 1900, and up to 30 more frost days were registered (Fig. 3.7). Snowfall day anomalies were positive in the spring of 1837 and 1853 mostly in the Alps, but they were negative in the Alps in the spring of 1785. The spring of 1785 also registered fewer wet days than in the 1871 to 1900 period and thus did not concur with the two other springs, that showed wet and cold conditions. In 1785, the frost days indeed showed a different spatial pattern with much larger frost day anomalies in the Swiss Plateau region compared to the Alps, which would correspond to an inversion situation. This suggests that synoptic conditions were different over Europe during 1785 compared to the two other cold springs.

Weather types allow a look at the synoptic conditions throughout the three cold springs. The late springs of 1837 and 1853 show a higher occurrence of northerly cyclonic situations
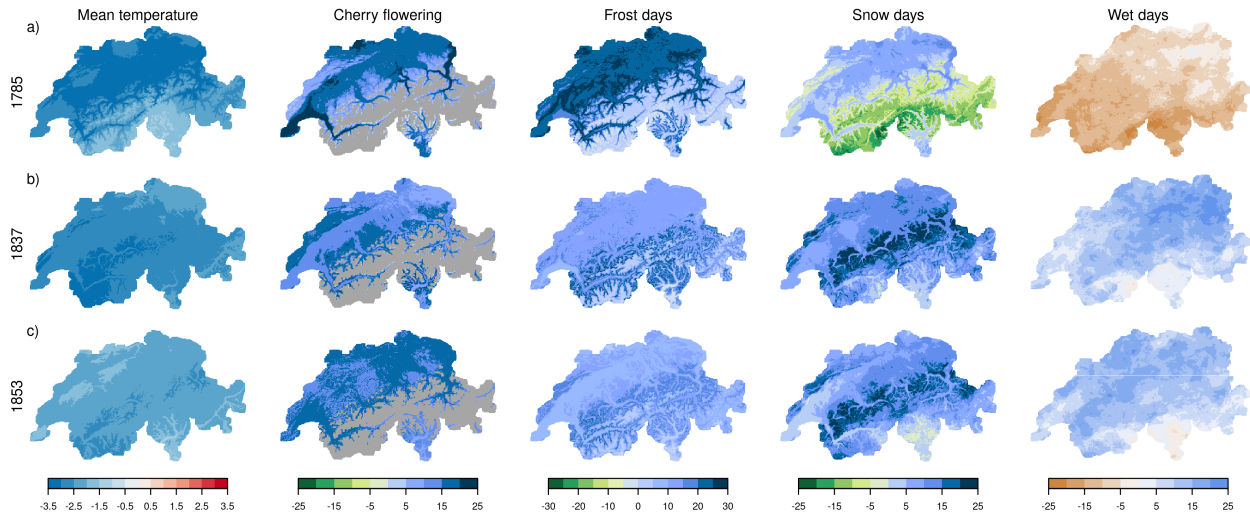
Figure 3.7: a) Temperature anomaly, b) anomaly in cherry flowering phenology, c) anomaly of the number of frost days, d) anomaly of the number of snow days, e) anomaly of the number of wet days for the cold springs (March to May) of 1785, 1837, 1853. All anomalies are calculated with respect to the 1871 to 1900 climatological mean. Grey areas for cherry flowering denote areas above 1600 m a.s.l.

(N) and cyclonic situations with westerly flow over Southern Europe (WC) compared to usual spring weather types in the entire period from 1763 to 2020 (see Schwander et al. (2017) for the description of weather types) (Fig. 3.8a). More cyclonic weather types are found also on average for all springs with temperatures below the 10th quantile (q10). The spring of 1785, however, showed an increase in weather types describing easterly, indifferent flow (E), and high-pressure situations over Europe (HP). To further evaluate this difference in weather types, we used the variance of bandpass-filtered daily pressure observations which give an insight into the "storminess", i.e. the frequency of passing of extra-tropical cyclones. We followed the approach of Brugnara et al. (2015), but only considered station data for calculating anomalies of the standard deviation. The pressure observations show that storminess decreased for northern stations in 1785, and it increased in 1837 and 1853 over Switzerland (Fig. 3.8b). Also, the average of the springs below q10 shows increased storminess except for two stations.

This is further confirmed by the monthly fields of geopotential height (anomalies) at the 500 hPa level during the three spring months March to May (Fig. 3.9). In February and March 1785, a trough was present over Central Europe leading to an advection of cold air from the north. This situation weakens through April and May, but the trough still remains throughout spring. Stations from several locations in Germany, Poland, and the Czech Republic, indeed, show all the same extended negative temperature anomalies throughout March until mid April. In 1837 and 1853, more zonal flow patterns seemed

to prevail between March and May and the average of springs below q10 similarly shows more zonal flow.

Historical sources confirm these cold spring weather conditions. In spring 1785, for six lakes reports about continued (partial) lake freezing were found until March (see Tab. 3.2). In March and April, several locations reported abundant snowfall. Due to feed shortage livestock starvation was reported from the Canton of Valais. In St Blaise in the Canton of Neuenburg, strong *Bise* was reported for March and April (Kopp, 1873) and that the first rain (not snow) after 4 months fell at the end of May. Both indicate specific synoptic conditions for this cold spring. For the springs of 1837 and 1853, fewer sources are available, but they reported abundant rain and snowfall, and frost impacts for various locations in Switzerland. These sources, thus, confirm that all three spring were especially cold and also agree with the classification of Pfister and Wanner (2021) which report cold conditions for all three springs with a category -3 for the Pfister temperature index.

Table 3.2: *Selection of registered weather impacts for the frost events and cold springs in Switzerland based on the Euro-Climhist database (Pfister et al., 2017) and further sources. The original sources are listed where possible and otherwise secondary sources.*

Time	Location	Impacts	Sources
Frost events			
1873 April	Sursee	complete damage of cherry harvest	MZA (1873)
1873 April	Marschlins	damage of walnut trees and grapes	MZA (1873)
1873 April	Switzerland	snow/frost damage on fruit trees and grapes	Appenzeller-Kalender (1874)
1957 April/May	Switzerland	considerable losses in fruit harvest	SBV (1958)
Cold springs			
1785 Jan–Apr	Lake Constance	water bodies frozen	Paffrath (1915)
1785 March	Lucerne	water bodies frozen	Staatsarchiv (1755-1829)
1785 March	Geneva	water bodies frozen, ice partially walkable	Forel (1892)
1785 March	Lake Constance	snowfall	Paffrath (1915)
1785 March	Thur river (Ct. of St Gall)	water bodies frozen	Braecker (1998)
1785 March	Lake Alpnach	water bodies frozen	Schaller-Donauer (1937)
1785 March	Lake Zurich	water bodies frozen	Müller (1878)
1785 March	Wattwil (Canton of St Gall)	several reports on abundant snow	Braecker (1998)
1785 March	Chur (Canton of Grisons)	reports on abundant snow, 9 d snowfall	Grimmer (2019)
1785 March	Lake Constance	reports on abundant snowfall	Paffrath (1915)
1785 March	Binn (Canton of Valais)	reports on birds frozen to death	Zennhäuser (2008)
1785 April	Lake Constance	snow impact, abundant snow, livestock starved	Paffrath (1915)
1785 April	Chur (Canton of Grisons)	reports on abundant snow, 6d snowfall	Grimmer (2019)
1785 April	Binn (Canton of Valais)	vegetation delayed, livestock starved	Zennhäuser (2008)

| Date	Location	Description	Reference
1785 March	St Blaise (Ct. of Neuenburg)	rigorous cold, abundant snow, and strong *Bise*	Kopp (1873)
1785 April	St Blaise (Ct. of Neuenburg)	abundant snow, cold, and strong *Bise*	Kopp (1873)
1785 May	Lake Constance	delayed vegetation and frost impact on vegetation	Paffrath (1915)
1785 May	Wattwil (Canton of St Gall)	fresh snow at higher elevations	Braecker (1998)
1837 March	Canton of Zurich	snow and rain quantities 'as expected for a January'	Vogel (1841)
1837 March	Simplon (Canton of Valais)	13 death due to avalanche	Joller (1888)
1837 April	Canton of Zurich	large snow and rain quantities	Vogel (1841)
1837 May	Canton of Zurich	large snow and rain quantities	Vogel (1841)
1837 May	Grindelwald (Ct. of Bern)	permanent snow cover	Strasser (1890)
1853 May	Canton of Zurich	large snow and rain quantities	Vogel (1841)
1853 May	Grindelwald (Ct. of Bern)	permanent snow cover	Strasser (1890)
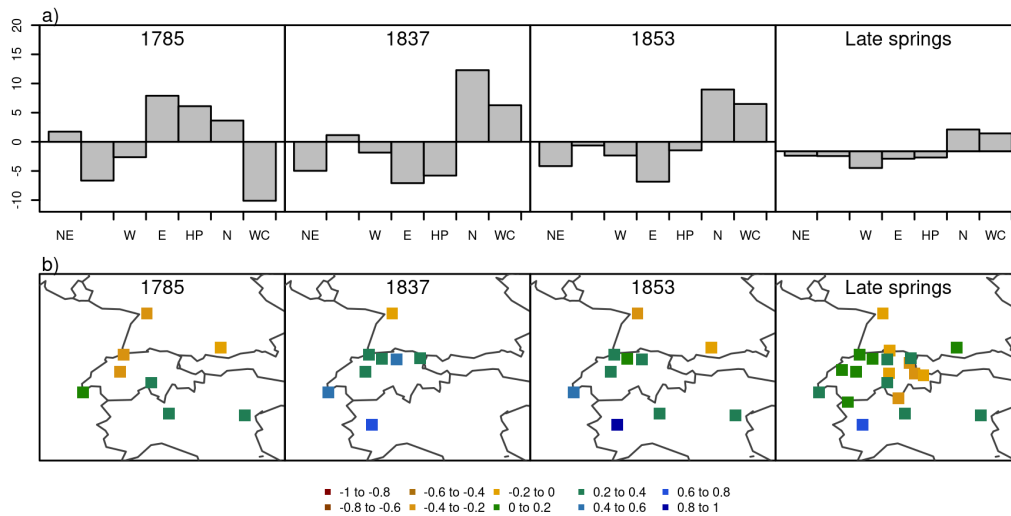
Figure 3.8: a) Anomalies of weather type frequencies for the three coldest springs and the mean of all springs below q10. The anomalies were calculated with respect to the mean frequency of weather types in March to April from 1763 to 2020 considering all weather types with a cumulative probability of 0.9. NE = Northeast, indifferent; WSW = West-southwest, cyclonic, flat pressure; W = Westerly flow over Northern Europe; E = East, indifferent; HP = High pressure over Europe; N = North, cyclonic; WC = Westerly flow over Southern Europe cyclonic (Schwander et al., 2017). b) Storminess based on pressure observations for the three coldest springs and the mean of all springs below q10. The anomaly of the standard deviation was calculated with respect to 1961 to 1990 because some series exhibit large gaps between 1871 and 1900.
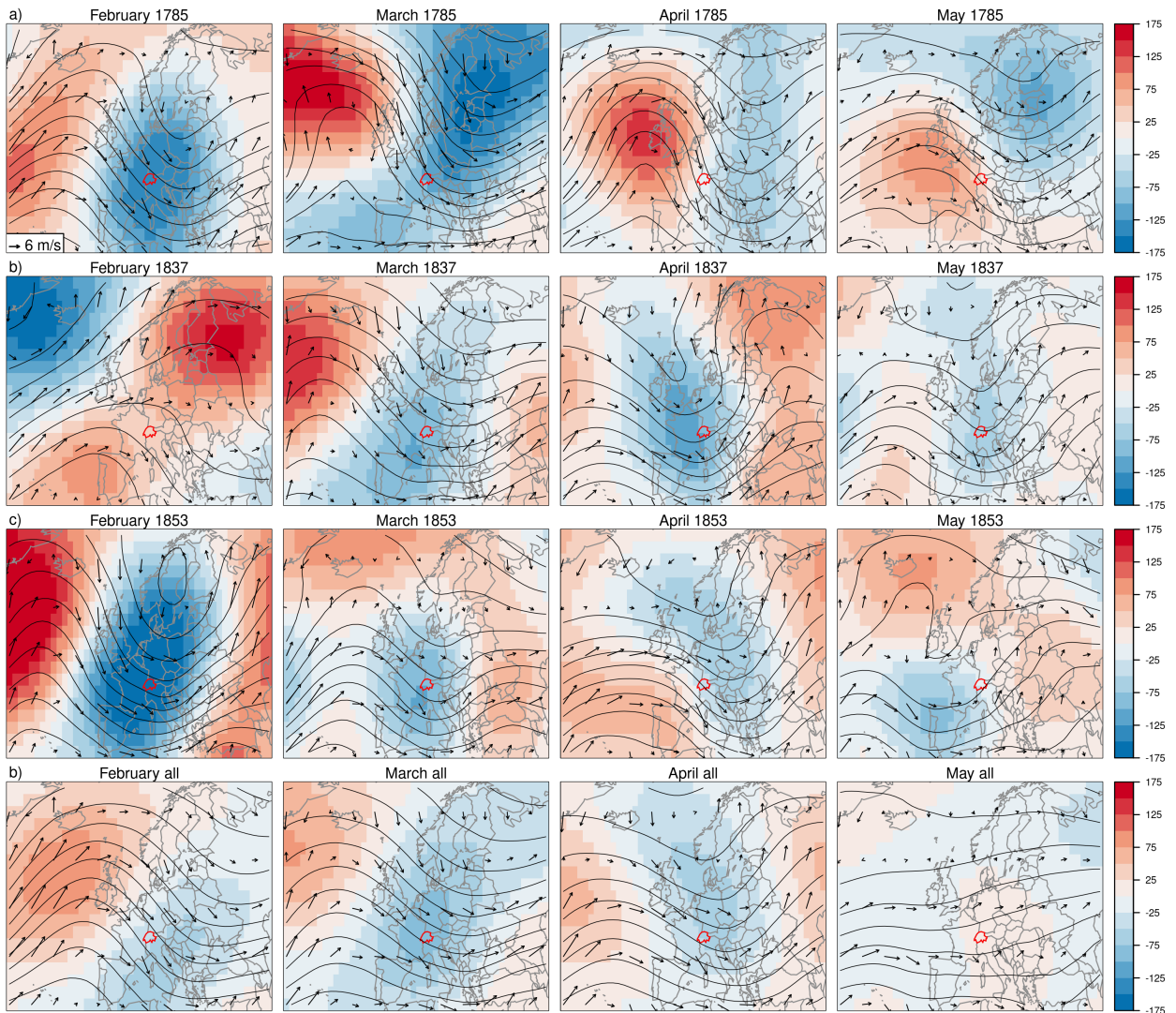
Figure 3.9: 500 hPa Geopotential height field and wind direction for the months of February to May of the three cold springs. Colors show anomalies with respect to the mean of 1871 to 1900, contours show absolute geopotential height field. Arrows show the wind field at 850 hPa. Switzerland is marked in darkred. a) 1785, b) 1837, c) 1853, and d) the composite of all springs below q10. The data is from ModE-RA (Valler et al., in review).

3.5 Discussion

Climate and phenological indices provide a useful way to study historical extreme spring events, such as cold springs or late frost events, and relate them to impacts, for example, the state of vegetation. All indices showed steep changes towards warmer conditions in the last climatological period from 1990 to 2020. These changes in temperature indices correspond to the widely reported trends for temperature development in Switzerland such as in e.g. Isotta et al. (2019) for monthly means, to changes in snowfall vs. rain (Serquet et al., 2011), and to the changes in spring phenology (Studer et al., 2005; Vitasse et al., 2018). The steep changes towards warmer conditions in the late 1980s have been found in a variety of time series across the world, including vegetation, temperature time series, and snow time series (Reid et al., 2016; Marty, 2008), however, mainly series linked to spring and winter conditions. Sippel et al. (2020) suggested that the changes, which are linked to the cold season temperature, stem from internal variability superimposed on a long-term warming trend.

For Switzerland, phenological models have been used to study for example past frost events (Vitasse et al., 2018) for different tree species and changes in future frost events for grapevines (Meier et al., 2018), but no attempts have been made to extend phenological predictions in space and time. The transferability of the phenological models may be limited in space (e.g. Basler, 2016), and also in time because sensitivities of the calibrated parameters may not be constant over time (Rutishauser et al., 2007). The comparison of historical phenological observations with our reconstruction shows systematic biases of several days for the series of Liestal, but high correlations, thus the reconstruction is able to depict the inter-annual variability of cherry flowering for Liestal. For the composite cherry flowering series, the bias is small with below 3 d, but correlation is also lower.

The indices allow us to gain insights into historical springs with unusual weather conditions. The warm spring of 1862 exhibited warm temperatures across the entire Switzerland, which was exceptional for this period, however, it is less exceptional in comparison to the recent warm springs such as 2011 or 2007. Temperature anomalies were high in spring 1862 in the gridded reconstruction, the Swiss series (Brugnara et al., 2022), and ModE-RA, but temperature anomalies were lower in 20CRv3. The three former data sets are all based on the same temperature series of Bern and Zurich. The geopotential height field in 20CRv3 does not point towards an exceptionally warm spring of 1862, which shows quite pronounced positive geopotential height anomalies over Europe and a ridge in 2011, but not for the year 1862. Similarly, ModE-RA does not show very pronounced ridge conditions either from March to May, but it does have high temperature anomalies.

Late frost events after a warm period in spring can be particularly damaging for example

to fruit harvest. For Switzerland, studies have evaluated how the frost risk has changed over the last decades, and how it may be affected by climate change in the future (Vitasse and Rebetez, 2018; Vitasse et al., 2018; Meier et al., 2018; Lhotka and Brönnimann, 2020), however historical events and their extent have not been studied. These studies rely, though, on daily minimum temperature which has shown different rates of changing compared to daily maximum or daily mean temperature (Scherrer and Begert, 2019). Since minimum temperature was not available in the past, we did not look at changes over time but focused on the representation of specific historical frost events. Two notable frost events occurred in the spring of 1873 and 1957. Harvest data for 1957 showed a considerable loss for apple, pear, and cherry trees (SBV, 1958), which also agrees with the frost index showing strong negative values. For the year 1873, only qualitative descriptions of frost damage were available. Since the frost index is based on daily mean temperature and not minimum temperature, it may not capture the extent of the frost event entirely. However, the data set allowed us to track past frost events based on phenology and frost days and relate them to historical descriptions of the events. This could be done as well for earlier events, such as the late frost in 1802.

Lastly, we considered the three springs 1785, 1837, and 1853 that registered the lowest temperatures from March to May in the Swiss reconstruction. Climate indices showed differences between 1785 and the two springs of 1837 and 1853 with respect to the occurrence of frost days, snowfall days, and wet days. Weather types, the storminess calculation, and the ModE-RA confirmed these differences. The spring of 1785 was under the influence of a pronounced cold trough with a higher occurrence of easterly, high-pressure, and northerly weather types. This led to particular cold, but also dry conditions. The frost day anomalies in the Swiss Plateau indicated likely prolonged inversion, and historical sources describe extended periods of *Bise* which can also lead to inversions and fog in the Swiss Plateau. Daily surface pressure fields over Europe would be needed to study the cold conditions in late winter and early spring of 1785 in more detail. In 1837 and 1853, a higher storminess was found in accordance with a more zonal flow and low-pressure systems passing leading to the above-average wet conditions. For the very cold winter of 1785, six of the large lakes of Switzerland reported that the lakes were frozen until March, which would also be indicative of cold winters. As suggested by Franssen and Scherrer (2008) lake freezing could be reproduced based on negative growing degree days for further phenological comparison.

The spring of 1785 followed the cold years after the Laki eruption which occurred in Iceland in 1783 (Yiou et al., 2014; Zambri et al., 2019), but the very cold period end of winter and beginning of spring of 1785 has not been studied in detail. Also, the spring of 1837 followed a volcanic eruption, namely the Cosiguna in Nicaragua in January 1835. After this eruption, several cold years were evident in tree and frost rings from Europe (Longpré et al., 2014). However, Longpré et al. (2014), also stated that a cooling trend was already

noted prior to the eruption. The spring of 1853 has not been related to cold conditions in previous literature, and for this spring the three data sets do not agree with respect to the magnitude of the negative temperature anomalies.

These cold spring conditions, in particular the unusually cold conditions in 1785, thus provide a rather unique case of cold spring conditions. Studying such weather in detail could still give relevant insights into mechanisms related to cold spring weather.

3.6 Conclusion

Climate and phenological indices allow us to depict changes in spring weather and to study extreme springs since the mid-18th century. The 258-year-long time series for the different indices all showed few changes for the first 200 years and a steep increase toward warmer conditions in the most recent decades, which has been shown by many studies. Some extreme spring events were, however, evident from the time series. Based on the different indices, we evaluated three cases of such extreme spring weather conditions since the mid-18th century. The spring of 1862 was exceptionally warm with respect to its climatological mean and it still ranks among today's warmest springs, though this ranking is highly dependent on the data set. Upper-level atmospheric fields indicate the warm weather conditions in spring 1862, but they are not comparable to the exceptionally warm conditions in spring 2011. The combination of phenology and frost days allows us to evaluate past frost events that caused damage to vegetation. Whereas for the warm summer of 1862, no frost damage was reported despite a cold air outbreak, for the two cases of 1873 and 1957, the frost index shows the affected areas and historical reports confirm the significance of these events.

In the period from 1763 to 2020, three springs showed very cold mean temperature from March to May of at most 5.1 °C. Whereas the springs of 1837 and 1853 showed cold and wet conditions, during spring 1785 fewer wet days than on average from 1871 to 1900 and, thus, dry conditions were registered. An evaluation of weather types, of a storminess index based on bandpass-filtered pressure data, and ModE-RA showed that the 1785 spring was related to more high-pressure conditions and northeasterly flow over Europe, which brought cold air towards Switzerland. The high frost day amounts in the Swiss Plateau and reports about *Bise* further suggest a synoptic situation favorable for prolonged inversion and fog in the Swiss Plateau in March extending to April. In 1837 and 1853, the zonal flow and mainly cyclonic conditions led to cold but also wet springs. Both, the spring of 1785 and 1837 occurred after volcanic eruptions in the extratropics and the subtropics.

The climate and phenological indices, thus, allowed us to get insights into different historical extreme spring events. It was possible to relate these springs to impacts through

historical sources and to evaluate the atmospheric conditions behind them by considering further data sets. Studying such past springs might also nowadays be interesting to better understand the causes of cold and warm springs. Modelling the phenology allowed us to relate the historical weather conditions in a straightforward manner to impacts, such as late frost events causing damage to harvests. But, phenological phases can also be relevant for agricultural modelling, and thus, may contribute to agricultural modelling of historical events in more detail.

Code availability

The code for the calculation of indices is available on github: https://github.com/imfeldn/swiss_indices/.

Data availability

Reconstructed daily precipitation and temperature data sets over the period 1763-01-02 to 2020-12-31 are published at the open-access repository PANGAEA under https://doi.org/10.1594/PANGAEA.950236. The climate and phenological indices for the period 1763 to 2020 described in this article are published at the open-access repository PANGAEA (Imfeld et al., in review).

Author contribution

NI performed the analyses and wrote the manuscript. KH helped with setting up the calibration of the phenological model and contributed to the manuscript. SB supervised the process and contributed to the manuscript.

Acknowledgements

Appendix

Phenological models

The cherry full flowering dates are estimated based on the photo thermal time model that has been proposed by various studies to model phenological phases (Basler, 2016; Meier et al., 2018; Hänninen, 1990). It is based on the growing degree days temperature response and a term that accounts for the photoperiod estimated based on the daylength L_i (Eq. 3.1 and 3.2). Temperatures are accumulated starting at day t_0. When S_{frc} reaches a specific threshold F_{crit}, the phenological phase happens. The parameters F_{crit}, T_{base}, and t_0 are calibrated based on the phenological observations from 1951 to 2020. The beech leaf unfolding dates are estimated based on the thermal time model. As for the photo thermal time model, it is based on the growing degree days temperature response, but daylength is not considered (Eq. 3.1 and 3.3).

$$R_g(T_i) = \begin{cases} 0 & \text{if } T_i \leq T_{base} \\ T_i - T_{base} & \text{if } T_i > T_{base} \end{cases} \tag{3.1}$$

$$S_{frc} = \sum_{n=t_0}^{n} \frac{L_i}{24} R_g \tag{3.2}$$

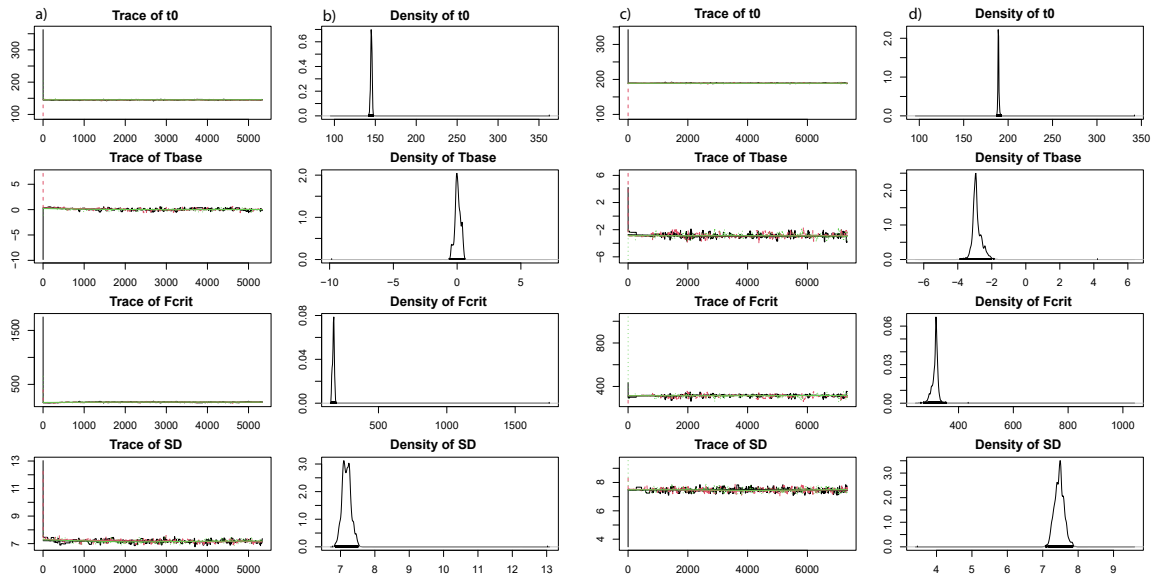$$S_{frc} = \sum_{n=t_0}^{n} R_g \tag{3.3}$$

Figure A.1: Convergence of the Markov Chain Monte Carlos DEzs algorithm for the calibration of the photo thermal time model (PTT) and the thermal time model (TT). a) Trace of the iterations after burn-in for the three chains and the four parameters. b) Marginal distribution of the four parameters based on the three chains. The first three parameters stem from the model, whereas the standard deviation is estimated during model calibration. See formula in Eq. 3.2 and 3.1 for the parameters. Note that t_0 does not start on 1st January, but on 21st September. c and d) are the same as a and b) but for the thermal time model and beech leaf unfolding. Note that we used 8000 iterations of the thermal time model to reach convergence.
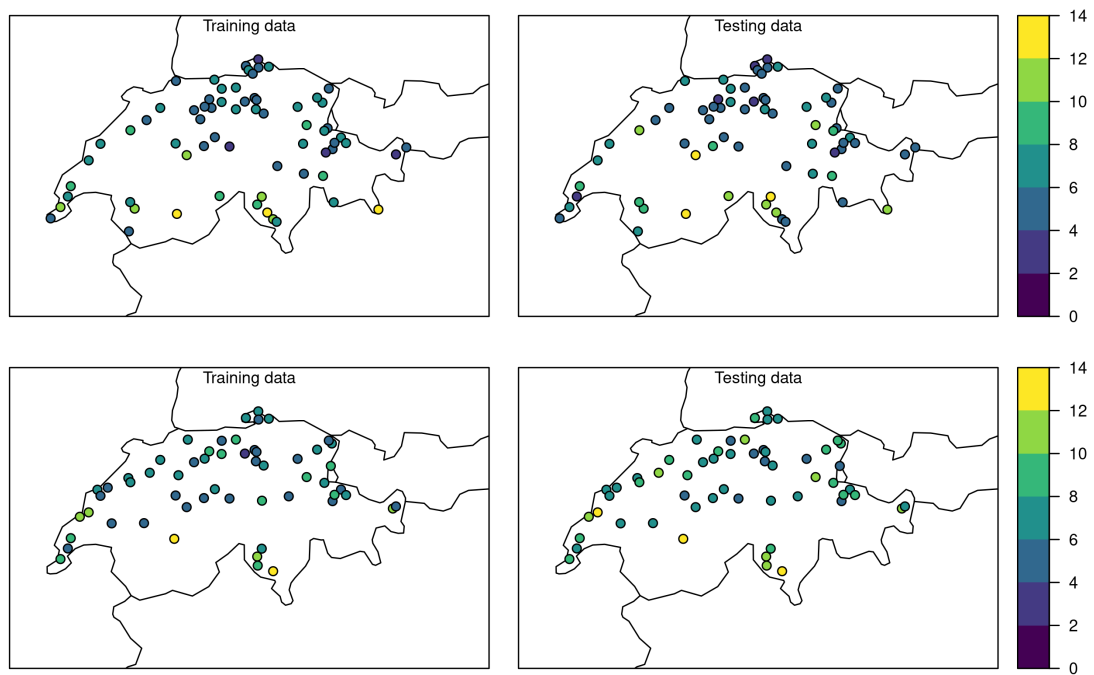
Figure A.2: Root mean square error in days of the cross-validation for cherry flowering (upper row) and beech leaf unfolding (lower row) observations from the Swiss Phenology Network for training data (even years/left column) and testing data (odd years/right column).
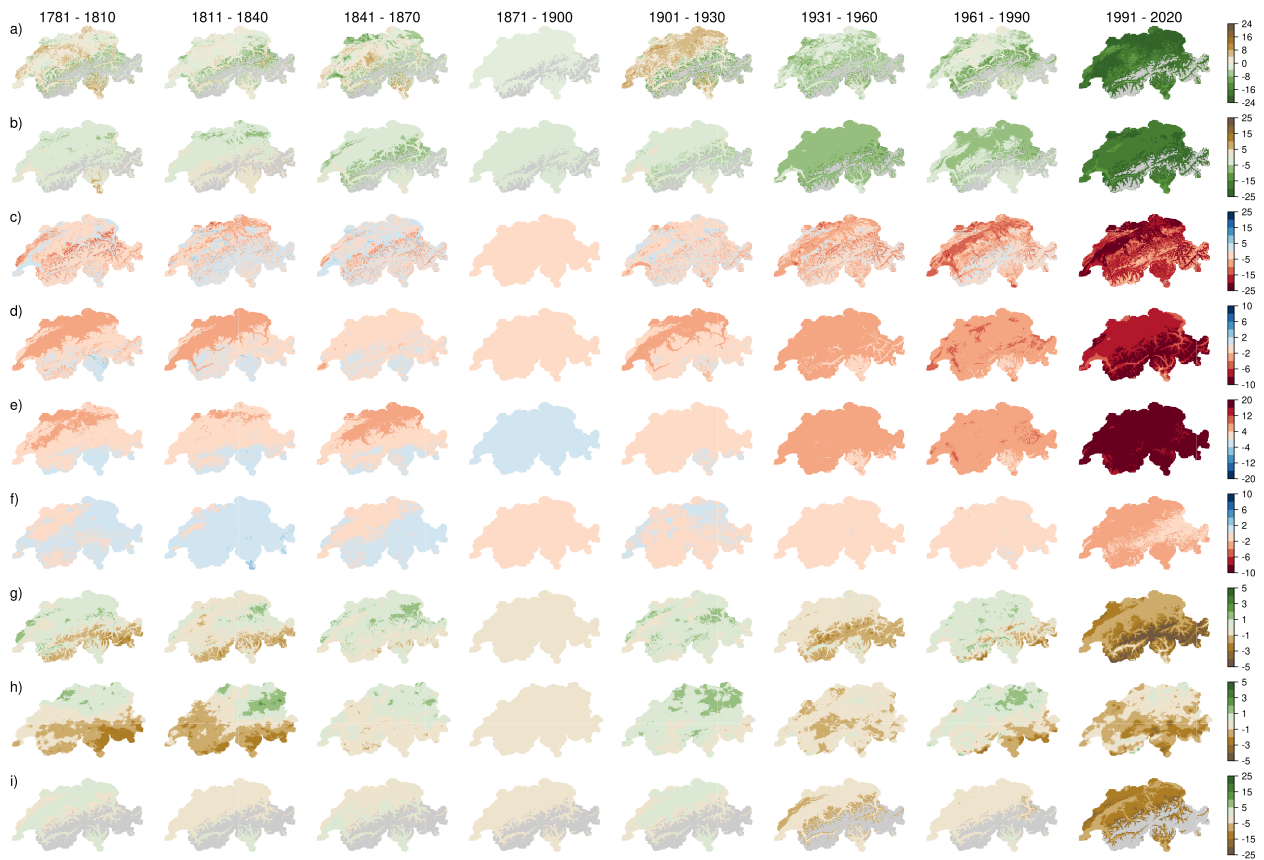
Figure A.3: Anomalies of 30-year climatology for climate indices for all six periods with respect to the pre-industrial reference period from 1871 to 1900. a) Growing season start, b) growing degree days, c) last frost day, d) the number of frost days, e) warm spell days, f) cold spell days, g) snowfall days, h) wet days, and i) cherry full flowering. Light grey areas depict areas, where the indices are 0 in more than 75 % of the years in a period or we do not consider it because the grid cells are above 1600 m a.s.l. (last row).

Figure A.4: a) Geopotential height anomalies (shading) and absolute values (contour) for the 500 hPa level for the mean of March-May, and for each spring month individu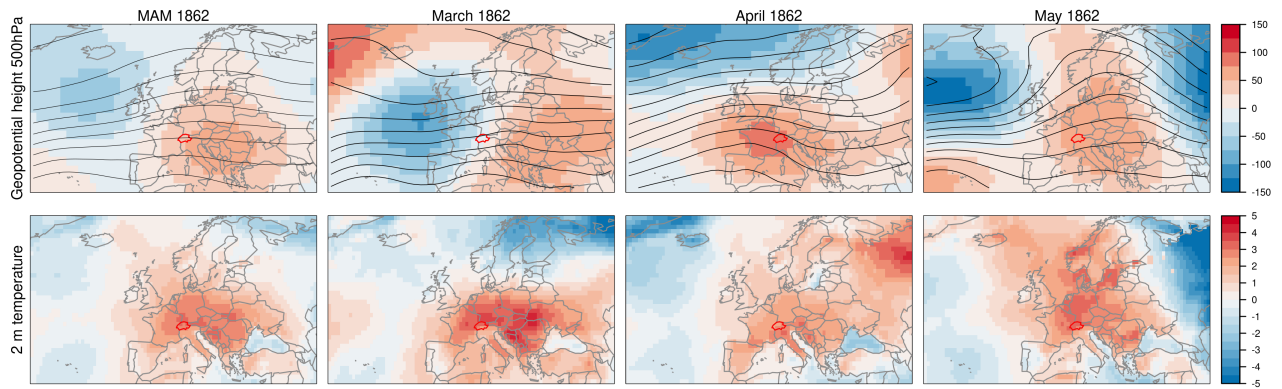ally in 1862. b) same as in a) but for 2 m temperature anomalies. Anomalies are calculated with respect to the 1871 to 1900 periods. The borders of Switzerland are marked in darkred. Data is from ModE-RA (Valler et al., in review).

Bibliography

Ambühl, E.: 100 Jahre Einschneien und Ausapern in Andermatt (1860/1960), Die Alpen, URL https://www.sac-cas.ch/index.php?eID=dumpFile&t=f&f=133729&token=e932334ef1e45fb867c0f664f81416f77eea1429, (last accessed 20 June 2023), 1961.

Appenzeller-Kalender: Appenzeller Kalender: Von der Witterung und Fruchtbarkeit vom Herbst 1872-1873, doi:10.5169/seals-373580, 1874.

Auchmann, R., Brugnara, Y., Rutishauser, T., Brönnimann, S., Gehrig, R., Pietragalla, B., Begert, M., Sigg, C., Knechtl, V., Calpini, B., and Konzelmann, T.: Quality Analysis and Classification of Data Series from the Swiss Phenology Network, Technical Report Meteoswiss, 271, 77 pp, URL https://www.meteoschweiz.admin.ch/dam/jcr:5220f36c-435d-4d46-b766-ba91b0dffe37/fachbericht-271.pdf, (last accessed 20 June 2023), 2018.

Basler, D.: Evaluating phenological models for the prediction of leaf-out dates in six temperate tree species across central Europe, Agricultural and Forest Meteorology, 217, 10–21, doi:10.1016/j.agrformet.2015.11.007, 2016.

Begert, M., Stöckli, R., and Croci-Maspoli, M.: Klimaentwicklung in der Schweiz - vorindustrielle Referenzperiode und Veränderung seit 1864 auf Basis der Temperaturmessung, Technical Report Meteoswiss, 274, 23 pp, URL "https://www.meteoswiss.admin.ch/dam/jcr:4c89a839-d577-47f1-aeb9-a30749ddaf2b/AB_Vorind_Refp_v1.1_de.pdf", (last accessed 30 June 2023), 2019.

Braecker, U.: Tagebücher 1779-1788 (Sämtliche Schriften 2), C.H.Beck/Haupt, Muenchen, 1998.

Brown, P. J., Bradley, R. S., and Keimig, F. T.: Changes in Extreme Climate Indices for the Northeastern United States, 1870–2005, Journal of Climate, 23, 6555 – 6572, doi:10.1175/2010JCLI3363.1, 2010.

Brugnara, Y., Auchmann, R., Brönnimann, S., Allan, R. J., Auer, I., Barriendos, M., Bergström, H., Bhend, J., Brázdil, R., Compo, G. P., Cornes, R. C., Dominguez-Castro, F., van Engelen, A. F. V., Filipiak, J., Holopainen, J., Jourdain, S., Kunz, M., Luterbacher, J., Maugeri, M., Mercalli, L., Moberg, A., Mock, C. J., Pichard, G., Řezníčková, L., van der Schrier, G., Slonosky, V., Ustrnul, Z., Valente, M. A., Wypych, A., and Yin, X.: A collection of sub-daily pressure and temperature observations for the early instrumental period with a focus on the" year without a summer" 1816, Climate of the Past, 11, 1027–1047, doi:10.5194/cp-11-1027-2015, 2015.

Brugnara, Y., Auchmann, R., Rutishauser, T., Gehrig, R., Pietragalla, B., Begert, M., Sigg, C., Knechtl, V., Konzelmann, T., Calpini, B., and Brönnimann, S.: Homogeneity

assessment of phenological records from the Swiss Phenology Network, International journal of biometeorology, 64, 71–81, doi:10.1007/s00484-019-01794-y, 2020a.

Brugnara, Y., Pfister, L., Villiger, L., Rohr, C., Isotta, F. A., and Brönnimann, S.: Early instrumental meteorological observations in Switzerland: 1708–1873, Earth System Science Data, 12, 1179–1190, doi:10.5194/essd-12-1179-2020, 2020b.

Brugnara, Y., Hari, C., Pfister, L., Valler, V., and Brönnimann, S.: Pre-industrial temperature variability on the Swiss Plateau derived from the instrumental daily series of Bern and Zurich, Climate of the Past Discussions, pp. 1–34, doi:10.5194/cp-2022-34, 2022.

Burgdorf, A.-M., Brönnimann, S., Adamson, G., Amano, T., Aono, Y., Barriopedro, D., Bullón, T., Camenisch, C., Camuffo, D., Daux, V., del Rosario Prieto, M., Dobrovolný, P., Gallego, D., García-Herrera, R., Gergis, Joelle Grab, S., Hannaford, M. J., Holopainen, J., Kelso, C., Kern, Z., Kiss, Andrea Kuan-Hui Lin, E., Loader, N. J., Možný, M., Nash, D., Nicholson, S. E., Pfister, C., Rodrigo, F. S., Rutishauser, T., Sharma, S., Takács, K., Vargas, E. T., and Vega, I.: DOCU-CLIM: A global documentary climate dataset for climate reconstructions, Scientific data, 10, 402, doi:10.1038/s41597-023-02303-y, 2023.

Collet, D.: Die doppelte Katastrophe: Klima und Kultur in der europäischen Hungerkrise 1770–1772., vol. 18 of *Umwelt und Gesellschaft*, Vandenhoeck & Ruprecht, doi:10.13109/9783666355929, 2018.

Cornes, R. C., van der Schrier, G., and Squintu, A. A.: A reappraisal of the thermal growing season length across Europe, International Journal of Climatology, 39, 1787–1795, doi:10.1002/joc.5913, 2019.

Defila, C. and Clot, B.: Phytophenological trends in Switzerland, International journal of biometeorology, 45, 203–207, doi:10.1007/s004840100101, 2001.

Diodato, N., Fratianni, S., and Bellocchi, G.: Reconstruction of snow days based on monthly climate indicators in the Swiss pre-alpine region, Regional Environmental Change, 20, 1–9, doi:10.1007/s10113-020-01639-0, 2020.

Domínguez-Castro, F., Reig, F., Vicente-Serrano, S. M., Aguilar, E., Peña-Angulo, D., Noguera, I., Revuelto, J., van der Schrier, G., and El Kenawy, A. M.: A multidecadal assessment of climate indices over Europe, Scientific data, 7, 125, doi:10.1038/s41597-020-0464-0, 2020.

Flückiger, S., Brönnimann, S., Holzkämper, A., Fuhrer, J., Krämer, D., Pfister, C., and Rohr, C.: Simulating crop yield losses in Switzerland for historical and present Tamb-

ora climate scenarios, Environmental Research Letters, 12, 074 026, doi:10.1088/1748-9326/aa7246, 2017.

Forel, F.-A.: Le Léman : monographie limnologique, F. Rouge, Lausanne, doi:10.5962/bhl.title.124608, 1892.

Franssen, H. J. H. and Scherrer, S. C.: Freezing of lakes on the Swiss plateau in the period 1901–2006, International Journal of Climatology, 28, 421–433, doi:https://doi.org/10.1002/joc.1553, 2008.

Fu, Y. H., Campioli, M., Demarée, G., Deckmyn, A., Hamdi, R., Janssens, I. A., and Deckmyn, G.: Bayesian calibration of the Unified budburst model in six temperate tree species, International journal of biometeorology, 56, 153–164, doi:10.1007/s00484-011-0408-7, 2012.

Füllemann, C., Begert, M., Croci-Maspoli, M., and Bönnimann, S.: Digitalisieren und Homogenisieren von historischen Klimadaten des Swiss NBCN: Resultate aus DigiHom, Arbeitsberichte der MeteoSchweiz, 236, URL https://www.meteoswiss.admin.ch/dam/jcr:c0d90a48-a05d-4ac9-9cf3-10769270d75e/ab236.pdf, (last accessed 21 June 2023), 2011.

Gelman, A. and Rubin, D. B.: Inference from iterative simulation using multiple sequences, Statistical science, 7, 457–472, doi:10.1214/ss/1177011136, 1992.

Grimmer, M.: The Meteorological Diaries of Johann Rudolf von Salis-Marschlins 1781-1800, Master's Thesis, University of Bern, URL https://occrdata.unibe.ch/students/theses/msc/283.pdf, 2019.

Hänninen, H.: Modelling bud dormancy release in trees from cool and temperate regions, Acta Forestalia Fennica, pp. 1–47, doi:10.14214/aff.7660, 1990.

Hartig, F., Minunno, F., Paul, S., Cameron, D., Ott, T., and Pichler, M.: BayesianTools: General-purpose MCMC and SMC samplers and tools for Bayesian statistics, R package version 0.1.8, URL https://github.com/florianhartig/bayesiantools, 2023.

Hufkens, K., Basler, D., Milliman, T., Melaas, E. K., and Richardson, A. D.: An integrated phenology modelling framework in r, Methods in Ecology and Evolution, 9, 1276–1285, doi:10.1111/2041-210X.12970, 2018.

Imfeld, N., Stucki, P., Brönnimann, S., Bader, S., Bürgi, M., Calanca, P., Gubler, S., Holzkämper, A., Hövel, L., Isotta, F. A., Kestenholz, C., Kotlarski, S., Mastai, A., Nussbaumer, S. U., Raible, C. C., Röthlisberger, M., Scherrer, S. C., Staub, K., Vicedo-Cabrera, A. M., Vogel, M.-M., Wehrli, K., Thomas, W., and Zumbühl, H. J.: Hot and dry summers in Switzerland. Causes and impacts of the record summers 1947,

2003, and 2018, Bern: Geographica Bernensia, Reihe G Grundlagenforschung G96, doi:10.4480/GB2022.G98.02, 2022.

Imfeld, N., Pfister, L., Brugnara, Y., and Brönnimann, S.: A 258-year-long data set of temperature and precipitation fields for Switzerland since 1763, Climate of the Past, 19, 703–729, doi:10.5194/cp-19-703-2023, 2023.

Imfeld, N., Hufkens, K., and Brönnimann, S.: Daily gridded temperature, precipitation, and phenological indices for Switzerland from 1763 to 2020, PANGAEA [data set], in review.

Isotta, F. A., Begert, M., and Frei, C.: Long-term consistent monthly temperature and precipitation grid data sets for Switzerland over the past 150 years, Journal of Geophysical Research: Atmospheres, 124, 3783–3799, doi:10.1029/2018JD029910, 2019.

Joller, F. J.: Collectaneen von Pfarrer Joller, Archiv des Geschichtsforschenden Vereins von Oberwallis, 5, 1888.

Kopp, C.: Résumé des observations météorologiques faites à Neuchâtel dans le 18ème siècle de 1760 à 1800, Bulletin de la Société Neuchâteloise de Sciences Naturelles, 9, 56–67, doi:10.5169/seals-88065, 1873.

Lhotka, O. and Brönnimann, S.: Possible Increase of Vegetation Exposure to Spring Frost under Climate Change in Switzerland, Atmosphere, 11, doi:10.3390/atmos11040391, 2020.

Longpré, M.-A., Stix, J., Burkert, C., Hansteen, T., and Kutterolf, S.: Sulfur budget and global climate impact of the A.D. 1835 eruption of Cosigüina volcano, Nicaragua, Geophysical Research Letters, 41, 6667–6675, doi:10.1002/2014GL061205, 2014.

Marty, C.: Regime shift of snow days in Switzerland, Geophysical Research Letters, 35, doi:10.1029/2008GL033998, 2008.

Meier, M. and Bigler, C.: Process-oriented models of autumn leaf phenology: ways to sound calibration and implications of uncertain projections, EGUsphere, 2023, 1–43, doi:10.5194/egusphere-2022-1423, 2023.

Meier, M., Fuhrer, J., and Holzkämper, A.: Changing risk of spring frost damage in grapevines due to climate change? A case study in the Swiss Rhone Valley, International journal of biometeorology, 62, 991–1002, doi:10.1007/s00484-018-1501-y, 2018.

MeteoSwiss: Witterungsberichte Schweiz 1861 – 1869, URL https://www.meteoswiss.admin.ch/dam/jcr:a4f1eb74-3a40-4476-bc56-64a27382bb5f/Witterungsberichte_1861-1869.pdf, (last accessed 25 July 2023), 2016.

MeteoSwiss: Documentation of MeteoSwiss Grid-Data Products. Daily Precipitation (final analysis): RhiresD, URL https://www.meteoswiss.admin.ch/dam/jcr:4f51f0f1-0fe3-48b5-9de0-15666327e63c/ProdDoc_RhiresD.pdf, (last accessed 30 June 2022), 2021a.

MeteoSwiss: Documentation of MeteoSwiss Grid-Data Products. Daily Mean, Minimum and Maximum Temperature: TabsD, TminD, TmaxD, URL https://www.meteoswiss.admin.ch/dam/jcr:818a4d17-cb0c-4e8b-92c6-1a1bdf5348b7/ProdDoc_TabsD.pdf, (last accessed 30 June 2022), 2021b.

MZA: Schweizerische Meteorlogische Beobachtungen, Annalen der Schweizerisch Meteorlogischen Zentralanstalt, URL https://www.meteoschweiz.admin.ch/assets/weather-archive/annalen-1873.pdf, (last accessed 25 July 2025), 1873.

Müller, C.: Joh. Heinrich Waser, der zürcherische Volkswirthschafter des 18. Jahrhunderts, seine Bestrebungen und Schicksale und sein statistischer Nachlass, fortgeführt bis zur Gegenwart, J.Herzog, Zurich, 1878.

Paffrath, J.: Schriften des Vereins für die Geschichte des Bodensees und seiner Umgebung, chap. Zum Wetterverlauf am Bodensee, Kommissionsverlag von Joh. Thom. Stettner, Lindau, 1915.

Parker, D. E., Legg, T. P., and Folland, C. K.: A new daily central England temperature series, 1772–1991, International Journal of Climatology, 12, 317–342, doi:10.1002/joc.3370120402, 1992.

Pfister, C. and Wanner, H.: Climate and Society in Europe: The Last Thousand Years, Haupt Verlag Bern, 2021.

Pfister, C., Rohr, C., and Jover, A. C. C.: Euro-Climhist: eine Datenplattform der Universität Bern zur Witterungs-, Klima-und Katastrophengeschichte, Wasser Energie Luft, 109, doi:10.7892/boris.97013, 2017.

Reid, P. C., Hari, R. E., Beaugrand, G., Livingstone, D. M., Marty, C., Straile, D., Barichivich, J., Goberville, E., Adrian, R., Aono, Y., Brown, R., Foster, J., Groisman, P., Hélaouët, P., Hsu, H.-H., Kirby, R., Knight, J., Kraberg, A., Li, J., Lo, T.-T., Myneni, R. B., North, R. P., Pounds, J. A., Sparks, T., Stübi, R., Tian, Y., Wiltshire, K. H., Xiao, D., and Zhu, Z.: Global impacts of the 1980s regime shift, Global Change Biology, 22, 682–703, doi:10.1111/gcb.13106, 2016.

Rutishauser, T., Luterbacher, J., and Wanner, H.: A 280-Year Long Series of Phenological Observations of Cherry Tree Blossoming Dates for Switzerland, in: Diploma thesis, University of Bern, pp. 1–122, 2003.

Rutishauser, T., Luterbacher, J., Jeanneret, F., Pfister, C., and Wanner, H.: A phenology-based reconstruction of interannual changes in past spring seasons, Journal of Geophysical Research: Biogeosciences, 112, doi:10.1029/2006JG000382, 2007.

SBV: Statistische Erhebungen und Schätzungen auf dem Gebiete der Landwirtschaft, 35. Jahresheft, p. 41 pp, URL https://www.sbv-usp.ch/fileadmin/sbvuspch/04_Medien/Publikationen/SES/Archiv/SES_1958-35.pdf, (last accessed, 10 April 2023), 1958.

Schaller-Donauer, A.: Chronik der Naturereignisse im Urnerland 1000-1800, Gotthardpost, 1937.

Scherrer, S. C. and Begert, M.: Effects of large-scale atmospheric flow and sunshine duration on the evolution of minimum and maximum temperature in Switzerland, Theoretical and Applied Climatology, 138, 227–235, doi:10.1007/s00704-019-02823-x, 2019.

Schwander, M., Brönnimann, S., Delaygue, G., Rohrer, M., Auchmann, R., and Brugnara, Y.: Reconstruction of Central European daily weather types back to 1763, International Journal of Climatology, 37, 30–44, doi:10.1002/joc.4974, 2017.

Serquet, G., Marty, C., Dulex, J.-P., and Rebetez, M.: Seasonal trends and temperature dependence of the snowfall/precipitation-day ratio in Switzerland, Geophysical Research Letters, 38, L07 703, doi:10.1029/2011GL046976, 2011.

Sippel, S., Fischer, E. M., Scherrer, S. C., Meinshausen, N., and Knutti, R.: Late 1980s abrupt cold season temperature change in Europe consistent with circulation variability and long-term warming, Environmental Research Letters, 15, 094 056, doi:10.1088/1748-9326/ab86f2, 2020.

Slivinski, L. C., Compo, G. P., Whitaker, J. S., Sardeshmukh, P. D., Giese, B. S., McColl, C., Allan, R., Yin, X., Vose, R., Titchner, H., Kennedy, J., Spencer, L. J., Ashcroft, L., Brönnimann, S., Brunet, M., Camuffo, D., Cornes, R., Cram, T. A., Crouthamel, R., Domínguez-Castro, F., Freeman, J. E., Gergis, J., Hawkins, E., Jones, P. D., Jourdain, S., Kaplan, A., Kubota, H., Le Blancq, F., Lee, T.-C., Lorrey, A., Luterbacher, J., Maugeri, M., Mock, C. J., Kent Moore, G., Przybylak, R., Pudmenzky, C., Reason, C., Slonosky, V. C., Smith, C. A., Tinz, B., Trewin, B., Valente, M. A., Wang, X. L., Wilkinson, C., Wood, K., and Wyszyński, P.: Towards a more reliable historical reanalysis: Improvements for version 3 of the Twentieth Century Reanalysis system, Quarterly Journal of the Royal Meteorological Society, 145, 2876–2908, doi:10.1002/qj.3598, 2019.

Slivinski, L. C., Compo, G. P., Sardeshmukh, P. D., Whitaker, J., McColl, C., Allan, R., Brohan, P., Yin, X., Smith, C., Spencer, L., , Vose, R. S., Rohrer, M., Conroy, R. P., Schuster, D. C., Kennedy, J. J., Ashcroft, L., Brönnimann, S., Brunet, M., Camuffo, D., Cornes, R., Cram, T. A., Domínguez-Castro, F., Freeman, J. E., Gergis,

J., Hawkins, E., Jones, P. D., Kubota, H., Lee, T. C., Lorrey, A. M., Luterbacher, J., Mock, C. J., Przybylak, R. K., Pudmenzky, C., Slonosky, V. C., Tinz, B., Trewin, B., Wang, X. L., Wilkinson, C., Wood, K., and Wyszyński, P.: An evaluation of the performance of the twentieth century reanalysis version 3, Journal of Climate, 34, 1417–1438, doi:10.1175/JCLI-D-20-0505.1, 2021.

Staatsarchiv: Unterschiedliche Begebenheiten und Ereignisse des Wetters, teils in Regenteils in Schneewetter, wie auch in Kälte und Erdstössen (1755-1829), 1755-1829.

Strasser, G.: Grindelwaldner Chroniken, Gletschermann. Familienblatt für Grindelwald, doi:10.3931/e-rara-78062, 1890.

Studer, S., Appenzeller, C., and Defila, C.: Inter-annual variability and decadal trends in alpine spring phenology: a multivariate analysis approach, Climatic Change, 73, 395–414, doi:10.1007/s10584-005-6886-z, 2005.

Ter Braak, C. J. and Vrugt, J. A.: Differential evolution Markov chain with snooker updater and fewer chains, Statistics and Computing, 18, 435–446, doi:10.1007/s11222-008-9104-9, 2008.

Valler, V., Franke, J., Brugnara, Y., Samakinwa, E., Hand, R., Lundstad, E., Burgdorf, A.-M., and Brönnimann, S.: ModE-RA – A global monthly paleo-reanalysis of the modern era (1421 to 2008), Sci. Data, in review.

Vitasse, Y. and Rebetez, M.: Unprecedented risk of spring frost damage in Switzerland and Germany in 2017, Climatic Change, 149, 233–246, doi:10.1007/s10584-018-2234-y, 2018.

Vitasse, Y., Schneider, L., Rixen, C., Christen, D., and Rebetez, M.: Increase in the risk of exposure of forest and fruit trees to spring frosts at higher elevations in Switzerland over the last four decades, Agricultural and Forest Meteorology, 248, 60–69, doi:10.1016/j.agrformet.2017.09.005, 2018.

Vogel, F.: Memorabilia Tigurina oder Chronik der Denkwürdigkeiten der Stadt und Landschaft Zürich, im Verlag des Verfassers und in Commission bey S. Höhr, doi:10.3931/e-rara-26390, 1841.

Wypych, A., Sulikowska, A., Ustrnul, Z., and Czekierda, D.: Variability of growing degree days in Poland in response to ongoing climate changes in Europe, International Journal of Biometeorology, 61, 49–59, doi:10.1007/s00484-016-1190-3, 2017.

Yiou, P., Boichu, M., Vautard, R., Vrac, M., Jourdain, S., Garnier, E., Fluteau, F., and Menut, L.: Ensemble meteorological reconstruction using circulation analogues of 1781–1785, Climate of the Past, 10, 797–809, doi:10.5194/cp-10-797-2014, 2014.

Zambri, B., Robock, A., Mills, M. J., and Schmidt, A.: Modeling the 1783–1784 Laki Eruption in Iceland: 2. Climate Impacts, Journal of Geophysical Research: Atmospheres, 124, 6770–6790, doi:10.1029/2018JD029554, 2019.

Zennhäuser, G.: Witterung und Klima eines Walliser Alpentals nach Aufzeichnungen (1770-1812) des Weibels Johann Ignaz Inderschmitten von Binn, Blätter aus der Walliser Geschichte 40, 40, URL https://doc.rero.ch/record/200964, (last accessed 12 September 2023), 2008.

Zhang, X., Alexander, L., Hegerl, G. C., Jones, P., Tank, A. K., Peterson, T. C., Trewin, B., and Zwiers, F. W.: Indices for monitoring changes in extremes based on daily temperature and precipitation data, WIREs Climate Change, 2, 851–870, doi:10.1002/wcc.147, 2011.

Zschokke, T.: Witterungsbeobachtungen in Aarau in den Jahren 1861-1865, vol. 1, Aarau, Sauerländer, URL https://abn-primo.hosted.exlibrisgroup.com/permalink/f/17uelnu/41ABN_ALEPH_DS000261569, 1865.

Zubler, E. M., Scherrer, S. C., Croci-Maspoli, M., Liniger, M. A., and Appenzeller, C.: Key climate indices in Switzerland; expected changes in a future climate, Climatic change, 123, 255–271, doi:10.1007/s10584-013-1041-8, 2014.

Chapter 4

Hot and dry summers in Switzerland - Causes and impacts of the record summers 1947, 2003, and 2018

This Chapter contains an introduction to the hot and dry summer of 1947 in Switzerland, and two sections about atmospheric dynamics of warm summers and about the summer half year of 2022 (Sect. 4.3 and 4.4) that have been published as part of a booklet on hot and dry summers in Switzerland. The booklet (article 1) has been written by 23 experts from different fields aimed at the general public. Article 2 has been written as an addendum at the end of the very warm summer half year of 2022.

Article 1:

Imfeld, N.; Stucki, P.; Brönnimann, S.; Bader, S.; Bürgi, M.; Calanca, P.; Gubler, S.; Holzkämper, A.; Hövel, L.; Isotta, F. A.; Kestenholz, C.; Kotlarski, S.; Mastai, A.; Nussbaumer, S. U.; Raible, C.; Röthlisberger, M.; Scherrer, S. C.; Staub, K.; Vicedo-Cabrera, A. M.; Vogel, M.M.; Wehrli, K.; Wohlgemuth T.; Zumbühl, H. J. (2022). Hot and dry summers in Switzerland. Causes and impacts of the record summers 1947, 2003, and 2018, (Reihe G Grundlagenforschung G98). Bern: Geographica Bernensia, DOI: 10.4480/GB2022.G98.03.

Article 2:

Imfeld, N.; Stucki, P.; Brönnimann, S.; Bürgi, M.; Calanca, P.; Holzkämper, A.; Isotta, F. A.; Nussbaumer, S. U.; Scherrer, S. C.; Staub, K.; Vicedo-Cabrera, A. M.; Wohlgemuth, T. und Zumbühl, H. J. (2022). 2022: Ein ziemlich normaler zukünftiger Sommer. Geographica Bernensia, G100, DOI: 10.4480/GB2022.G100.

Abstract

The last summer half years were marked by new temperature records, for example, the longest heat wave ever measured in southern Switzerland in the summer of 2022. Nine out of the top ten warmest summer half years occurred in the 21st century, with the exception of the summer of 1947. This summer half year has been exceptionally warm and dry, in particular for its climatological period. Here, we place the summer of 1947 into the context of the 258-year-long daily reconstruction of daily temperature and compare different hot summers across the centuries based on climate indices. Further, we explain the main processes of how extremely hot summers happen, from how air warms to why heat waves can re-occur throughout an entire summer. In 1947, the repeated occurrence of blocking situations over Europe played a pivotal role in generating a very warm summer. Finally, we look at the impacts of the hot and dry summer half year of 2022 and place the summer into context with its mean climate, and a future climate showing that this summer is not extreme, but a fairly normal summer.

4.1 Introduction

The last two summer half years (April - September) were marked by new temperature records, for example, the longest and most intense heat wave ever recorded in late August in northern and southern Switzerland (MeteoSchweiz, 2023). While new temperature records have been occurring throughout the year, they are particularly striking in the summer months, since the consequences of the high temperatures are significant, e.g., in terms of heat-related deaths and melting glaciers (e.g. Ragettli et al., 2019; GLAMOS, 2022). Warm summers have, however, occurred throughout history, and studying historical warm summers can be valuable, despite them no longer being among the warmest. Historical extreme summers are relevant, for example, to put them in context with past climate and to study how extreme they were relative to their mean climate, they can serve as storylines for future extreme summers, and we can learn about the impacts of historical warm summers.

A period of remarkably warm summers occurred in Europe in the late 1940s. In Switzerland, the summer of 1947 has been the record summer for many years. Only in the 21st century, warmer summer half-year temperatures were registered in 2003, 2018, 2022, and 2023. In addition to 1947, the summers of 1949 and 1945 also showed unusually high temperatures for this time (Imfeld et al., 2022, p. 8-9). These summers were not only warm but also unusually dry. The summer half year of 1947 is still the driest summer in parts of northern Switzerland since 1864. The prolonged hot and dry conditions led to severe consequences for ecosystems and society, such as dried-out lakes, losses in agriculture, forest damages, and glacier melting described as unprecedented at that time (Imfeld et al., 2022).

In the following Chapter, we describe the climatological context of the summer of 1947 and past hot summers based on the new daily temperature reconstruction spanning 258 years (Imfeld et al., 2023) and based on the Swiss plateau series (Brugnara et al., 2022). A climatological description of the summer half year of 1947 has already been presented in section 2 of the brochure (Imfeld et al., 2022, p. 8-9). Then, a section on the atmospheric dynamics of hot summers in general with a brief look at the summer of 1947 follows which corresponded to section 3 in the brochure. Further, we put the summer of 2022 into context with the almost 160-year-long record of the Swiss mean temperature and precipitation and describe the impacts as they have been observed by the end of September 2022.

4.2 Hot summers in the 258-year-long temperature reconstruction

Based on the merged Swiss Plateau series from Bern and Zurich (Brugnara et al., 2022), and extended with the newly measured data for 2023 (the mean of observation from Bern/Zollikofen and Zurich/Fluntern), the summer half year of 1947 ranks as the fifth warmest in the record since 1763 with an anomaly of 2.91 °C with respect to the 1871 to 1900 period. The Swiss Plateau series is used, because the temperature fields are not yet updated until September 2023. With anomalies of 3.04 and 3.12 °C, the summer half years of 2022 and 2023 just recently became the third and fourth warmest summer half years recorded in Switzerland after 2018 and 2003. Among the top ten warmest summer half years, with 1947, only one summer from the 20th century remains, indicating how exceptionally warm this summer half year has been.
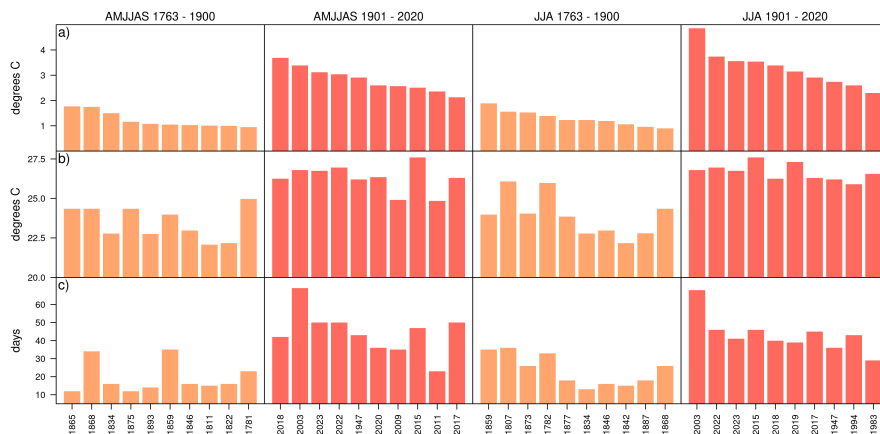
Figure 4.1: Ranking of the ten warmest summer half years (AMJJAS) and summer months (JJA) for two periods from 1763 to 1900 and from 1901 to 2020 based on the anomalies with respect to the pre-industrial reference period (Begert and Frei, 2018). a) Mean temperature anomaly, b) maximum daily mean temperature, c) number of summer days with daily mean temperature above 20 ° C. The ranking is based on the Swiss Plateau series (Brugnara et al., 2022) because it is possible to extend it to 2023.

Separating the Swiss temperature series with its extension to 2023 (Brugnara et al., 2022) into a period before the pre-industrial mean (including the pre-industrial mean) and after the pre-industrial mean periods, allows us to look at early warm summer half years (Fig. 4.1a). With anomalies of 1.77 and 1.75 °C above the pre-industrial mean, the summers of 1865 and 1868 were the warmest before 1901, but their anomalies barely reached half the anomaly of 2018. The warmest daily mean temperatures of the warmest summers in the early period ranged between 22.10 and 25.00 °C, whereas in the recent period maximum

daily mean temperatures of the top ten summer half years range between 24.90 and 27.60 °C. The largest amount of days above 20 °C (hereafter denoted as summer days) in the entire period from 1763 to 2023 was registered in 2003 with 69 d (Fig. 4.1c). In the early period before 1901, the highest number of summer days was registered in 1859 with 35 d.

Considering only the summer months June to August, the summer of 2003 is still the most extreme with an anomaly of 4.85 °C. The summer of 1947 only ranks 8th, but other warm summers of the 20th century such as 1983 and 1994 are among the top ten as well. Very warm summers before 1901 were, for example, 1859 and 1807 with anomalies of 1.90 and 1.60 °C, but as expected considerably cooler than the hottest ten summers.
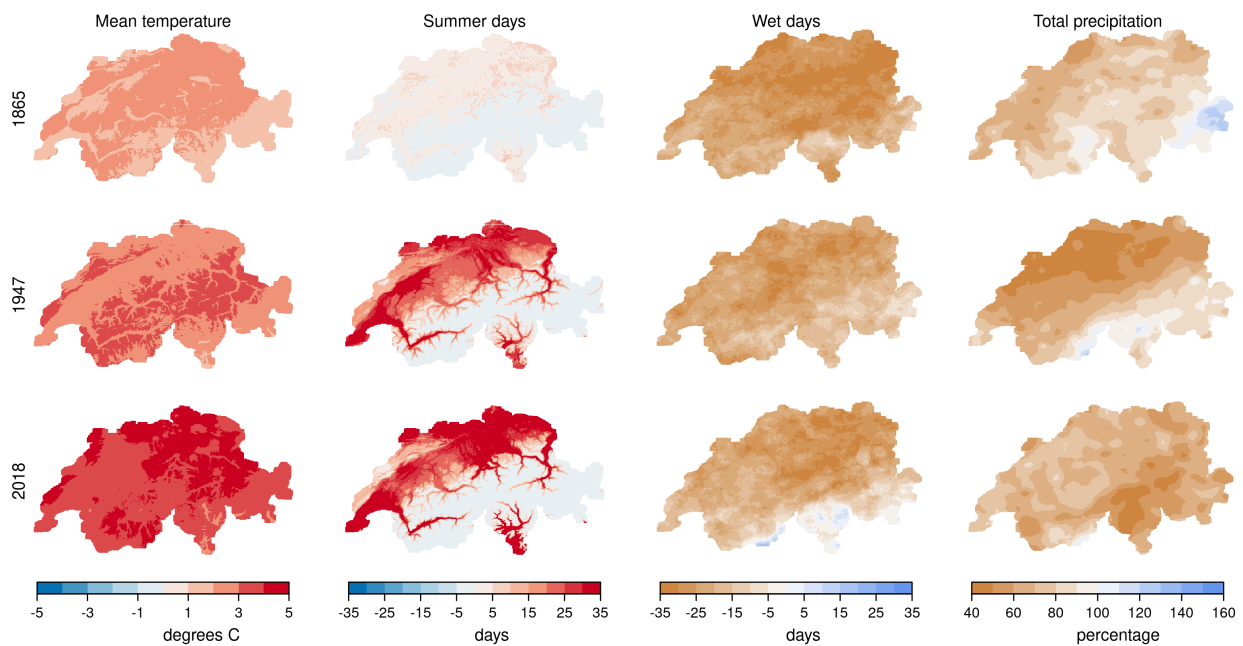
Figure 4.2: a) Anomaly of April - September mean daily temperature, b) anomaly of summer days (> 20 °C), c) anomaly of wet days (days >= 1 mm), and d) anomaly of total precipitation (in %) for the three warm summer half years 1865, 1947, and 2018 based on the gridded reconstruction for Switzerland. All anomalies are calculated with respect to April - September 1871 to 1900.

For further comparison, we consider the warmest summers of both periods, namely 1865 and 2003, and compare them to 1947 (Fig. 4.2). These summer half years currently also correspond to the warmest in each century. In the summer half year of 1865, based on our definition of summer days (days > 20 °C), rarely any summer days have been registered. For the later two years of 1947 and 2018, in some areas up to 65 d more summer days were reached compared to the 1871 to 1900 mean. Regarding wet days (days >= 1 mm), 1865 shows for a large area wet day anomalies of up to 35 d, in particular in eastern Switzerland (Fig. 4.2c). In 1947, entire Switzerland showed below average wet

days, whereas, in 2018, mainly the canton of Ticino in southern Switzerland did not register below average wet days. For total precipitation, the lowest anomalies are registered in 1947 in northern Switzerland, whereas in 1865, the eastern mountainous areas show around average precipitation sums (Fig. 4.2d). In comparison, in 2018, especially in southern Switzerland below average precipitation sums were registered. The summer half years of 1947 and 2018 are also among the years with the most negative water balance considering the Swiss Plateau (Imfeld et al., 2022, see p. 8).
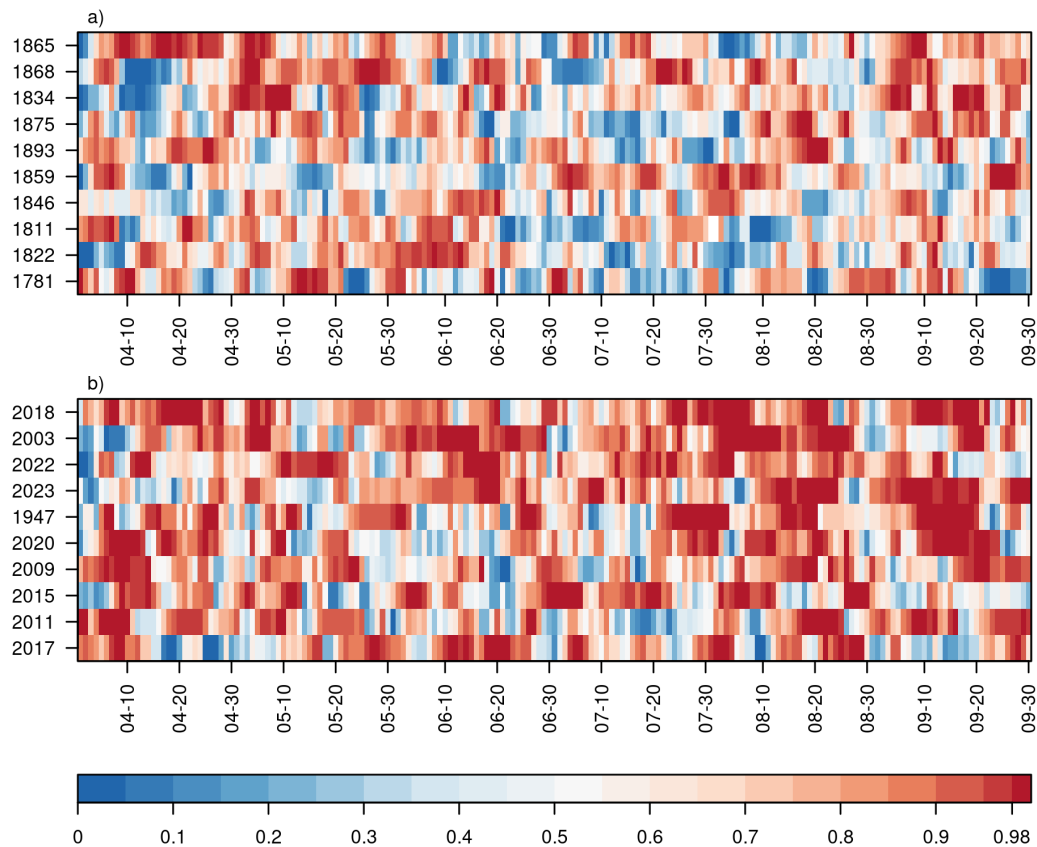
Figure 4.3: Heat waves based on the percentile of daily mean temperature during April to September for the ten warmest summer half years and for the two periods a) between 1763 and 1900, and b) between 1901 and 2023. The daily mean temperature from the Swiss Plateau series is used (Brugnara et al., 2022). For every year, the color represents the percentile of the respective day. Percentiles are calculated for every day of the year between 1871 and 1900 using a 5 d moving window centered at the day of interest.

Heat waves are a relevant contributor to the high temperature anomalies of very hot summers. In the summer of 1947, a total of five heat waves were recorded at the station of Basel/Binningen in northern Switzerland. One way to look at heat waves is by considering the days when the 90th percentile is surpassed during at least 6 consecutive days. This is referred to as the Warm Spell Duration Index (WSDI) (e.g. in Molina et al., 2020).

In Fig. 4.3, the percentile of every day from April to September is shown for the Swiss Plateau series for the warmest ten summers in both periods. For this mean series, in 1947, only four periods fulfilled the WSDI definition (05-25 to 06-03, 07-22 to 08-03, 08-13 to 08-20, and 09-08 to 09-20), but other areas in Switzerland registered five heat waves (Fig. 4.3b). Note that since there is no daily maximum temperature for the entire period, we considered the daily mean temperature to look at indications of heat waves. In the early period (Fig. 4.3a), the warm summer of 1865 shows prolonged warm April temperatures and warm September temperatures, contributing to the warm summer, but no heat waves from June to August. For the second period from 1901 to 2023 (Fig. 4.3b), particularly long heat waves are known for 2003 and 2018 (Black et al., 2004; Spensberger et al., 2020).

In the next section, we explore the mechanisms behind heat waves and hot summers in general and, also, focus on the summer of 1947.

4.3 Atmospheric dynamics: From a hot air parcel to a very hot summer

by Noemi Imfeld and Matthias Röthlisberger

In this article, we shed light on the formation of heat waves on various spatial and temporal scales. Starting with an individual air parcel, we discuss how an air parcel changes its temperature, in which weather systems heat waves develop, and how individual heat waves can evolve into an entire extreme summer. In addition, we summarise the most important synoptic features of the summer of 1947.

4.3.1 How does air change its temperature?

Our journey through the spatial and temporal scales of heat waves begins with an individual air parcel, for example, the air that was located about 100 metres above Bern at 2 p.m. on the 13th August 2003, and was around 30 °C warm at that time. To understand how this air parcel could become so warm, we can examine the air parcels' path on its journey through the atmosphere. This path is called "trajectory." Along its trajectory, an air parcel's temperature changes on the one hand due to pressure changes resulting from sinking (i.e., subsiding) or ascending motion, which results in compression or expansion of the air parcel (so-called "adiabatic" temperature changes). On the other hand, its temperature is affected by radiation, turbulence, or phase transformations of water (e.g. condensation of water vapour), which are referred to as "diabatic" temperature changes. Figures 4.4a and b show this interplay of adiabatic and diabatic processes along the trajectory of the air parcel located over Bern at 2 p.m. on 13th August 2003 (colored trajectory in Fig. 4.4). On 3rd August, this air parcel was still at a pressure level of 600 hPa (about 4500 m a.s.l.) over the Atlantic and then subsided to 800 hPa over the eastern Atlantic and England until 8th August. During this process, the air parcel warmed by 20 °C, whereby periods of strong subsidence were also associated with strong temperature increases (Fig. 4.4b). During the last three days prior to the arrival in Bern, the air parcel was located near the ground in the lowermost kilometre of the atmosphere. During this time, the temperature evolution decoupled from the pressure evolution, as diabatic processes started to strongly influence the temperature and the air parcel hardly moved vertically anymore. The jagged pattern in Figure 4.4b shows the classical diurnal cycle in temperature, arising from diabatic heating during the day and diabatic cooling at night by radiation, sensible heat fluxes, and turbulence.

During heat waves in Central Europe, the near-surface air is heated both by subsidence and by diabatic processes (Bieli et al., 2015; Zschenderlein et al., 2019). Contrary to common notions, this heat wave air mostly approaches Central Europe from northwest to northeast

and only in rare cases from the climatologically warmer southerly regions (Zschenderlein et al., 2019). This is illustrated exemplarily by the trajectories of the air parcels that reached Bern between 6th and 13th August 2003, which mainly approached Switzerland from northeast and which were located over the Atlantic Ocean a few days before (Fig. 4.4a). In cases when air masses from southerly regions approach Central Europe, they usually ascend over the colder air in Central Europe and therefore often do not reach the surface at all. However, the relative importance of compression, diabatic processes, and the simple horizontal transport of warm air for heat waves is still a subject of active research.
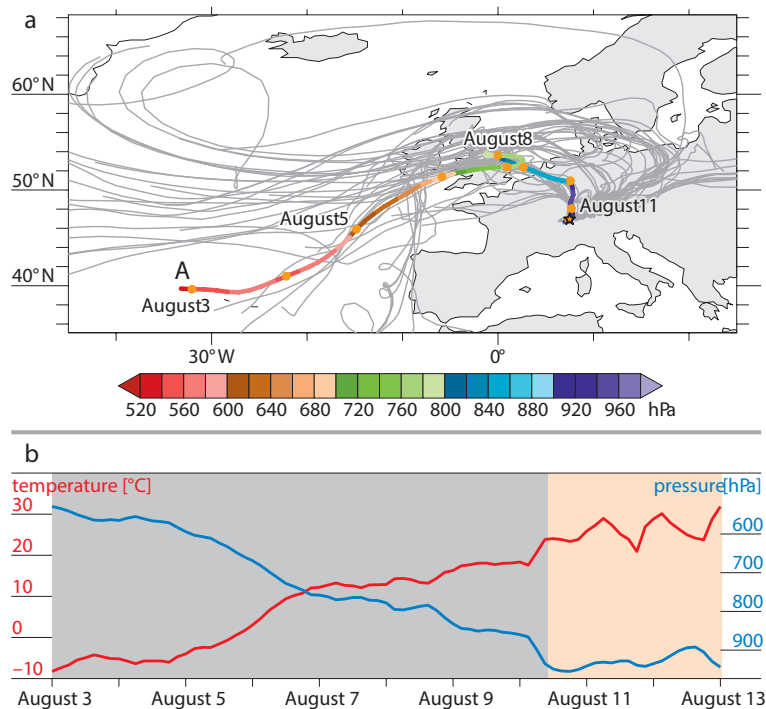
Figure 4.4: a) Trajectories of the air parcels arriving in Bern from 6th to 13th August 2003 at about 100 m above ground (in grey) based on ERA-5 (Hersbach et al., 2020). The trajectory of the air parcel with an arrival time of 2 p.m. local time on 13th August (the hottest day of the summer in Bern) is coloured by its pressure. b) Evolution of pressure (blue) and temperature (red) in the air parcel A. The grey and orange shading in (b) indicate periods during which temperature changes in air parcel A were primarily adiabatic and diabatic, respectively.

4.3.2 Synoptic scale – weather systems and heat waves

Whether and where heat waves develop is related to the synoptic-scale circulation (i.e., the large-scale circulation over several thousand kilometres) in the middle and upper troposphere (5000 – 12 000 m a.s.l.). At these heights is the jet stream, a band of strong

westerly winds that undulates from west to east. These waves of the jet stream, the so-called "Rossby waves", steer and modulate the occurrence of high- and low-pressure areas and thereby determine to a large extent how the surface temperature changes. This relationship is illustrated in Fig. 4.5a – c, which show the jet stream at 300 hPa (wind vectors), surface temperature anomalies, and sea level pressure for three days at 12 UTC during the summer of 1947. The largest positive temperature anomalies in Western Europe at all time steps are found in the central and eastern part of a "ridge", which is the region where the jet stream describes a poleward deflection. The negative temperature anomalies further east, however, are located below a "trough", i.e., below an equatorward deflection of the jet stream. Positive temperature anomalies occur in the central and eastern part of the ridge because there the air is descending near the surface and the middle troposphere and thereby heated adiabatically. This adiabatic warming leads to cloud-free skies, as cloud droplets and ice crystals evaporate or melt and sublimate during subsidence. The descending of the air thus also leads to stronger solar radiation, which diabatically warms the air near the surface (Pfahl and Wernli, 2012). If a ridge is located over a region for a particularly long time, this typically favours the development of heat waves, since the air near the surface can warm up over several days (Zschenderlein et al., 2019; Pfahl and Wernli, 2012; Sousa et al., 2018; Röthlisberger and Martius, 2019). This often happens when the Rossby waves reach a particularly large amplitude (i.e., extension in a north-south direction), thereby reducing their phase speed and deforming strongly (this process is called Rossby wave breaking) (Altenhoff et al., 2008). Such ridges can remain stationary for days and sometimes even weeks (in these cases they are called "blocks" or "blocking high-pressure systems"), and shift the normal west-east propagation of low-pressure systems to the north or south (Woollings et al., 2018). In central and northern Europe, heat waves occur mainly in association with blocks (Pfahl and Wernli, 2012). Also, during the heat waves in the summer of 1947, several blocking high-pressure systems were located over Europe, however at different positions (green lines in Fig. 4.5a – c).

4.3.3   From a heat wave to a very hot summer

Individual heat waves are thus strongly related to particular synoptic-scale weather systems, but how do individual heat waves become an entire extremely hot summer? Answering this question in detail is difficult because, at any location of the globe, only very few seasonal heat extremes occurred since weather data have been collected continuously and reliably. However, it is clear that the duration and temporal organisation of heat waves (and the weather systems responsible for them) play a key role. During the extremely hot summers of 2003 and 2018 in Europe, as well as 2010 in western Russia, several but also particularly long-lasting heat waves occurred Fink et al. (2004); Black et al. (2004); Spensberger et al. (2020); Schneidereit et al. (2012); Trenberth and Fasullo (2012), which
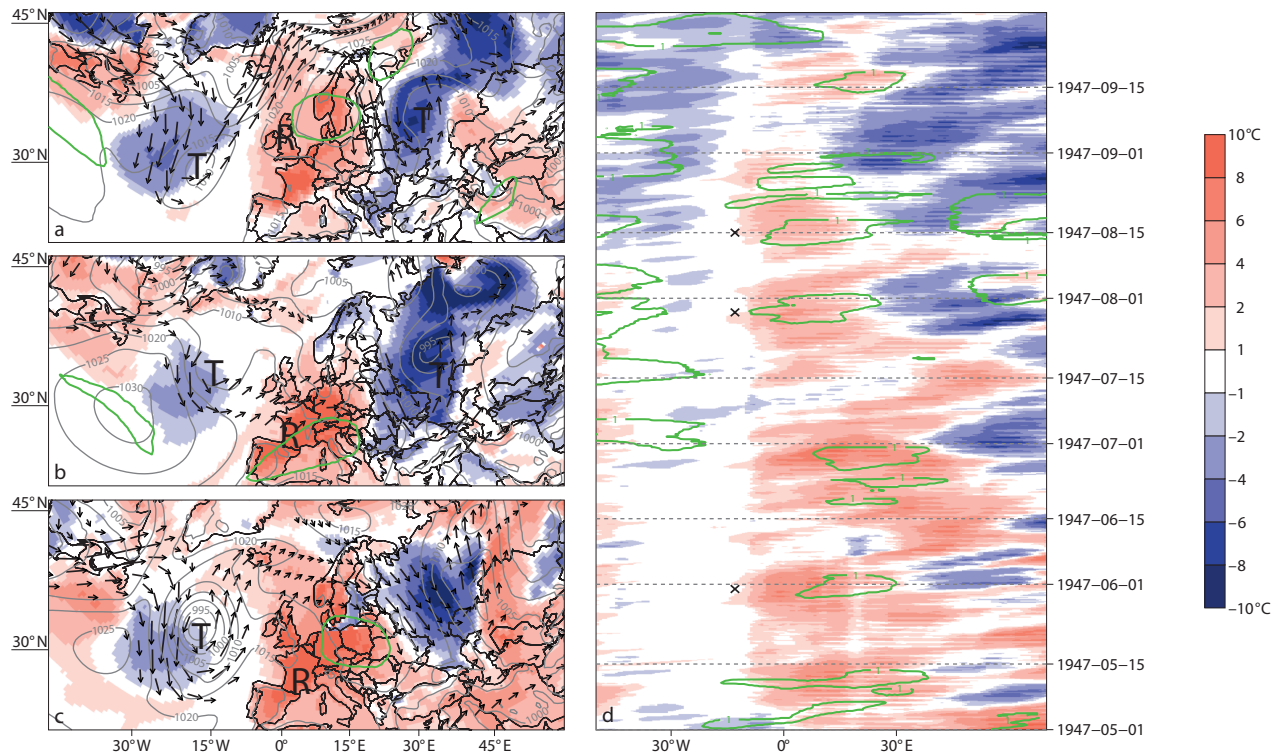
Figure 4.5: a – c) Meteorological situation during three heat days on a) 31st May, b) 29th July, and c) 15th August 1947 at 2 p.m. local time. Temperature anomalies are calculated relative to the 1931 – 1960 daily climatology at 2 p.m. (shading). The jet stream is apparent from the vectors, which show the 300 hPa wind wherever its velocity exceeds 18 m/s. Surface pressure (in hPa) is shown as grey lines. Green lines show blocked areas, troughs and ridges are labeled with T and R, respectively. d) Longitude-time plot of May to September 1947 hourly temperature anomalies averaged over 35 °C – 65 °C N (shading) and blocks (green lines). The three crosses indicate the times for which maps are shown in the left column. The data are from the reanalysis 20CRv3 (Slivinski et al., 2019).

were associated with long-lasting blocks, especially during the summer of 2010 in western Russia (Schneidereit et al., 2012; Fragkoulidis et al., 2018). Such a long-lasting block is typically repeatedly reinforced by ridges that form to the west of the block and are absorbed by the block (Woollings et al., 2018; Shutts, 1983; Steinfeld and Pfahl, 2019). In addition, it is known that the recurrent formation of ridges in the same location (even without a block) can lead to particularly long-lasting heat waves (Röthlisberger et al., 2019). The temporally clustered occurrence of blocks and ridges is influenced by so-called teleconnections, climatic connections between widely separated areas. These modulate the triggering, propagation, and breaking of Rossby waves, thus influencing the frequency of midlatitude blocks and ridges (Imfeld et al., 2022, p. 12). Heat summers over land also usually occur in conjunction with drought whereby heat and drought mutually reinforce

each other through land-atmosphere feedback.

4.3.4   1947: A summer with many blocks over Europe

Between May and September 1947, several, as well as unusually strong heat waves occurred in succession. The temperature anomalies averaged between 35 ° N and 65 ° N (Fig. 4.5d) were almost continuously strongly positive between May and September and interrupted only by short episodes with average temperatures. Blocks were repeatedly present over Europe throughout the summer – depending on the area, their frequency in the summer of 1947 was up to three times higher than the average for these months in the period 1931 – 1960 (Fig. 4.6a; the term "frequency" here refers to the fraction of time steps in the 1947 summer during which blocks occurred at each grid point). The frequent blocking situations in 1947 can be explained by the fact that resemblant large-scale flow patterns with a ridge over Europe (Fig. 4.5a – c) established in a recurrent manner including large-scale subsidence over Europe (Fig. 4.6c). The recurrence of similar flow patterns had led to a particularly large number of different blocks, depending on the region up to four blocks more than in the average of the years 1931 – 1960 (Fig. 4.6b), which corresponds roughly to a doubling of the number of blocks compared to climatology. This indicates that especially the temporal organisation of these blocks (i.e., their recurrence in a relatively short period) may have played a pivotal role in generating the extremely hot summer of 1947. The summer of 1947 thus exhibits the decisive characteristics of a heat summer described above.
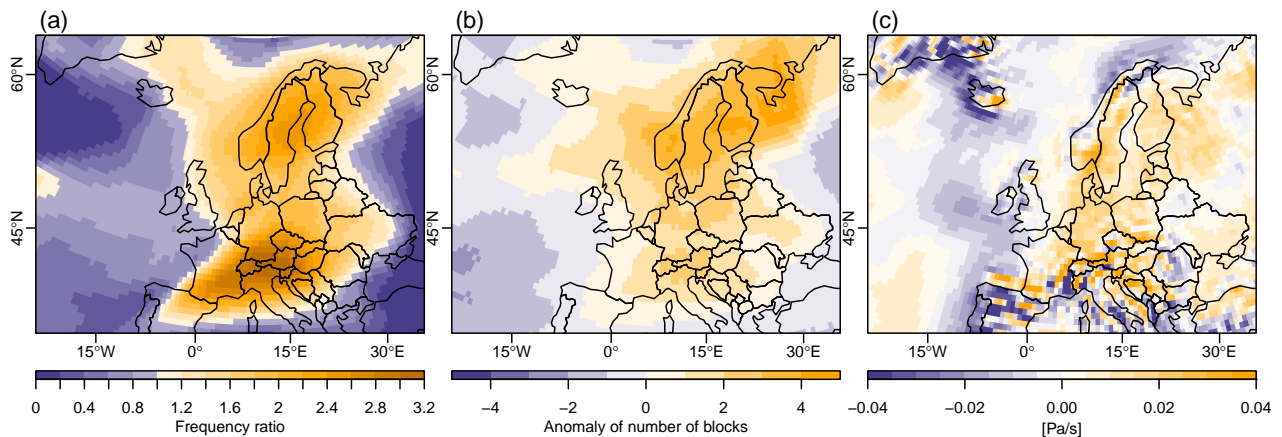
Figure 4.6: a) ratio of the frequency of blocks in summer 1947 (May to September) and the May to September climatology from 1931 – 1960; b) anomaly of number of blocks relative to the 1931 – 1960 climatology [same months as in (a)]. c) Anomaly of vertical motion at 700 hPa relative to the 1931 - 1960 climatology [same months as in (a)]. Positive values mean that air is sinking as pressure increases. The data are from the reanalysis 20CRv3 (Slivinski et al., 2019).

4.4 2022: A fairly normal future summer

by Imfeld, N., P. Stucki, S. Brönnimann, M. Bürgi, P. Calanca, A. Holzkämper, F. A. Isotta, S. U. Nussbaumer, S. C. Scherrer, K. Staub, A. M. Vicedo-Cabrera, T. Wohlgemuth und H. J. Zumbühl

The summer of 2022 gained wide-spread attention with its weather and climate extremes and their unmistakable consequences. In Switzerland, temperatures climbed above 30 °C as early as May, followed by several heat waves. The drought, which had already prevailed since the beginning of the year, lasted until August. The effects were immediately visible. Lake levels reached record lows, melting glaciers exposed objects and a pass, forests suffered and fire bans were imposed. But how extreme was the summer really? After the end of the meteorological summer half year, it is time for a ranking. This shows that the summer of 2022 was not as extreme in comparison as one might think, but is the harbinger of a new climate.

The summer half year 2022 was the third warmest in Switzerland since measurements began. In the series of measurements from 1864 onward, four years stand out from the rest: 2003, 2018, 2022, and 1947 (Fig. 4.7, top). Looking at the deviation from the prevailing climate in each case (Fig. 4.7, topright), 1947 and 2003 are the most striking, while the summer of 2022 is further behind, at about 0.65 °C [1]. Thus, more extreme temperatures would be possible. The drought throughout the summer half year (Fig. 4.7, bottom) was ultimately less severe than had been feared in midsummer because locally rather intense precipitation set in from mid-August. For the Swiss Plateau region (an average of the stations Bern/Zollikofen, Basel/Binningen, Zurich/Fluntern, and Geneva/Cointrin), the summer half year 2022 belongs to the years with below average precipitation amounts, but not to the extreme ones (Fig. 4.7, bottom). The driest summer half year, by some margin, is still that of 1947.

4.4.1 Heat in Switzerland and Europe

The three most pronounced heat periods in the summer of 2022 occurred in mid-June, mid-July, and early August (Fig. 4.8, top). In Geneva, 38 hot days (maximum temperature ≥ 30 °C) were recorded until mid-August, the second-highest number since measurements began in 1864. The record is still held by the heat summer of 2003 with 50 hot days. In Lugano, the number of hot days in 2022 was almost the same as in 1947, namely 35 d; in

---

[1]The prevailing climate for each summer is calculated by fitting a spline to the time series of the Swiss mean summer temperatures/precipitation. The spline was smoothed to correspond to a 20-year Gaussian filter as it is depicted in Imfeld et al. (2022, p. 8). Anomalies are calculated with respect to this spline at each time step. A normal distribution is fitted based on these anomalies and depicted in Fig. 4.7, right column)
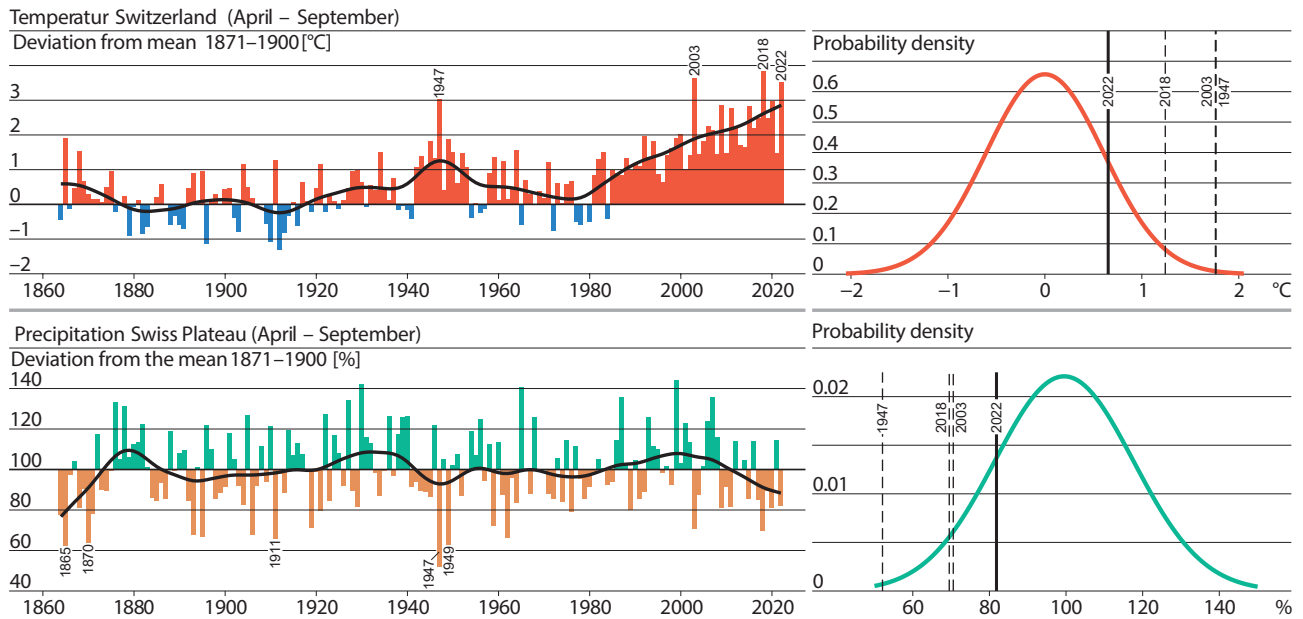
Figure 4.7: Development of the Swiss mean temperature (Begert and Frei, 2018) (deviation in °C) and the mean precipitation (deviation in %). The deviations refer to the pre-industrial average from 1871 to 1900. The black curve shows the smoothed development (spline). The figures on the right show the distributions relative to the prevailing climate. Swiss Plateau: an average of four stations (see text). Values for 2022 are based on measurements and forecast data. Data: MeteoSwiss

the summer of 2003, the number was 47 d. In Basel/Binningen, the number of hot days in 2022 was 33 d, ranking third behind 1947 (43 d) and 2003 (41 d) (Fig. 4.8, bottom). Compared to 1947, however, the individual heat waves were less long and less intense. 1947 was exceptional, as there were five waves in total, the last one in September (Imfeld et al., 2022).

Large parts of Europe were also characterized by extreme heat and drought in the summer of 2022. London, for example, recorded temperatures of 40 °C for the first time (Copernicus, 2022a). The average summer temperature in Europe (June - August) was by far the highest since records began (Copernicus, 2022b). The first two heat waves over Western Europe were characterized by strong meridional ridges that built up from Spain via France to the North Sea (in the second wave to central Scandinavia). Accordingly, the heat waves ran from the Iberian Peninsula through France and southern England to the northeast. The shorter August wave was characterized by a strong temperature gradient over the continent, with a trough positioned over the northwest and a ridge of high pressure in the southeast. The pronounced drought and high temperatures had far-reaching consequences, for example, for agriculture, forests, and glaciers.
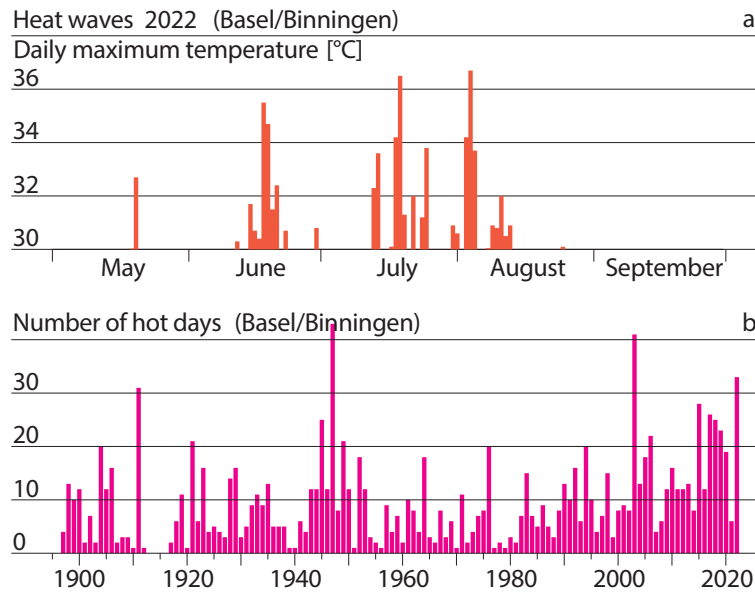
Figure 4.8: a) Days with a maximum temperature greater than or equal to 30 °C for the summer of 2022. b) Number of hot days (maximum temperature ≥ 30 °C) in the summer months April to September from 1898 to 2022. Data: Basel/Binningen from MeteoSwiss.

4.4.2 Agriculture and forests

After a long drought in July, rainfall in the second half of August 2022 north of the Alps partially alleviated the precarious situation in agriculture, for example in grass cutting or water access for alpine cattle (Schweizer Bauernverband, 2022). Nevertheless, insured damage to crops amounted to an estimated 10 million Swiss francs (SDA, 2022). In addition to the drought, crops suffered from frost damage in spring and hail damage in June. In the western part of the Central Plateau and south of the Alps, the drought was much more pronounced: it started already in winter and lasted until the end of summer. Due to the low water levels, irrigation had to be restricted. The consequences of the drought for agriculture were correspondingly severe. Without irrigation, for example, the quality of the potato harvest was reduced. Corn yields were also severely reduced in many places. The consequences of the drought were also strongly felt in fodder production: In many places, hay stocks for the winter had to be fed in the summer. This was compounded by socio-economic problems caused by the pandemic, inflation, and the war in Ukraine, a major exporter of cereals, which resulted in high prices for (imported) concentrated feed. In contrast, above-average yields were recorded for winter crops such as winter wheat, which this year, like most other crops, matured unusually early and were also less exposed to the summer drought. A historic record was set this year on Lake Geneva for the ripening of Chasselas (Agroscope, 2022). Swiss forests also suffered greatly from the drought. Already at the beginning of August, premature leaf discoloration was reported for the Ajoie, the

Laufental, the Klettgau, the Lägerngrat, the Hardwald in Basel, the Lower Valais and for the Canton Ticino in the Mendrisiotto. While in northern Switzerland the damage patterns were less extreme than during the drought of summer 2018, heat and drought, particularly in Valais and Mendrisiotto affected the forests similarly to the summer of 2003 (WSL, 2022). Aside from observations of early leaf discoloration, no current forest damage figures are yet available. The intense precipitation at the end of August and in September reduced drought stress, but if similarly warm and dry summers follow with only short recovery periods in between the resilience of forests will reduce (Frei et al., 2022). A large forest fire occurred in February at Monte Gambarogno in Ticino (approx. 200 ha), but no large fires were recorded during the summer of 2022.

4.4.3 Glaciers

The descriptions of the glacier melt in the summer of 2022 use a similar vocabulary as in the record summer of 1947, which at that time was called a "catastrophic year" (Imfeld et al., 2022) for the glaciers, especially in the Eastern Alps: The summer of 2022 was also catastrophic for Swiss glaciers. In addition to the high temperatures, this was due to the fact that very little snow had fallen in the winter of 2021/22 and the glaciers had already become heavily depleted early in the summer. Normally, the snow cover on the glacier protects the underlying ice from melting. This snow cover had disappeared about a month earlier than usual in the summer of 2022.

To date, the most negative annual mass balance was measured in 1947, and the most negative summer balance in 2003 (Imfeld et al., 2022). These melting rates from the summer of 2003 have now been greatly exceeded in the Swiss Alps in 2022, as the latest data from the Swiss glacier measurement network GLAMOS show. This year, glaciers lost 6 % of their volume (GLAMOS, 2022). Such a melt rate has never been measured before. The hot summers of the late 1940s were followed by a series of colder summers and, in some cases, winters with high precipitation, slowing or even halting glacier retreat until the 1980s. With almost annual recurrences of extreme glacier melt, such as in recent years, many of Switzerland's smaller glaciers, such as the Witenwasseren (Fig. 4.9), will disappear within the next few decades. This year, mass balance measurements on three glaciers had to be abandoned because of a lack of ice at the measurement sites or because the glaciers had become too small to carry out a meaningful measurement program. (GLAMOS, 2022).

4.4.4 Heat and health

Over the summer of 2022 (mid-June to early September), the Swiss Federal Statistical Office reported excess mortality of about 1700 persons for 11 consecutive weeks, especially in the age group over 65 years (BFS, 2022). Such a long and high excess mortality in

Figure 4.9: The Witenwasseren glacier in the canton of Uri melted heavily in the summer of 2022, leaving debris and a proglacial lake in the forefront. As early as August, the glacier had practically no more accumulation area left (photo Isabelle Gärtner-Roer, 23th August 2022).

the summer half year is exceptional. The reasons are probably both independent and interactive effects of the COVID-19 pandemic and the heat. For example, there may have been increased heat-related deaths in patients with chronic conditions who had somewhat less health care due to the pandemic. Known sequelae of COVID-19 include cardiovascular conditions, which in turn are a risk factor for heat-related deaths. However, it is too early for an overall assessment and an objective classification in comparison with the heat summers of 2003 or 1947: the official publication of the causes of death in 2022 is not expected until mid-2024. If heat summers become the norm in the future, the healthcare system could also be more burdened during the summer months due to demographic change (the population is getting older).

4.4.5   How exceptional will a summer like 2022 be in the future?

Overall, Switzerland experienced a very hot and dry summer in 2022. Compared to previous record summers, however, it was less dry than, for example, 1947 and less hot than the record summer of 2003. Nevertheless, there were serious consequences in agriculture and forestry, and in glacier melt. How exceptional will a summer like 2022 be in a future climate? The Swiss climate scenarios CH2018 provide an answer (CH2018, 2018). The

temperature will continue to rise rapidly. Dry periods in summer will become longer, and heavy precipitation more intense. Overall, summer precipitation will probably decrease. If we compare the mean temperature of the summer half years of 2022, 2018, 2003, and 1947 with the expected climate at the end of the 21st century, assuming an optimistic scenario (RCP2.6), then the summer of 2022 would be slightly warmer than average (Fig. 4.10) (Imfeld et al., 2022). In a pessimistic scenario (RCP8.5), 2022 would be a very cool summer. In a scenario with partially implemented climate protection measures (RCP4.5), the summers of 2003, 2018, and 2022 roughly correspond to an average expected summer. When we consider the impacts of this summer, we must keep in mind that 2022 was a fairly normal future summer.
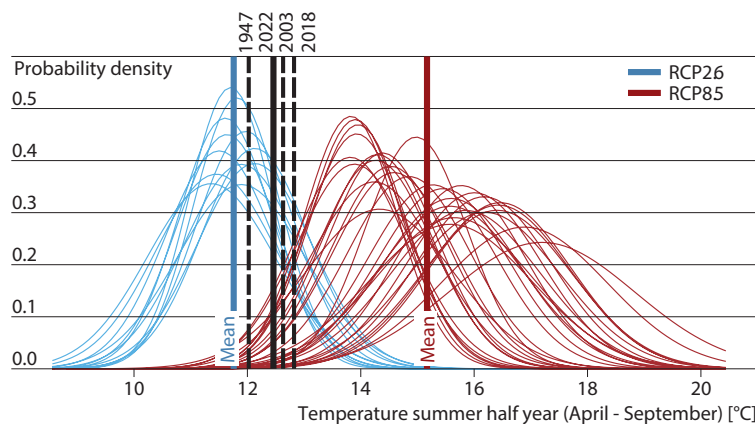

Figure 4.10: Distribution of the temperature of the summer half year (April - September) for the period at the end of the century (2070 - 2099). For each climate model simulation, a normal distribution was fitted (thin coloured lines), the trend in the data was not removed. The coloured vertical lines show the mean value over all summer half-year temperatures of the respective RCP. Also shown are the observed temperatures for the summer half years of 1947 (12.0 °C), 2003 (12.6 °C), 2018 (12.8 °C), and 2022 (12.5 °C). The Swiss average temperature was determined for all data as in (Begert and Frei, 2018). The data for 2022 are based on measurements and forecast data.

Bibliography

Agroscope: Frühreife-Rekord bei Trauben, www.agroscope.admin.ch/agroscope/de/home/aktuell/newsroom/2022/08-02_fruehreife-rekord-trauben.html, last accessed 26 September 2022, 2022.

Altenhoff, A. M., Martius, O., Croci-Maspoli, M., Schwierz, C., and Davies, H. C.: Linkage of atmospheric blocks and synoptic-scale Rossby waves: a climatological analysis, Tellus A: Dynamic Meteorology and Oceanography, 60, 1053–1063, doi:10.1111/j.1600-0870.2008.00354.x, 2008.

Begert, M. and Frei, C.: Long-term area-mean temperature series for Switzerland — Combining homogenized station data and high resolution grid data, International Journal of Climatology, 38, 2792–2807, doi:10.1002/joc.5460, 2018.

BFS: Sterblichkeit, Todesursachen, https://www.bfs.admin.ch/bfs/de/home/statistiken/gesundheit/gesundheitszustand/sterblichkeit-todesursachen.html, last accessed 26 September 2022, 2022.

Bieli, M., Pfahl, S., and Wernli, H.: A Lagrangian investigation of hot and cold temperature extremes in Europe, Quarterly Journal of the Royal Meteorological Society, 141, 98–108, doi:10.1002/qj.2339, 2015.

Black, E., Blackburn, M., Harrison, G., Hoskins, B., and Methven, J.: Factors contributing to the summer 2003 European heatwave, Weather, 59, 217–223, doi:10.1256/wea.74.04, 2004.

Brugnara, Y., Hari, C., Pfister, L., Valler, V., and Brönnimann, S.: Pre-industrial Temperature Variability on the Swiss Plateau Derived from the Instrumental Daily Series of Bern and Zurich, Climate of the Past Discussions, pp. 1–34, doi:10.5194/cp-2022-34, 2022.

CH2018: CH2018 - Climate scenarios for Switzerland, Technical Report, National Centre for Climate Services, p. 271, 2018.

Copernicus: Climate bulletin, Surface air temperature for July 2022, https://climate.copernicus.eu/surface-air-temperature-july-2022, (last accessed 20 September 2022), 2022a.

Copernicus: Climate bulletin, Surface air temperature for August 2022, https://climate.copernicus.eu/surface-air-temperature-august-2022, (last accessed 20 September 2022), 2022b.

Fink, A. H., Brücher, T., Krüger, A., Leckebusch, G. C., Pinto, J. G., and Ulbrich, U.: The 2003 European summer heatwaves and drought –synoptic diagnosis and impacts, Weather, 59, 209–216, doi:10.1256/wea.73.04, 2004.

Fragkoulidis, G., Wirth, V., Bossmann, P., and Fink, A. H.: Linking Northern Hemisphere temperature extremes to Rossby wave packets, Quarterly Journal of the Royal Meteorological Society, 144, 553–566, doi:10.1002/qj.3228, 2018.

Frei, E., Gossner, M., Vitasse, Y., Queloz, V., and Wohlgemuth, T.: Laubfall im Sommer als Indiz für späteres Buchensterben, Wald und Holz, 103:9, 10–13, 2022.

GLAMOS: Schlimmer als 2003: Schweizer Gletscher schmolzen wie noch nie. Medienmitteilung SCNAT, https://scnat.ch/de/uuid/i/2e076759-0234-567e-9bfb-2cdfebd6ff34-Schlimmer_als_2003_Schweizer_Gletscher_schmolzen_wie_noch_nie, 28 September 2022, 2022.

Hersbach, H., Bell, B., Berrisford, P., Hirahara, S., Horányi, A., Muñoz-Sabater, J., Nicolas, J., Peubey, C., Radu, R., Schepers, D., et al.: The ERA5 global reanalysis, Quarterly Journal of the Royal Meteorological Society, 146, 1999–2049, doi:10.1002/qj.3803, 2020.

Imfeld, N., Stucki, P., Brönnimann, S., Bader, S., Bürgi, M., Calanca, P., Gubler, S., Holzkämper, A., Hövel, L. B., Isotta, F. A., et al.: Hot and dry summers in Switzerland. Causes and impacts of the record summers 1947, 2003, and 2018, doi:10.4480/GB2022.G98.03, 2022.

Imfeld, N., Pfister, L., Brugnara, Y., and Brönnimann, S.: A 258-year-long data set of temperature and precipitation fields for Switzerland since 1763, Climate of the Past, 19, 703–729, doi:10.5194/cp-19-703-2023, 2023.

MeteoSchweiz: Klimabulletin Sommer 2023, https://www.meteoswiss.admin.ch/dam/jcr:0e1fd75c-b5ed-487a-ab72-535a0f3f07a7/Klimabulletin-Sommer-2023-de.pdf, (last accessed 6 October 2023), 2023.

Molina, M., Sánchez, E., and Gutiérrez, C.: Future heat waves over the Mediterranean from an Euro-CORDEX regional climate model ensemble, Scientific reports, 10, 8801, doi:10.1038/s41598-020-65663-0, 2020.

Pfahl, S. and Wernli, H.: Quantifying the relevance of atmospheric blocking for co-located temperature extremes in the Northern Hemisphere on (sub-)daily time scales, Geophysical Research Letters, 39, doi:10.1029/2012GL052261, 2012.

Ragettli, M. S., Vicedo-Cabrera, A. M., Flückiger, B., and Röösli, M.: Impact of the warm summer 2015 on emergency hospital admissions in Switzerland, Environmental health, 18, 1–10, doi:10.1186/s12940-019-0507-1, 2019.

Röthlisberger, M., Frossard, L., Bosart, L. F., Keyser, D., and Martius, O.: Recurrent synoptic-scale Rossby wave patterns and their effect on the persistence of cold and hot spells, Journal of Climate, 32, 3207–3226, doi:10.1175/JCLI-D-18-0664.1, 2019.

Röthlisberger, M. and Martius, O.: Quantifying the Local Effect of Northern Hemisphere Atmospheric Blocks on the Persistence of Summer Hot and Dry Spells, Geophysical Research Letters, 46, 10 101–10 111, doi:10.1029/2019GL083745, 2019.

Schneidereit, A., Schubert, S., Vargin, P., Lunkeit, F., Zhu, X., Peters, D. H. W., and Fraedrich, K.: Large-Scale Flow and the Long-Lasting Blocking High over Russia: Summer 2010, Monthly Weather Review, 140, 2967 – 2981, doi:10.1175/MWR-D-11-00249.1, 2012.

Schweizer Bauernverband, S.: AGRISTAT, Statistisches Monatsheft 22-08, https://www.sbv-usp.ch/fileadmin/sbvuspch/04_Medien/Publikationen/Agristat/Archiv/AGRISTAT_2022/Publikation_AGRISTAT_2022-08.pdf, (last accessed 20 September 2022), 2022.

SDA: Trockene Monate wirken sich verheerend auf Schweizer Äcker aus., sRF 4 News, 09-01-2022, 2022.

Shutts, G. J.: The propagation of eddies in diffluent jetstreams: Eddy vorticity forcing of 'blocking' flow fields, Quarterly Journal of the Royal Meteorological Society, 109, 737–761, doi:10.1002/qj.49710946204, 1983.

Slivinski, L. C., Compo, G. P., Whitaker, J. S., Sardeshmukh, P. D., Giese, B. S., Mc-Coll, C., Allan, R., Yin, X., Vose, R., Titchner, H., et al.: Towards a more reliable historical reanalysis: Improvements for version 3 of the Twentieth Century Reanalysis system, Quarterly Journal of the Royal Meteorological Society, 145, 2876–2908, doi:10.1002/qj.3598, 2019.

Sousa, P. M., Trigo, R. M., Barriopedro, D., Soares, P. M., and Santos, J. A.: European temperature responses to blocking and ridge regional patterns, Climate Dynamics, 50, 457–477, doi:10.1007/s00382-017-3620-2, 2018.

Spensberger, C., Madonna, E., Boettcher, M., Grams, C. M., Papritz, L., Quinting, J. F., Röthlisberger, M., Sprenger, M., and Zschenderlein, P.: Dynamics of concurrent and sequential Central European and Scandinavian heatwaves, Quarterly Journal of the Royal Meteorological Society, 146, 2998–3013, doi:10.1002/qj.3822, 2020.

Steinfeld, D. and Pfahl, S.: The role of latent heating in atmospheric blocking dynamics: a global climatology, Climate Dynamics, 53, 6159–6180, doi:10.1007/s00382-019-04919-6, 2019.

Trenberth, K. E. and Fasullo, J. T.: Climate extremes and climate change: The Russian heat wave and other climate extremes of 2010, Journal of Geophysical Research: Atmospheres, 117, doi:10.1029/2012JD018020, 2012.

Woollings, T., Barriopedro, D., Methven, J., Son, S.-W., Martius, O., Harvey, B., Sillmann, J., Lupo, A. R., and Seneviratne, S.: Blocking and its response to climate change, Current climate change reports, 4, 287–300, doi:10.1007/s40641-018-0108-z, 2018.

WSL: WSL internal survey among employees in August., 2022.

Zschenderlein, P., Fink, A. H., Pfahl, S., and Wernli, H.: Processes determining heat waves across different European climates, Quarterly Journal of the Royal Meteorological Society, 145, 2973–2989, doi:10.1002/qj.3599, 2019.

Chapter 5

Conclusions and outlook

5.1 Conclusions

Studying past climate variability is relevant for understanding mechanisms and processes behind multi-decadal variability, long-term climate changes, and past extreme events. While long-term data sets have contributed to studying monthly to seasonal variability over the past centuries, some research questions require daily data, which have so far not been available in a spatio-temporally complete way.

In this thesis, a new high-resolution (1x1 km^2) gridded reconstruction of daily mean temperature and daily precipitation sums based on early instrumental data was presented, which extends the currently available data sets to cover a total of 258 years for Switzerland (Chapter 2). Based on this gridded data set, new analyses and applications are possible. For example, extreme climate anomalies can be studied such as the wet and cold period of 1769 to 1771 in Central Europe (Collet, 2018). The main findings concerning this reconstruction are:

- The analog resampling method with subsequent data assimilation and quantile mapping proved to be a feasible method for reconstructing meteorological fields from early instrumental data to study climate and weather over several centuries. It is a computationally efficient and stable method for reconstructing fields when little observational information is available because it is based on physically plausible samples.

- Despite the low availability of observations before 1864, the cross-validation and the comparison to independent data showed promising results for temperature, although with spatial differences in reconstruction skill, particularly in the Alpine regions. For precipitation, the skill of the reconstructions is lower, but adding precipitation

occurrence (wet days) leads to improved results at specific locations. For the early period, in particular, for precipitation, analyses based on the reconstruction need to be evaluated carefully. While the data are suitable for studying individual events, for example, calculating trends may lead to spurious results due to temporal inhomogeneities.

- Including precipitation occurrence as a variable improves the wet day reconstruction considerably. This suggests that it is worth investing in the rather tedious work of digitizing precipitation occurrence from, for example, weather diaries. However, consistent quality control of precipitation occurrence data is needed which is less straightforward than for other variables.

In Chapter 3, we studied the occurrence of historical extreme springs over the 258-year-long period looking at unusually warm and cold springs, and at springs for which frost damage due to late frosts was reported. Historical reports allowed us to contextualize the daily-based climate indices and the phenological phases from the gridded reconstruction with socio-ecological impacts experienced at that time. The main conclusions of this study are:

- Climate and phenological indices for eight 30-year periods show little variability in the years up to 1930, which is in stark contrast to the last 30 years depicting the strong spring warming due to climate change. This has been shown in many studies before, but until now it has not been possible to show the warming trend using climate indices going back to the late 18th century.

- The three springs of 1785, 1837, and 1853 were exceptionally cold in the period from 1763 to 2020. While the springs of 1837 and 1853 seem to follow a typical cold and wet spring pattern, during the spring of 1785 a cold air outbreak and inversion in March led to continuous cold weather in the Swiss Plateau. These exceptionally cold temperatures are seen in different climate indices and in the cherry flowering phenology which showed delays of up to 25 d in the Swiss Plateau.

- Calibrating phenological models based on phenological observations seems to adequately represent the phenology of the past. However, the choice of the phenological model and the calibration period may influence the reconstruction of historical phenology. Evaluating the effects of the model and calibration period would require further studies beyond the scope of the presented thesis.

Lastly, we presented a Chapter on hot and dry summers in Switzerland with a particular focus on the hot and dry summer of 1947 and 2022 (Chapt. 4). The summer half year of 1947 was with an anomaly of 2.91 °C based on a long series from Bern and Zurich for many years the record summer, and still ranks as the fifth warmest summer half year since

1756. It is also still the driest summer half year in parts of northern Switzerland since 1864. Concerning the atmospheric dynamics, 1947 was particularly interesting because of the high number of blockings that occurred throughout the summer half year, leading to a total of five heat waves in Basel/Binningen. More in-depth research would be needed to study what led to the warm and dry conditions in the late 1940s. Further, we showed that a summer as it occurred in 2022, was not particularly hot for its mean climate, and that it was also a fairly normal summer in a future climate when a scenario with emission reductions (RCP2.6) is considered.

5.2 Outlook

The results presented here showed that the ARM is a feasible method for the generation of meteorological fields based on early instrumental data to study climate and weather over several centuries. However, the results and case studies raised further questions about reconstruction methods, analyses of climate variability and impacts, and the need for more variables. Here, I propose a selection of research directions as a follow-up to this thesis:

- The backbone of any reconstruction method is its input data. The reconstruction showed that it is possible to include information on precipitation occurrence to get a more accurate representation of wet days. This confirms that it is worth investing in digitizing more data for precipitation occurrence, for example from weather diaries. Furthermore, some of the temperature series may be affected by radiation biases due to their exposures (e.g. Hürzeler et al., 2020). Homogenization can reduce such biases in the mean, but correcting radiation errors at a daily resolution is difficult because they are related to the daily weather conditions. Continuing thorough examinations of biases and corrections thereof is relevant for future attempts to reconstruct historical weather (Wallis et al., 2023; Brugnara et al., 2022).

- The selection of best analogue days lacks a temporal relation of the analogue days themselves. Through the assimilation of temperature observations, the temporal relation is improved since the observations themselves contain the temporal structure. However, this is not the case for the precipitation fields that stem from resampling and are only bias-corrected. It may be worthwhile to test temporal criteria in the analogue selection, as this could improve the representation of e.g. passing cold fronts and cyclones, especially for precipitation and also for areas where little data is available for temperature assimilation. A simple approach is to calculate analog days based on moving windows over several days (Yiou et al., 2014).

- With the current reconstruction no information on the uncertainty of the fields is published, which could however be provided through an analogue ensemble and the

examination of Gower distances from the resampling. It would be an advantage to publish uncertainty estimates, for example, by making available the entire ensemble created in the reconstruction process.

- New developments and testing of new reconstruction methods may provide better results by overcoming inherent problems of analogue based reconstructions, such as a poor representation of extreme events due to a small reference data set, i.e. a small analogue pool. Attempts have been made to reconstruct daily fields for Europe based on machine learning using gap-filling approaches. Such approaches could be further explored.

- Extensions of the data set could be made in space, time, and for more variables. Pappert et al. (2022) and the European reconstructions for 1782 to 1785 and 1807 in Sect.1.3 showed that the ARM with subsequent data assimilation can be extended covering larger areas of Europe, though with reduced skill where observation density is low. Reconstructing the area of Europe for temperature and pressure may help in studying, for example, the synoptic conditions during past cold air outbreaks, which is not possible with the Swiss reconstruction. Such single case studies could be extended to an entire data set since observations are available further back in time (Brugnara et al., 2015; Camuffo et al., 2006). For some applications, such as agricultural modelling (e.g. Flückiger et al., 2017) more variables are needed, such as daily minimum and maximum temperature, sunshine duration, but also wind fields may be relevant as they have been downscaled for Switzerland for the period from 1961 to 2020 (Miralles et al., 2022). All of this opens up opportunities for the expansion of the data set.

- Lastly, we presented in Chapter 3 a simple reconstruction of phenology using process-oriented phenological models calibrated with observations from the Swiss Phenology Network. These phenological estimates provide a good basis to study historical phenology and relate them to e.g. historical sources. However, the sensitivity of the calibrated parameters in the phenology models may not be stationary over time. Different models may lead to different estimates in the past due to their parameter sensitivities. Since the late 1980s, a considerable advancement of phenology has been observed (e.g. Vitasse et al., 2018). Very early starts of phenological phases are used to calibrate and estimate phenology for a period where such early starts were rather rare - this might influence how parameters are calibrated. Studying the effects of the calibration period, as well as the model and the parameter sensitivities can contribute to a better reconstruction of past phenology and a better understanding of the responses of phenology and phenological models over long climatic periods.

Bibliography

Brugnara, Y., Auchmann, R., Brönnimann, S., Allan, R. J., Auer, I., Barriendos, M., Bergström, H., Bhend, J., Brázdil, R., Compo, G. P., Cornes, R. C., Dominguez-Castro, F., van Engelen, A. F. V., Filipiak, J., Holopainen, J., Jourdain, S., Kunz, M., Luterbacher, J., Maugeri, M., Mercalli, L., Moberg, A., Mock, C. J., Pichard, G., Řezníčková, L., van der Schrier, G., Slonosky, V., Ustrnul, Z., Valente, M. A., Wypych, A., and Yin, X.: A collection of sub-daily pressure and temperature observations for the early instrumental period with a focus on the" year without a summer" 1816, Climate of the Past, 11, 1027–1047, doi:10.5194/cp-11-1027-2015, 2015.

Brugnara, Y., Hari, C., Pfister, L., Valler, V., and Brönnimann, S.: Pre-industrial Temperature Variability on the Swiss Plateau Derived from the Instrumental Daily Series of Bern and Zurich, Climate of the Past Discussions, pp. 1–34, doi:10.5194/cp-2022-34, 2022.

Camuffo, D., Cocheo, C., and Sturaro, G.: Corrections of systematic errors, data homogenisation and climatic analysis of the Padova pressure series (1725-1999), Climatic Change, 78, 493–514, doi:10.1007/s10584-006-9052-3, 2006.

Collet, D.: Die doppelte Katastrophe: Klima und Kultur in der europäischen Hungerkrise 1770–1772., vol. 18 of *Umwelt und Gesellschaft*, Vandenhoeck & Ruprecht, doi:10.13109/9783666355929, 2018.

Flückiger, S., Brönnimann, S., Holzkämper, A., Fuhrer, J., Krämer, D., Pfister, C., and Rohr, C.: Simulating crop yield losses in Switzerland for historical and present Tambora climate scenarios, Environmental Research Letters, 12, 074 026, doi:10.1088/1748-9326/aa7246, 2017.

Hürzeler, A., Brugnara, Y., and Brönnimann, S.: The meteorological record from St. Gall, 1812–1853. Swiss Early Instrumental Meteorological Series, Bern: Geographica Bernensia, G96, 87–95, doi:10.4480/GB2020.G96.07, 2020.

Miralles, O., Steinfeld, D., Martius, O., and Davison, A. C.: Downscaling of Historical Wind Fields over Switzerland Using Generative Adversarial Networks, Artificial Intelligence for the Earth Systems, 1, e220 018, doi:10.1175/AIES-D-22-0018.1, 2022.

Pappert, D., Barriendos, M., Brugnara, Y., Imfeld, N., Jourdain, S., Przybylak, R., Rohr, C., and Brönnimann, S.: Statistical reconstruction of daily temperature and sea-level pressure in Europe for the severe winter 1788/9, Climate of the Past Discussions, pp. 1–35, 2022.

Vitasse, Y., Schneider, L., Rixen, C., Christen, D., and Rebetez, M.: Increase in the risk of exposure of forest and fruit trees to spring frosts at higher elevations in Switzerland over the last four decades, Agricultural and Forest Meteorology, 248, 60–69, doi:10.1016/j.agrformet.2017.09.005, 2018.

Wallis, E., Osborn, T., and Taylor, M.: Estimating exposure biases in early instrumental land surface temperature data, Tech. rep., EGU23-8119, Copernicus Meetings, 2023.

Yiou, P., Boichu, M., Vautard, R., Vrac, M., Jourdain, S., Garnier, E., Fluteau, F., and Menut, L.: Ensemble meteorological reconstruction using circulation analogues of 1781 - 1785, Climate of the Past, 10, 797–809, doi:10.5194/cp-10-797-2014, 2014.

Appendix A

Statistical reconstruction of daily temperature and sea level pressure in Europe for the severe winter 1788/89

Duncan Pappert[1,2], Mariano Barriendos[3], Yuri Brugnara[1,2], **Noemi Imfeld**[1,2], Sylvie Jourdain[4], Rajmund Przybylak[5,6], Christian Rohr[7], and Stefan Brönnimann[1,2]

1. Institute of Geography, University of Bern, Bern, Switzerland.
2. Oeschger Centre for Climate Change Research, University of Bern, Bern, Switzerland.
3. Department of History and Archaeology, University of Barcelona, Barcelona, Spain 4. Direction de la Climatologie et des Service Climatiques, Météo-France, Toulouse, France.
5. Faculty of Earth Sciences and Spatial Management, Nicolaus Copernicus University, Toruń, Poland
6. Centre for Climate Change Research, Nicolaus Copernicus University, Toruń, Poland.
7. Institute of History, University of Bern, Bern, Switzerland.

A.1 Abstract

The winter 1788/89 was one of the coldest winters Europe had witnessed in the past 300 years. Fortunately, for historical climatologists, this extreme event occurred at a time when many stations across Europe, both private and as part of coordinated networks, were making quantitative observations of the weather. This means that several dozen early instrumental series are available to carry out an in-depth study of this severe cold spell. While there have been attempts to present daily spatial information for this winter, there is more to be done to understand the weather variability and day-to-day processes that characterised this weather extreme. In this study, we seek to reconstruct daily spatial high-resolution temperature and sea level pressure fields of the winter 1788/89 in Europe from November through February. The reconstruction is performed with an analogue resampling method (ARM) that uses both historical instrumental data and a weather type classification. Analogue reconstructions are then post-processed through an ensemble Kalman fitting (EnKF) technique. Validation experiments show good skill for both reconstructed variables, which manage to capture the dynamics of the extreme in relation to the large-scale circulation. These results are promising for more such studies to be undertaken, focusing on different extreme events and other regions in Europe and perhaps even further back in time. The dataset presented in this study may be of sufficient quality to allow historians to better assess the environmental and social impacts of the harsh weather.

Acknowledgement

First of all, I would like to thank Prof. Stefan Brönnimann for giving me the opportunity to work for a few more years in his group and pursue a PhD on the topic of historical weather reconstruction. Thank you for the feedback and guidance over the last years. His enthusiasm and dedication to his research have always inspired me.

I would like to thank the University of Bern, the Oeschger Centre for Climate Change Research, and the SNSF for making this PhD project possible. Thank you, Ed Hawkins, for evaluating this thesis as an external examiner.

Thanks a lot, Alistair, Clotilde, and Eric for proofreading parts of my thesis. Thanks to all my colleagues on the 4th and 5th floors of the GIUB for the enlightening coffee and lunch breaks, for the fun climbing activities, and for the beers we shared after work. Thanks also to Stefanie and Katrin, my former colleagues of the Climandes project, for the extended virtual coffee breaks and supporting conversations during the pandemic.

Thanks to my family and friends for supporting me throughout my studies. And thank you, Al, for being there these past few months.

Declaration

under Art. 28 Para. 2 RSL 05

Last, first name: Imfeld, Noemi

Matriculation number: 09-062-621

Program: PhD. in Climate Sciences

Bachelor ☐ Master ☐ Dissertation ☒

Thesis title: A daily reconstruction of historical weather to study past climate variability and impacts

Thesis supervisor: Prof. Dr. Stefan Brönnimann

I hereby declare that this submission is my own work and that, to the best of my knowledge and belief, it contains no material previously published or written by another person, except where due acknowledgement has been made in the text. In accordance with academic rules and ethical conduct, I have fully cited and referenced all material and results that are not original to this work. I am well aware of the fact that, on the basis of Article 36 Paragraph 1 Letter o of the University Law of 5 September 1996, the Senate is entitled to deny the title awarded on the basis of this work if proven otherwise.

Bern, 31th October 2023

Signature: